Karlsruher Institut für Technologie

Bachelor Thesis

Shear-wave and Compression-wave velocity as Failure Indicator for uniaxial Compressive Strength Tests with Rock Samples

The preparation of this bachelor thesis was supported by the Federal Waterways Engineering and Research Institute (BAW).

Henri Winkler

Geophysik

First Supervisor: Prof. Dr. Thomas Bohlen
Second Supervisors: Dr.-Ing. Julia Götz Eberhard Kunz

Abstract

The evaluation of compressive strength in rock and ground samples is a fundamental component of geotechnical testing. It provides critical data, including stress-strain graphs, that allows for the calculation of various mechanical moduli. When the Federal Waterways Engineering and Research Institute (Bundesanstalt für Wasserbau, BAW) tests compressive strength sensors are attached around the rock samples to measure lateral stress. These sensors have a high risk of damage when the samples are pressured to failure, which is standard testing protocol following the DIN 18141-1:2014 [1] and DIN EN ISO 17892-7:2018 [2]. Preserving the sensors while following these protocols to ensure accurate mechanical moduli calculations has become an urgent challenge.

The primary objective of this Bachelor Thesis is to predict sample failure during uniaxial compressive strength tests using changes in seismic wave velocity under varying pressure conditions, thereby allowing for the timely cessation of testing to protect both sensors and samples. The preferred time window for indicator detection was set at 10 to 30 seconds before the stress peak. The study evaluates indicators, such as the peaks of P- and S-wave velocity, and the last inflection points before the stress peak of P- and S-wave velocity.

A total of 35 cylindrical samples were subjected to compressive strength tests following established standards (DIN 18141-1:2014 and DIN EN ISO 17892-7:2018), while measuring P- and S-wave velocities. Of these, 21 samples were made of Conduro plaster, with different diameters, and 14 were composed of Cordierite Pearl Gneiss. However, the Gneiss samples could not be pressured to failure, limiting the meaningfulness of the data.

The research findings suggest that the velocity peaks of both P-wave and S-wave are unsuitable as indicators for sample failure, as they do not consistently fall within the chosen 10-30 second time window. However, the inflection points of the S-wave velocity show promise, with consistent time windows for Conduro samples and potential suitability for certain conditions. To enhance the capabilities of the experimental setup and accommodate a broader range of testable samples, the study recommends the use of transducers with expanded capabilities and an adapter to connect these transducers to a 600 kN pressure plate. These hardware enhancements, coupled with a data analysis workflow that operates during testing, could lead to the practical application of the derived indicator for sample failure.

While the S-wave velocity inflection point currently holds potential as an indicator for sample failure, further research with a diverse range of materials is needed to validate its applicability under varying conditions. In conclusion, this research contributes to the development of a more efficient and sensor-preserving approach to evaluating the compressive strength of rock and ground samples, opening doors to improved testing methods and reduced resource expenditure.

Contents

1 Introduction

When working with rock and ground samples, the test for compressive strength is essential. Compressive strength and the data collected during the test, a stress-strain graph, enable one to calculate many mechanical moduli. When the Federal Waterways Engineering and Research Institute (Bundesanstalt für Wasserbau, BAW) tests compressive strength, and mechanic moduli of solid samples, sensors are attached around them to measure lateral stress. These sensors tend to break when testing the samples till failure. For an accurate calculation of the mechanical moduli, it is crucial to apply force to the samples until most of the linear stress-strain relation is revealed. To ensure this, the BAW tests samples until failure following the DIN 18141-1:2014 [1] and DIN EN ISO 17892-7:2018 [2], which endangers the sensors. Theoretically testing for mechanical moduli could be done without breaking the sensors to save money.

To secure accurate calculations of the mechanical moduli without breaking the sensors, one needs to apply enough vertical force to reveal the linear stress-strain relation while not straining the samples to failure. Due to the common inhomogeneous and isotropic nature of rock and ground samples, general recommendations of compressive strengths based on rock and ground types are too inaccurate to rely on [15] p. 49 table 3.1.

As a research object of this Bachelor Thesis, we thought to use the effect of increasing and decreasing seismic wave velocity under varying pressure to predict sample failure during the testing. That would allow applying strong enough vertical force to show most or all of the linear stress-strain relation and then stopping the testing before the sample fails, thus leaving the testing material and sensors intact.

2

Theory

2.1. Seismic Body Waves

Seismic waves are split into two categories, surface and body waves. For this study, only the body waves are important. The seismic body waves can be split into two different types, which differ in the way the ground particle move, while transporting the kinetic energy from the source outwards. The Primary wave (P-wave) or compressional wave is a longitudinal wave, as it is polarised in the direction of the wave propagation (see figure 2.1), while the Secondary wave (S-wave) or shear wave is a transverse wave as it is polarised perpendicular to the direction of wave propagation

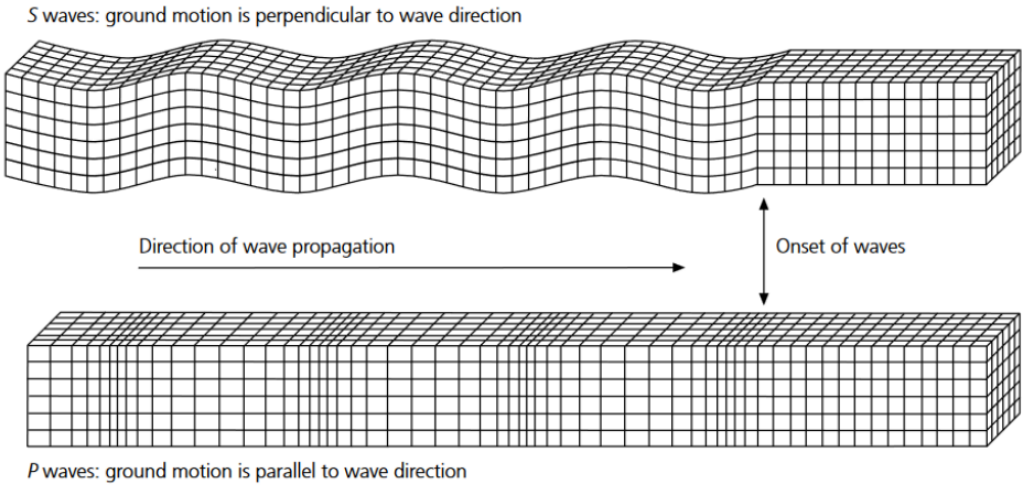

Figure 2.1: The ground motion in relation to the direction of wave propagation. With the transverse S-waves ground motion being perpendicular to wave direction (top) and the longitudinal P-waves ground motion being parallel to wave direction (bottom). The graphic also indicates what the wave onset looks like ([14]).

2.2. Huygens Principle and Travel Time

Huygens states that all points of a wavefront of sound in a transmitting medium can be regarded as new sources of wavelets that expand spherically at a rate depending on their velocities. The sum of these spherical wavelets forms a new wavefront. The wave is refracted and reflected at boundary surfaces of different mediums, which differ in their physical properties.

To simplify wave propagation, the Huygens principle for seismic waves is used to view the body wave propagation along a ray. The mathematical justification of the ray theory can be derived from a high-frequency approximation of the acoustic wave equation ([12]). With our testing frequency being 1.1 MHz, we are in a sufficiently high-frequency range to apply this approximation. This leads to the travel times of P- and S-waves being computed as

$$t_p = \frac{x}{v_p}, \quad t_s = \frac{x}{v_s} \tag{2.1}$$

With x being the distance travelled and v_p and v_s being the corresponding P- and S-wave velocities. In this thesis the distance travelled x will be the initial length of the samples l_0 and the length of the samples thereafter l.

2.3. Microcracks

For the later discussion, it is imperative to examine the behaviour of microcracks under increasing load. As Simmons et al. [13] wrote in 1976, cracks are produced when the local stress exceeds the local strength. This can happen through a variety of causes, from external forces to spatial and temporal changes in temperature, which induce microcracking as a result of differential thermal expansion between grains with different thermoelastic moduli and thermal conductivities ([7]).
The emergence of microcracks or bigger cracks leads to slower wave velocities, while the closing of existing cracks leads to higher velocities. Griffiths et al. [5] state that with increasing uniaxial load, the first microcracks to close are those perpendicular to the direction of the applied stress, followed by those at lower angles. For propagation and the stress direction perpendicular to the fibre direction of isotropic materials, the data collected by Prosser [10] demonstrated a linear relation between normalized velocity shift and stress.

Based on this information, we expect the following wave velocity behaviour during the compressive strength tests. **1.** The velocities will gradually increase as stress increases, brought about by the microcracks closing under higher pressures. **2.** The velocities will peak, signalling that most microcracks are closed. **3.** Then the velocities will decrease, while the stress increases. During increasing load, new microcracks emerge that grow and connect, creating macro instability until the velocities reach a new local minimum, before the sample failure.

2.4. Geometry Factor

The Geometry Factor k is a simple positive number, showing the relation between the diameter and length of the samples. It is calculated by dividing the length l of the sample by its diameter d, as mandated by the DIN 18141-1:2014 [1].

$$k = \frac{l}{d}$$

For this study, the Geometry Factor k was chosen to be around 2 for consistent testing and because anything out of the range of 1 - 2.5 is deemed unusable due to briquette danger or possible bending ([9]).

2.5. Material Properties

2.5.1. Compressive Stress and Compressive Strength

The compressive stress σ is, as mentioned in DIN 18141-1:2014 [1], the axial force F divided by the initial cross-sectional area A.

$$\sigma = \frac{F}{A} \tag{2.2}$$

The compressive strength σ_u is the maximum stress σ_{max} the material can take before failing.

$$\sigma_u = \sigma_{max} = \frac{F_{max}}{A} \tag{2.3}$$

2.5.2. Strain

The strain ε, as defined in DIN 18141-1:2014 [1], is the relation of the axial length change of the sample Δl_m to the initial sample length l_m. Shortenings and compressions have positive signs.

$$\varepsilon = \frac{\Delta l_m}{l_m} \tag{2.4}$$

2.5.3. Stress-Strain Curve and Modulus of Elasticity

When visualizing a compressive strength test through a stress-strain curve, three sections are apparent ([4]). Figure 2.2 is an example, showing these three sections and other points of interest along the curve.

The first section, **I**, is the linear elastic section during which the sample shows linear elastic properties, meaning that the strain is reversible, and Hooke's law is still applicable. The slope of the linear curve portion is used to calculate the elastic modulus. The yield strength is the highest stress under which the sample behaves as linear elastic, functioning as a border point between the first and second section ([4]).

The second section, **II**, is called the nonlinear elastic section during which the sample deformation is still reversible but not proportional to the applied stress. The curve's peak is the compressive strength, the highest stress the sample can support, and also separates the elastic and plastic sections ([4]).

The third section, **III**, is called the nonlinear plastic section because after the compressive strength is reached the sample partially deforms plastically ([4]).

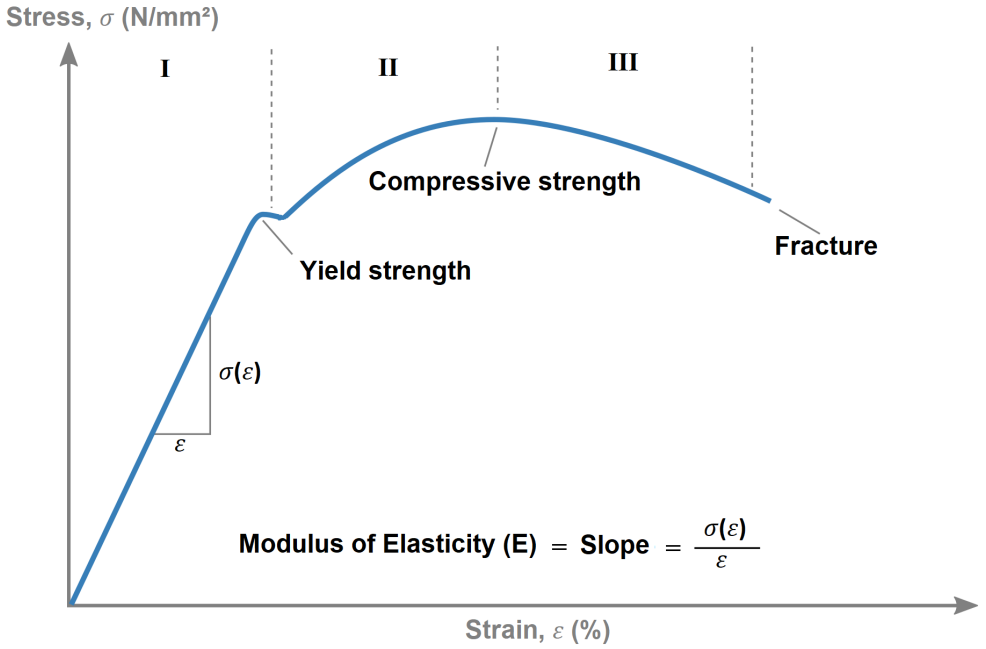

Figure 2.2: An exemplary compression stress-strain curve, showing the 3 sections, **I** linear elastic section, **II** nonlinear elastic section, and **III** nonlinear plastic section. The yield strength is the highest stress under which the sample behaves linear elastic. The curves peak is the compressive strength, the highest stress the sample can support. Also shown in the figure is the formula for the modulus of elasticity, since it is derived using the slope of the curve in the linear elastic section ([4]).

The modulus of elasticity or Young's modulus gives the proportional relation between stress σ and strain ε during the linear-elastic behaviour of a solid material during a deformation.

For the calculation of the modulus we look at the slope (see figure 2.2) coming from the linear part of the stress-strain curve ([6]).
The slope is the tensile stress $\sigma(\varepsilon)$ divided by the lateral strain of the test probe ε.

$$E = \frac{\sigma(\varepsilon)}{\varepsilon} \tag{2.5}$$

3
Methods

3.1. Experimental Equipment

3.1.1. Hydraulic Press Z600

The hydraulic press Z600, by the company ZwickRoell, was used to apply force during the testing. It has a maximum force output of 600 kN, according to *Vorteile und Merkmale der Z600* [17] the force is measured by a DMS Force Transducer and is calibrated according to ISO 7500-1 in class 0.5 and class 1.

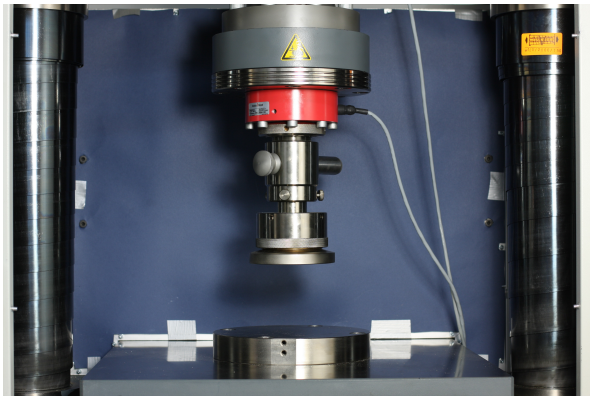

Figure 3.1: The hydraulic press in close up, showing the pressure plate (in this picture the 100 kN pressure plate) and the bottom steel plate, between which the piezo sensors [3] [16] were fixed.

3.1.2. Syrosonic ultrasonic device and Electro-Acoustic Transducers by GL Testsystems

To measure the transit time of the seismic waves through the samples, the Syrosonic ultrasonic device [16] was used. The Syrosonic set includes two electro-acoustic transducers [3] (seen in figure 3.2), which generate acoustic waves through singular piezo components located deep within the transducer. The casing is made of steel, covered in an anti-corrosion layer, and the round contact surface of the two transducers has a diameter of 80 mm. These robust casings make the transducers ideal for testing under high pressure.

The piezo enables them to measure with different frequencies (0.5 MHz, 1.1 MHz and 3.6 MHz), and the extended steel casing creates deadtimes of 22.63 μs for the P-waves and 40.73 μs for the S-waves.

Figure 3.2: The two piezo electro-acoustic transducers by the company GL Testsystems (1 and 3) [3], with a round contact surface diameter of 80 mm attached to their adapters (2 bottom and 4 top).

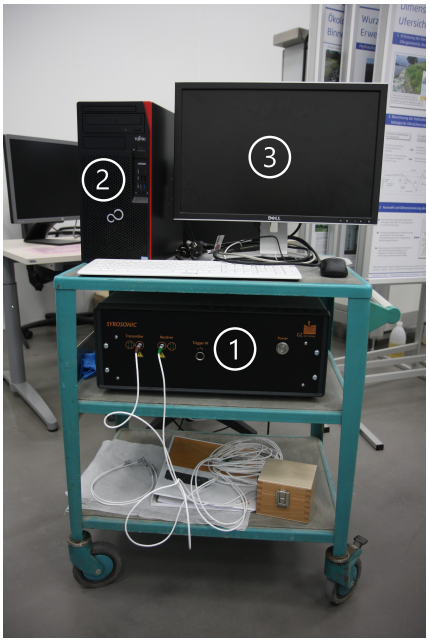

Figure 3.3: The Syrosonic workstation including (1) the Syrosonic by [16], (2) a computer to which the Syrosonic is connected and (3) a screen to visualize the Syrosonic Software.

During the tests, the Syrosonic was set to measure with 1.1 MHz and measure continuously during the tests, with measuring intervals of 4 seconds. For every interval, it shows the received signal with a resolution of 10 nanoseconds and exports it. This precise measurement is important because velocity changes due to stress are small, typically below 0.1 % ([11]). The graphical interface of the Syrosonic software was used to set the window length of the signal and the window in which the signal amplification was automatically set. The Syrosonics software internal arrival time picker was not used for the analysis.

The Syrosonic workstation, which can be seen in figure 3.3, is made up of the Syrosonic itself, together with a personal computer (PC) and a screen. Because of strict software licensing, the Syrosonic can only be connected to this one PC, not to the one controlling the Z600. That means that for the acoustic transducer to measure during a Z600 experiment, one had to switch to the Syrosonic PC right after starting the Z600 experiment, to start the automatic transit time measuring. This led to a one to four-second delay between the starting time of the Z600 experiment and the start of the transit time measuring. Because the Z600 experiments start with the hydraulic press slowly increasing its force to the pre-load of 100 N, there was always enough time to trigger the Syrosonic without losing measurements.

3.1.3. Transducer Adapter

To connect the hydraulic press and the electro-acoustic transducer [3], a steel adapter was designed. This adapter is mounted to the Z600 through the pressure plate connection, which ensures easy connecting and negligible leeway when force is applied. The top transducer was then pressed into the adapter. To secure the transducer in place, a rubber ring was built into the inside of the recess. The bottom transducer was placed on top of the bottom adapter to ensure a flat connecting surface with the steel plate. There was no other fixation needed because there was only vertical force applied. This led to initial leeway when lateral force was applied, but after pushing the transducer all the way into the adapter, the leeway decreased to a negligible amount. The transducer, with the associated adapters can be seen in figure 3.2.

3.2. Samples

The samples are drill cores of cordierite pearl gneiss, marlstone, concrete with a big grain size and plaster, cut into smaller cylinders. The origins of the gneiss is the floodgate Kachlet in Passau, the exact GK4-DHDN coordinates are 4603697.17 (E) / 5383262.51 (N) and the drill depth is 8 m to 9 m.

The process of preparation will be discussed in the next section.

3.2.1. Sample Preparation

All the drill cores arrived in sealed tubes that were 1 m long and had a diameter of 10 cm. Most cores showed damage because they became bridled and broke in unfortunate places after transportation and natural dehydration. This led to some sections of a core being unusable. The first step of sample preparation was to assess the cores and decide the number of pieces each would be cut into.

The samples should have a length between 6 cm and 10 cm, with corresponding diameters of 3 cm to 5 cm, after DIN 18141-1:2014 [1]. We chose small samples because this would increase the chance of sample failure during the compressive strength tests. Leaving a leeway of around 20 % - 50 % for the length of the samples, the cores were cut into 3 to 7 pieces each, using a stationary diamond rock saw. The cut core piece is then placed in the centre of the concrete cube mould, and freshly mixed plaster (conduro) is poured around it to fix it in place (see a) in figure 3.4). After a minimum of 3 hours, the plaster will have solidified enough to allow the metal box containing the core piece to be placed under a drill, similar to step b) in figure 3.4 for the next step of preparation.

(a) Plaster fixation

(b) Drill placement

Figure 3.4: a) Two core pieces of Cordierite Pearl Gneiss fixed in the centre of a metal box by conduro plaster. **b)** A conduro plaster block placed under a drill with 5 cm diameter. The conduro block, as well as the core pieces in metal boxes are fixed under the drill by a metal ring mount, secured in place by two screws on the ends of the mount.

Depending on what size the samples should be, the diameter of the drill is chosen. The box is then fixed in the correct place by the metal ring mount, which is held on top of the block or box by two screws at the ends of the mount. This ensures little to no movement of the fixed object during drilling and allows enough space to drill out a single solid sample. The drilling has to be done with great care and under continuous water flow to avoid getting the drill stuck, breaking the sample, and making it unusable.

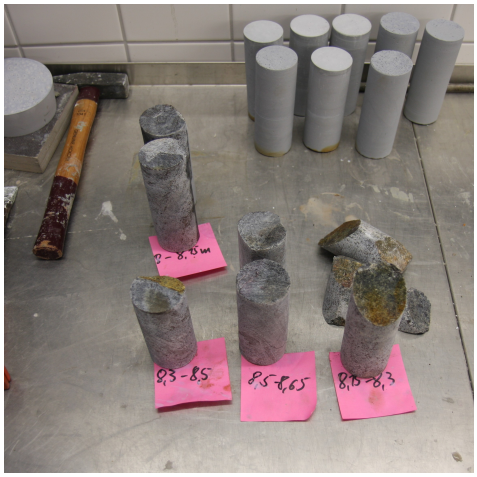

Figure 3.5: Uncut gneiss (in the front) and uncut plaster (in the back) samples with 3 cm diameter.

After successful drilling, the sample has the right diameters but is too long and has uneven edges. To achieve a cylinder with parallel planes and the desired length, the sample is fixed into a diamond rock saw. After marking the cutoff points for the wanted length, the edges are cutoff without taking the sample out of the fixed position in the saws mounting. That ensures parallel planes for the sample cylinder. The cut should be as clean and parallel as possible because every ripple in the surface or slight difference in orientation can lead to weaker signals.

Most of the gneiss samples had a small protrusion of 1 mm - 4 mm at one or both faces,

which occurred during the cutting of the rough edges. The gneiss was very sturdy, which led to the diamond saw blade slowly bending outwards during the cut. These protrusions were later filed down, to achieve smooth and parallel faces. This led to them being slightly shorter than wanted, not always reaching the desired 1:2 ratio of diameter to length.

After successful drilling, cutting and filing, the finished samples are weighed, and the final length and diameter are measured following the DIN 18141-1:2014 [1] specifications.

The gneiss samples with 50 mm proved too sturdy for the 100 kN pressure plate of the hydraulic press, meaning that they didn't fail, even after maximum force output. In an effort to create gneiss samples that break under the 100 kN plate, the 50 mm diameter samples were reused after testing. They were once again plastered, drilled and cut, but to a diameter of 30 mm and lengths around 60 mm. These samples are named "G 30er ...".

3.3. Problems with Measuring

During tests with the Syrosonic with natural samples and rough concrete, a problem arose. No matter how much pressure or coupling paste was applied to the concrete or the marlstone samples, the Syrosonic did not show a signal. Even with the highest gain of 80 dB, which the Syrosonic automatically set, one could only see noise. When the samples were tested with a different electro-acoustic transducer, the "Pundit 200 Pulse Echo", they showed a clear signal. Initially, this led us to believe that the plane surface of the natural samples was too rough for the Syrosonic transducer. But even after cutting them again and even covering the plane surfaces with just enough plaster to make them as smooth as possible, the Syrsonic couldn't read a signal.

We realized that the concrete and the marlstone samples have bigger grain sizes than the gneiss and the plaster and that the Pundit ultrasonic device measures with 54 kHz, which is about a tenth of the 500 kHz of the lowest signal frequency of the Syrosonic transducers. These findings pointed to a frequency-depended dampening effect as an explication for the missing signals. After multiple tests with materials of different grain sizes, we are sure this is the reason behind the missing signals. This meant that the materials that we were going to test using the Syrosonic had to have very small grain sizes and had to be very compact.

3.4. Experimental Setup and Presets

The experimental setup consists of the Z600 hydraulic press, equipped with the 100 kN pressure plate together with the mentioned adapters and electro-acoustic transducers. The Z600 is connected to a PC which allows the operation of the press via the software TextXpert running on the PC.
The transducers are connected to the Syrosonic, which is connected to the second PC. The second PC was set up close enough to the first one, to allow for simultaneous excess.

To secure reproducible and reliable tests, a solid form fitter with an adaptable diameter is used to place the bottom transducer in the centre of the bottom steel plate. Before testing, a small amount of coupling paste is applied to the top and bottom area of the probes, and they are placed in the middle of the lower transducer. This guarantees the best possible coupling between the surface of the transducer, where the piezo crystal is located, and the probes surface.

The TestXpert software preset for the Z600 is as followed:

Versuchsdefinition or type of testing

Type of testing is set to pressure (*Druck*).

Startposition or starting position

Set the starting position to sample height plus 2 mm. Set the speed with which the press reaches the starting position (*Geschwindigkeit Startposition*) to 50 mm/min.

Vorkraft or pre-load

Set the pre-load (*Vorkraft*), usually 100 N, set the speed for the pre-load (*Geschwindigkeit*) to 0.5 mm/min and set the pre-load holding time (*Vorkraft Haltezeit*) to 300 s.

Probedaten or sample data

The sample geometry for the cross section (*Probenform für die Querschnittberechnung*) is set to round (*Rundprobe*), the sample diameter can be input, the cross-section correction factor (*Querschnittkorrekturfaktor*) is set to 1. The negative cross-section correction value (*negativer Querschnittkorrekturwert*) is set to 0 mm^2.

Setzphase or setting phase

Setting cycles are disabled.

Messphase or measuring phase

Non cyclic Measuring
For compressive strength testing, cyclic measuring phase (*Messphase*) is disabled.

Cyclic Measuring
When cyclic measuring is enabled, one can set the Number of cycles (*Anzahl der Zyklen*), the pressure at the load point of the cycles (*Druck am Belastungspunkt der Zyklen*) (in N/mm^2), gain (*Zunahme*) (in N/mm^2), holding time at the relief point of the cycles (*Haltezeit am Entlastungspunkt der Zyklen*) (in s), and the speed of the cycles (*Geschwindigkeit der Zyklen*) (in %L0/min). Set the relief point of the cycles (in N/mm^2), gain (in N) and holding time (in s) at the relief point. Chose the holding at the relief point of the cycles, the speed of the cycles (in $\%l_0$/min), whether the cycles should start at the relief point or not, whether to start with pre-load after each cycle or not, and whether only specific cycles should get detected or not. The chosen settings for the tests can be found in chapter 3.8.

Belastungsphase or stress phase

For the stress phase, the setting "pressure until the end of testing" (*Belastung bis Prüfungsende*) is enabled and the speed at which the hydraulic press moves (*Geschwindigkeit bis Prüfungsende*) is set to be strain regulated (*Dehnungsgeregelt*).

Prüfungsende or end of testing

The Force cut-off threshold *Kraftabschaltschwelle* is set to 30 %, the usual setting for soil samples. The maximum force drop-off *Kraftabfall* is set to 5 kN, the setting for rock samples. These settings enable us to switch sample types without changing the *Prüfungsende* settings. In addition, set the upper force limit (*Kraftgrenze*) just below the maximum force of the test head (98 kN for the 100 kN pressure plate). The lower force limit, which must be negative, was set to -5 N, and the maximum change in length (*maximale Längenänderung*) is set to 21 %, which is the setting for soil samples. A maximum test duration (*maximale Versuchdauer*) can be set, but is not required.

Ergebnisse or results

In Results (*Ergebnisse*), you can select the curve signs, units and names for the results and graphs.

Bruchuntersuchung or break analysis

Set the amount of measuring data sets for break analysis (*Anzahl der Messdatensätze für Bruchuntersuchung*) to 5, the load spike (*Kraftsprung*) to 5 %, the negative and positive stretch strain (*negative und positive Dehungsspannung*) to 10 %.

Aktion nach Prüfung or action after testing

The maximum load at the end of the test (*maximal zulässige Kraft am Prüfungsende*) is set to 50 N and the relief velocity (*Geschwindigkeit der Entlastung*) is set to 50 mm/min.

Messwertspeicher or data storing

A displacement interval of 0.01 mm, a time interval of 1 s and a force interval of 100 N are set and all activated to guarantee enough measuring points. Between 1000 and 5000 measured values per test are ideal.

Regelparameter or control parameters

In the Control parameters area (*Regelparameter*), Controlled Positioned (*Geregelt Positioniert*) is selected, with a delay at speed changeover (*Verzögerung bei Geschwindigkeitsumschaltung*) of 100.

Parameter fürs Protokoll or protocol parameters

In protocol parameters *Parameter fürs Protokoll*, one can enter the header data, extra information and comments.

Protokolle or protocol

In Protocol *Protokolle*, select the `Protocol_BAW_2166` preset.

Exportschnitstelle or export interface

In this setting, one can choose how to export the data, and the log.

After the configurations are set, the hydraulic press is manually moved, with a speed of 200 mm/min for longer distances and 50 mm/min for precise movements, to create contact between the transducer and the sample without overstepping the pre-load force of 100 N. This is an important step to spread the coupling paste evenly on the surface and to ensure that the two transducers sit tightly in their respective adapters without any give. If this step is overlooked or not done correctly, it can lead to the transducers being slowly pushed into the adapters during the test. This paired with a force-controlled compression of the hydraulic press, can lead to long and slow experiments, which are harder to process and evaluate.

Before the measuring can start, Syrosonics measuring window and the automatic gain window have to be set in the GL Testsystem software. For this, automatic measuring is started for P- and S-wave signals and the parameters are chosen depending on the signal. Contingent on the probe length, either a 90 µs window from 0 µs to 90 µs or from 30 µs to 120 µs is chosen. For the gain window, one has to look at the first-time arrival and set the window around that arrival time, to prevent irregular spikes in the signal to trigger unwanted gain chances.

3.5. Experimental Conduct and Data Collection

Z600

With the correct TestXpert settings chosen and the Syrosonic parameters set, one can press the "Start" button in the Z600 software, shortly followed by pressing the "Automatic Measuring" button in the Syrosonic software, to start measuring for the hydraulic press and the electro-acoustic transducers.

After the test is finished the data is exported as a .txt file, copied and saved for further analysis.

Syrosonic

The Syrosonic measures every 4 seconds and saves the snapshot as a .txt file in the dedicated folder. After a sample was tested to failure, or the Z600 test has been stopped, one has to click "Stop measurement" in Syrosonics software. This will make the device take one last snapshot and export a single conclusion file with all the automatically picked first arrival times. Due to the inconsistency of the automatic picker, we will not be using the conclusion file but rather all the singular snapshot files for our further analysis.

3.6. Preliminary Tests

Preliminary tests were made to ensure the experimental setup would work as planned and to figure out a fast and reliable workflow for testing, collecting data, and processing the data. A compact workflow was necessary to stay within the given time frame while testing around 50 conduro plaster samples to failure during compressive strength tests and cyclic stress tests.

During tests with marlstone and concrete, it became apparent that the lowest testing frequency of the GL Testsystems acoustic transducers, with 500 kHz, was too high to produce a readable signal. The high frequency led to such strong dampening in materials with particle sizes over 10 μm that not even testing on small samples with lengths of 50 mm - 70 mm would produce a readable signal. This was a big setback and would ultimately limit the sample material to the conduro plaster, a highly homogeneous and isotropic mix with small particle size, and a cordierite pearl gneiss from the watergate Kachlet in Germany.

During these tests, the right amount of coupling paste was found to be a small drop with a diameter between 2 mm - 4 mm, depending on if the samples had a 30 mm or 50 mm diameter. When using too much coupling paste it would spill over the surface edges, and the initial pre-loading would take significantly longer, without improving the measured signal in any noticeable way. Any less paste and the signal would significantly worsen.

The preliminary tests also helped find the best way to set the gain window of the Syrosonic software. Sometimes signals, both compressional and shear waves, had spikes in the middle of the signal or shortly after the first arrival time, which would end up affecting the automatic gain. To prevent this, one would look at the signal before starting the compressive strength test and set the gain window borders significantly in front and close behind the first onset. This would ensure an appropriately boosted signal over the whole test.

The automatic picker of the Syrosonic was found to be too inaccurate and not adjustable enough, sometimes picking peaks with an error of 0.5 µs. It would only pick the strongest peak in the set window, not taking into account first arrival times or how consistent the peak is. Because of this, a Python code was written to analyse and process the collected data.

3.7. Code for Analysis

During the preliminary tests a total of five different codes were written (`rename_files.py`, `manuel_picker.py`, `auto_picker.py`, `results.py`, `inflection_point.py`, `distortions.py`, and `compare.py`. In the following sections, I will go over them briefly, describe their purpose and what they do in the order they were used during the analysis.

3.7.1. `rename_files.py`

The data exported by the Syrosonic consists of two types of files. The first type is the "conclusion" file, in which all the automatically picked first arrival times are collected, together with some information about the measuring series. The second type is the collection of all the P- and S-wave signal snapshots which occurred every four seconds during the

measuring. These snapshots are named like this `seriesname_date_time_numberofsnapshot`. These names are laborious to process in scripts, which is why I wrote the `rename_files.py` script. It was used to rename the exported signal files of the Syrosonic to make them easier to use in further analysis without losing any valuable information. The new name is like the following example "`name_date_time_00x`".

3.7.2. `manuel_picker.py`

Because this paper explores the relative changes of mechanical properties of materials and is not dependent on accurate P- and S-wave velocities, we would pick strong and consistent peaks in the signal as reference points for transit time changes, as opposed to first arrival times. These consistent picks will henceforth be called arrival times. The `manuel_picker.py` script enabled me to set a defined window in the P- and S-wave signals to pick peaks within. It would find the strongest peaks in the chosen window for one snapshot, depending on the parameters set, record the peaks and mark them in the chosen snapshot. Usually, 8 to 15 snapshots are chosen per measuring series, depending on the number of snapshots per series. They would also be spread out enough to enable me to see trends and find consistent peaks. The strongest and most consistent peak is recorded and used as a start-off point for the following analysis script. This means the arrival times of the strongest peak in the P- and S-wave signal in the first snapshot would be used for further analysis. The actual picking is done with the next script `auto_picker.py`.

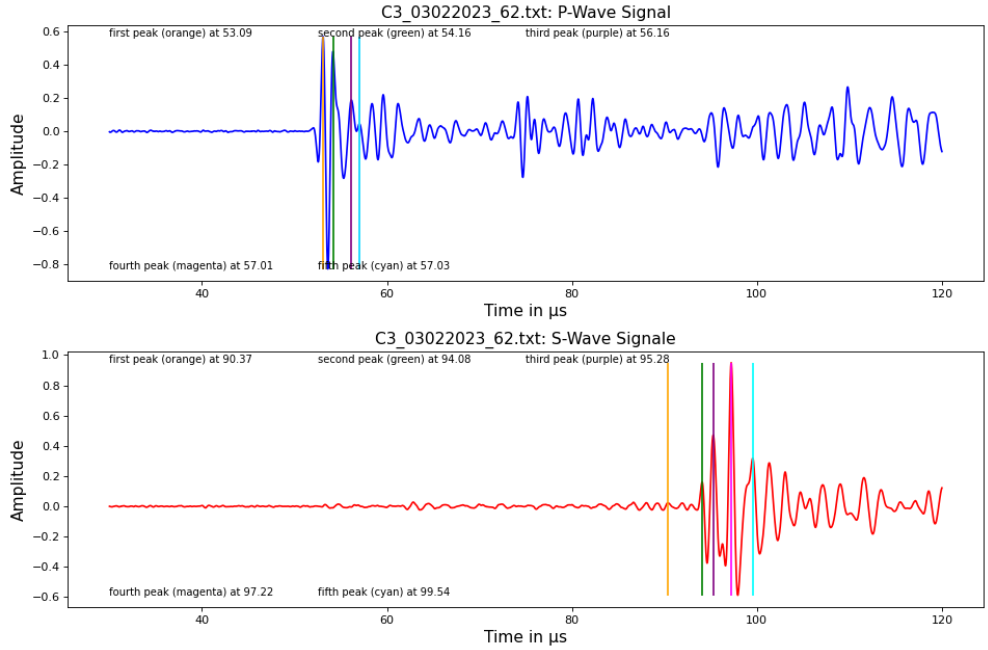

Figure 3.6: Example snapshot 62 from the sample C3, after analysis through the `manuel_picker.py` script. The amplitude is normalized for easier readability.

3.7.3. `auto_picker.py`

The auto-picker script picks the arrival times and extracts gain and signal strength data from the snapshot files. It needs the input of the two mentioned arrival times. Those are manually found with the `manuel_picker.py` script, and a given time window, usually 10 μs to 20 μs wide, to function properly. The script uses `find_peaks` from the `scipy.signal` pack to search for peaks in the snapshot signals. It picks the arrival times based on the arrival time of the last snapshot and the strength of the peaks in the chosen time window, except for the first pick, which uses the mentioned input arrival times.
The picked arrival times of each snapshot of every measuring series are exported into a single file, which is used in the last step of the analysis. The gain and signal strength information is also saved and exported respectively, into single files for further use.

3.7.4. `inflection_point.py`

The `inflection_point.py` script takes the velocity and stress data to determine the second derivative of the velocity curve, to find the number of inflection points, their location and at what stress levels they appeared (IP), for both P- and S-wave velocities for every sample. It also gives the time from the inflection point to the stress peak (TIP).

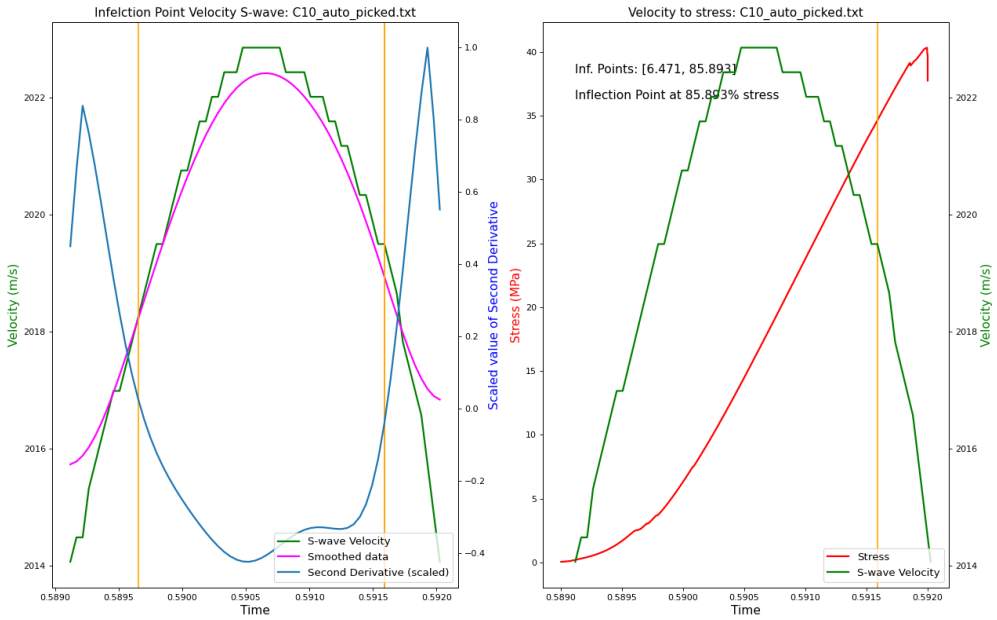

Figure 3.7: Example of sample C10, after analysis through the `inflection_point.py` script. Showing the inflection points on the velocity data and at what stress levels they occur, over the time of the test (x-axes). The velocity (green) is shown in m/s and the stress (red) is shown in MPa.

The script uses a Gaussian filter to create a smoothed data set with the same amount of data points as the original velocity data set. It then calculates the first and second derivatives of the smoothed data set, creating arrays with the same length as the original data set. When searching for inflection points, one has to look for the zero points in the second derivative. Since the second derivative array has relatively few data points (60 to 70 for an average

5-minute compressive strength test), it rarely includes a true 0. To find inflection points under those circumstances the script checks for sign changes within the second derivative and chooses one of the data points of such a sign change. This leads to the position of inflection points having an error of 1 s to 2 s. This problem and possible solutions will be mentioned in the discussion of error.

3.7.5. `results.py`

The `results.py` script is a collection of classes, all written to simplify and visualize the data provided by the `auto_picker.py` script. It was used to determine the percentage of stress at which the velocities peak (PPC) and the time between velocity peak and stress peak (TPP).

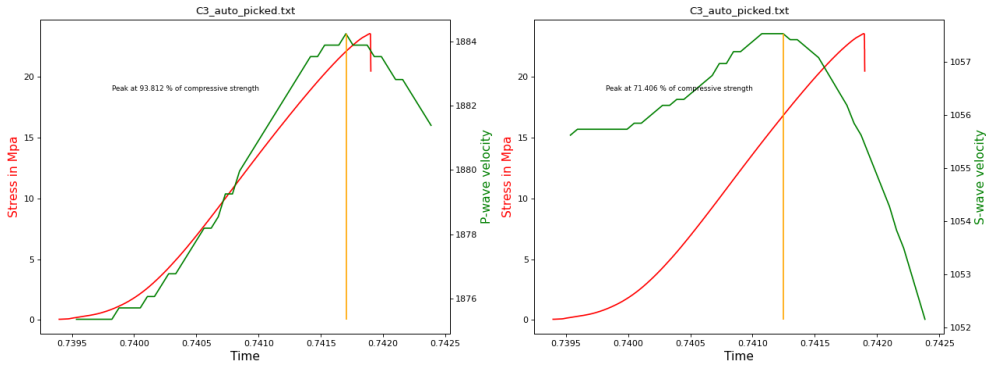

Figure 3.8: Example of sample C3, after analysis through the `results.py` script. Showing the wave velocity and stress during the test.

3.7.6. `distortion.py`

The `distortion.py` script was written to examine the velocity errors created by physical changes of the sample during testing. It uses additional compression data collected by the Z600 to evaluate the impact of small length changes on the wave velocities. It visualizes the velocities derived from using the static sample length and the dynamic sample length, and compares them.

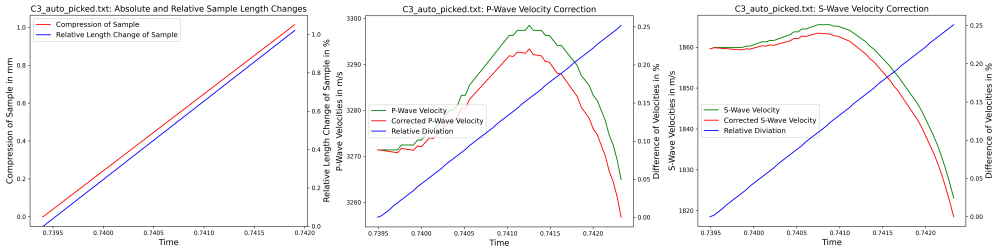

Figure 3.9: Example of sample C3, after analysis through the `distortion.py` script. **(left)** Showing the absolute (red) and relative (blue) sample length changes. **(middle/right)** depicts the P- and S-wave velocities derived by using the static sample length (green) and the dynamic sample length (red).

3.7.7. `compare.py`

The `compare.py` script is used to visualize the gained sample data of PPC, TPP, IP, TIP, by comparing it to the other samples. The comparisons between different samples is used to discuss the viability of the velocity peak and the velocity inflection point as indicators for sample failure in chapter 6.

3.8. Experiments

The experiments followed the workflow that was developed during the preliminary testing.

Figure 3.10: Flowchart representing the workflow for the experiments with corresponding chapters in brackets. From preparing samples (3.2.1) to setting up the Syrosonic and Z600 (3.4) to performing the test (3.5) to collecting the data (3.5) to analyzing and interpreting the data using the written python scripts (3.7).

Over the course of the experiments we tested 12 conduro samples with a diameter of 50 mm (can be seen in figure 3.5), 9 conduro samples with a diameter of 30 mm, 6 cordierite pearl gneiss samples with a 50 mm diameter (can be seen in figure 3.5), and 8 cordierite pearl gneiss samples with a diameter of 30 mm. The time that one non-cyclic test took, from positioning the sample and setting the correct window in the software, to the cleanup of the sample, was between 2 min and 8 min. Most tests took around 5 minutes.

Table 3.1: Material, names, and geometry factor of all samples that were tested during the main experiments.

Material	Names	geometry factor
Conduro Plaster	C1 - C12	1.928 - 1.999
Conduro Plaster	C 30er 1 - C 30er 9	1.926 - 2.055
Cordierite Pearl Gneiss	G1 - G6	1.621 - 2.007
Cordierite Pearl Gneiss	G 30er 1 - G 30er 6.2	1.244 - 2.136

The conduro plaster samples C 30er 2 to C 30er 7 were tested with a different preset for the Z600, while the processes for the Syrosonic stayed the same. We tested them under cyclic load to see how changing loads, would affect wave velocities. There were two different cyclic presets, one with 50 cycles and one with 100 cycles, both cycling between 25 % and 75 % of the compressive strength of the conduro plaster.

4

Measured Material Properties

4.1. Conduro Plaster

The Conduro Plaster is a fast-hardening plaster, meaning it becomes solid within a few hours after mixing. After solidifying, the plaster dries out further, increasing its compressive strength. How the compressive strength differs depending on the curing time does not matter for this study. Since not all samples were created on the same day, the plaster samples dried for different lengths of time, which led to different compressive strengths within the same mix of plaster.

4.1.1. 50 mm Diameter Samples

The 50 mm conduro samples have an average geometry factor of k = 1.959, with the lowest being 1.928 from C11 and the highest being 1.999 from C2. All the geometry factors are very close to the optimal k_{opt} = 2.0 and thus meet the standard of the DIN-18141-2:2014 [1]. The signal strength peaks of the P- and S-waves differ substantially, between 0.04 mV (sample C2 S-wave) and 20.38 (sample C12 S-wave), and are only listed to be able to be referred to later for possible explanations of outlier data or unreadable signals.

The P-wave velocity of the 50 mm conduro samples averaged 3398.05 m/s, with the highest coming from C12 with 3528.28 m/s and the lowest from C1 with 3253.15 m/s. The S-wave velocity averaged at 2011.39 m/s, with the highest coming from C1 with 2238.58 m/s and the lowest from C3 with 1865.50 m/s (see table 4.1). The average velocity ratio (VR = $\frac{v_p}{v_s}$) is 1.694, with the highest being C3 with 1.768 and the lowest coming from C1 with 1.453. All velocity ratios are in the expected range and don't give any reason to doubt the measured velocities.

The average compressive strength of all 50 mm conduro samples was 31.952 MPa, with the lowest being 23.233 MPa from C1 and the highest being 45.568 MPa from C12. This large difference can be explained by the fact that the plaster for samples C1 to C12 was all prepared on the same day, but the samples had curing times of different lengths. C1 to C3 had two days, C4 to C6 had five days, and C7 to C12 had six days to harden. This can be seen in the compressive strengths in table 4.1.

The figures showing the corresponding stress, P-wave and S-wave velocities can be found in the Appendix.

Table 4.1: Sample name and date of testing, geometry factor k, maximum signal strength (mV), maximum velocity (m/s), compressive strength (MPa) and velocity ratio of the Conduro plaster samples C1 to C12.

Sample a. date	k	Signalstr. (mV)		Velocity (m/s)		σ_u (MPa)	VR
		P-wave	S-wave	P-wave	S-wave		
C1 (03.02.23)	1.945	1.64	0.08	3253.15	2238.58	23.233	1.453
C2 (03.02.23)	1.999	0.29	0.04	3381.46	2224.92	24.544	1.52
C3 (03.02.23)	1.973	0.88	2.89	3298.51	1865.5	23.568	1.768
C4 (06.02.23)	1.989	8.3	3.65	3295.47	1912.73	25.158	1.723
C5 (06.02.23)	1.965	3.89	6.21	3328.86	1922.03	26.728	1.732
C6 (06.02.23)	1.973	8.49	8.04	3376.27	1947.21	29.009	1.734
C7 (07.02.23)	1.962	10.02	12.17	3444.64	2014.46	35.378	1.71
C8 (07.02.23)	1.938	14.58	14.3	3357.27	1970.36	29.662	1.704
C9 (07.02.23)	1.945	6.02	12.39	3501.79	1992.08	39.633	1.758
C10 (07.02.23)	1.931	8.04	9.53	3494.08	2022.85	40.346	1.727
C11 (07.02.23)	1.928	6.26	14.74	3516.79	2018.24	40.597	1.743
C12 (07.02.23)	1.964	15.36	20.38	3528.28	2007.69	45.568	1.757

The percentage of the compressive strength at which the velocities of the 50 mm conduro samples peaked (PPC) is 80.46 % for the P-wave, with the highest being 99.8 % from C10 and the lowest being 46.31 % from C2. The average PPC of the S-wave is 47.79 %, with the highest being 71.56 % from C4 and the lowest being 25.13 % from C2 (see table 4.2). The average PPC of the S-wave, as well as the individual S-wave PPCs, are lower than the P-wave PPCs. This phenomenon will be mentioned and discussed in chapter 6.1.

The time from the velocity peak to the stress peak (TPP) of the P-wave velocity was an average of 34.5 s, with the longest being 97.9 s from C2 and the shortest being -4.4 s from C8. The velocity peak of C8 occurred shortly before the stress peak and remained at its peak value until shortly after the stress peak (see figure C8 in the Appendix). The average S-wave velocity TPP of 92.1 s is longer than its P-wave counterpart. This also applies to each sample individually. The highest S-wave TPP is 130.6 s from C2, and the lowest is 43.1 s from C4 (see table 4.2).

Table 4.2: Sample name, percentage of compressive strength at which the velocity peak occurred (PPC), and the time from the velocity peak to the stress peak (TPP) in seconds of the Conduro plaster samples C1 to C12.

Sample	PPC (%)		TPP (s)	
	P-wave	S-wave	P-wave	S-wave
C1	54.97	46.52	81.6	93.7
C2	46.31	25.13	97.9	130.6
C3	71.95	51.24	54.5	86.7
C4	74.51	71.56	39.1	43.1
C5	62.09	37.249	63.1	100.1
C6	86.4	36.36	25.5	103.3
C7	99.31	45.16	-0.3	90.0
C8	97.93	61.55	-4.4	58.6
C9	83.0	47.28	35.6	100.1
C10	99.8	48.09	1.6	106.1
C11	92.07	42.25	20.0	114.0
C12	97.14	61.05	-0.4	79.0

The percentage of the compressive strength at which the last inflection points (IP), before the stress peak, in the velocities data occurred averaged 61.25 % for the P-wave and 89.14 % for the S-wave (table 4.3). The reason for the P-wave average being lower is that for 5 out of the 12 samples, namely C3, C7, C8, C10, and C12, the inflection point occurs before the velocity peak (see figures in 7). The average P-wave IP for the samples where the IP occurred after the velocity peak (see table 4.3) is 90.77 % and thus, slightly higher than the S-wave IP.

Table 4.3: Sample name, percentage of compressive strength at which an inflection point (IP) occurred, of the Conduro plaster samples C1 to C12. I chose the penultimate and last inflection points for this data set since those are the relevant ones. They usually occur before and after the velocity peak. The table also shows the time (in seconds) between an inflection point occurring and the peak stress (TIP).

Sample	P-wave IP (%)		S-wave IP (%)		P-wave TIP (s)		S-wave TIP (s)	
	penult.	last	penult.	last	penult.	last	penult.	last
C1	54.97	94.31	16.93	96.07	138.1	16.9	81.6	12.9
C2	17.91	86.50	5.39	88.69	142.9	32.2	171.6	28.1
C3	-	32.66	20.53	99.30	-	115.4	135.4	2.9
C4	27.13	86.23	39.80	88.97	99.9	23.0	83.7	18.9
C5	7.03	88.31	5.85	83.41	157.5	21.9	161.6	30.2
C6	16.42	91.50	4.51	86.40	140.3	17.2	177.2	25.4
C7	-	19.02	11.22	85.83	-	134.7	151.0	24.7
C8	-	21.74	15.44	86.52	-	119.9	132.1	21.9
C9	17.19	89.29	6.66	87.35	160.6	23.5	192.9	27.6
C10	-	13.62	6.47	85.89	-	177.3	202.4	35.1
C11	17.44	99.23	6.49	97.55	165.2	2.9	195.1	7.2
C12	-	12.57	2.80	83.64	-	184.2	224.7	34.6

The time from the inflection points to the stress peak (TIP) for the P-wave is an average of 72.4 s. The longest is 184.2 s from C12, and the shortest is 2.9 s from C11. The average S-wave TIP is 22.4 s, with the longest being 35.1 s from C10 and the shortest being 2.9 s from C3. Again, if samples C3, C7, C8, C10, and C12 are excluded, the average P-wave TIP is 19.7 s, with the longest being 32.2 s from C2 and the shortest being 2.9 s from C11.

4.1.2. 30 mm Diameter Samples

The 30 mm conduro samples have an average geometry factor of k = 2.002, with the lowest being 1.926 from C 30er 5 and the highest being 2.055 from C 30er 8 (table 4.4). All the geometry factors are very close to the optimal k_{opt} = 2.0 and thus meet the standard of the DIN-18141-1:2014 [1].

The signal strength peaks of the P- and S-waves are higher than the peaks of the 50 mm samples and differ substantially from each other. The weakest signal strength was 5.17 mV from C 30er 2, and the strongest was 109.51 mV from C 30er 5. They are only listed to be able to be referred to them later for possible explanations of outlier data or unreadable signals.

The P-wave velocity of the 30 mm conduro samples averaged 3581.36 m/s, with the highest coming from C 30er 4 with 3624.06 m/s and the lowest from C 30er 1 with 3533.68 m/s. The S-wave velocity averaged 2093.19 m/s, with the highest being C 30er 5 with 2129.43 m/s and the lowest from C 30er 2 with 1971.8 m/s. The average velocity ratio is 1.711, with the highest coming from C 30er 2 with 1.8 and the lowest being 1.679 from C 30er 5 (see table 4.4). All velocity ratios are in the expected range and don't give any reason to doubt the measured velocities.

The average compressive strength of all 30 mm conduro samples was 51.848 MPa, with the lowest being 36.194 MPa from C 30er 2 and the highest being 61.665 MPa from C 30er 9. The curing times of the 30 mm samples were all long enough as not to lead to strongly varying compressive strengths (table 4.4).

The figures showing the corresponding stress, P-wave and S-waves can be found in the Appendix.

Table 4.4: Sample name and date of testing, geometry factor k, maximum signal strength (mV), maximum velocity (m/s), compressive strength (MPa) and velocity ratio of the Conduro plaster samples C 30er 1 to C 30er 9.

Sample a. date	k	Signalstr. (mV)		Velocity (m/s)		σ_u (MPa)	VR
		P-wave	S-wave	P-wave	S-wave		
C 30er 1 (16.02.23)	2.041	7.29	11.02	3533.68	2039.2	43.445	1.733
C 30er 2 Z (17.02.23)	2.009	5.17	24.41	3549.01	1971.8	36.194	1.8
C 30er 3 Z (17.02.23)	2.021	14.88	84.07	3574.02	2116.42	58.495	1.689
C 30er 4 Z (17.02.23)	1.929	14.23	80.52	3624.06	2122.31	50.618	1.708
C 30er 5 Z (20.02.23)	1.926	8.76	109.51	3575.85	2129.43	55.958	1.679
C 30er 6 Z (20.02.23)	2.012	20.24	39.34	3564.27	2107.74	48.641	1.691
C 30er 7 Z (20.02.23)	2.023	11.35	74.58	3601.42	2117.16	53.095	1.701
C 30er 8 (21.02.23)	2.055	6.84	107.67	3602.68	2109.33	58.524	1.708
C 30er 9 (21.02.23)	2.006	17.26	57.54	3607.27	2125.35	61.665	1.697

The percentage of the compressive strength at which the velocities of the 30 mm conduro samples peaked (PPC) is 90.1 % for the P-wave, with the highest being 99.73 % from C 30er 5 and the lowest being 27.61 % from C 30er 2. The average PPC of the S-wave is 84.55 %, with the highest being 99.46 % from C 30er 2 and the lowest being 70.0 % from C 30er 3 (see table 4.5). The average PPC of the S-wave, as well as the individual S-wave PPCs, are lower than the P-wave PPCs. Except for C 30er 2, where the P-wave velocity looks like it is shifted around 50 s backwards. This phenomenon will be mentioned and discussed in chapter 6.1.

The time from the velocity peak to the stress peak (TPP) of the P-wave velocity is 5.76 s on average, with the longest being 56.5 s from C 30er 2 and the shortest being -2.0 s from C 30er 7. The average S-wave velocity TPP of 19.49 s is longer than its P-wave counterpart. This also applies to each sample individually, except to C 30er 2, where the P-wave velocity peak occurs 56.5 s before the stress peak and the S-wave velocity peaks right around the stress peak. The highest S-wave TPP is 38.7 s from C 30er 3, and the lowest is -0.3 s from C 30er 2 (see table 4.5).

Table 4.5: Sample name, percentage of compressive strength at which the velocity peak occurred (PPC), and the time from the velocity peak to the stress peak (TPP) in seconds of the Conduro plaster samples C 30er 1 to C 30er 9.

Sample	PPC (%)		TPP (s)	
	P-wave	S-wave	P-wave	S-wave
C 30er 1	99.27	94.15	1.0	9.2
C 30er 2 Z	27.61	99.46	56.5	-0.3
C 30er 3 Z	99.38	70.01	-0.3	38.7
C 30er 4 Z	97.80	75.41	-0.8	27.3
C 30er 5 Z	99.73	86.73	-0.3	16.7
C 30er 6 Z	99.73	78.75	0.5	25.0
C 30er 7 Z	98.74	82.19	-2.0	22.6
C 30er 8	94.44	83.45	-1.8	22.5
C 30er 9	94.22	90.8	-1.0	13.7

The percentage of the compressive strength at which the last inflection points (IP), before

the stress peak, in the velocities data from the 30 mm conduro samples occurred averaged 46.34 % for the P-wave and 79.65 % for the S-wave (see table 4.6). Due to the inflection points in the velocity data of all nine 30er Conduro samples, occurring before the velocity peak, the average P-wave IP is lower than the S-wave IP (see figures in the Appendix). Whereas for the S-wave IP, only C 30er 1 and C 30er 2 had inflection points before the velocity peak, leading to a higher IP and shorter TIPs.

The time from the inflection points to the stress peak (TIP) for the P-wave is an average of 71.4 s. The longest is 163.9 s from sample C 30er 1, and the shortest is 10.5 s from sample C 30er 3. The average S-wave TIP is 25.6 s, with the longest being 136.1 s from sample C 30er 1, and the shortest being 2.4 s from sample C 30er 8. To visualize the outlier data from C 30er 1, if the sample is excluded for the S-wave average, the new average TIP would be 11.8 s long.

Table 4.6: Sample name, percentage of compressive strength at which an inflection point (IP) occurred, of the Conduro plaster samples C 30er 1 to C 30er 9. For this data set, I chose the penultimate and last inflection points, since those are the relevant ones. The cyclic measured samples are C 30er 2 Z to C 30er 7 Z. The table also shows the time (in seconds) between an inflection point occurring and the peak stress (TIP).

Sample	P-wave IP (%)		S-wave IP (%)		P-wave TIP (s)		S-wave TIP (s)	
C 30er 1	-	1.76	-	6.56	-	163.9	-	136.1
C 30er 2 Z	49.04	86.75	42.55	49.04	40.1	12.3	80.7	40.5
C 30er 3 Z	89.59	92.66	37.17	95.62	14.5	10.5	74.8	6.5
C 30er 4 Z	34.4	44.45	35.58	90.46	99.9	55.6	63.6	11.3
C 30er 5 Z	35.65	41.44	33.60	96.50	105.4	65.1	73.2	4.7
C 30er 6 Z	82.8	87.08	37.95	90.99	21.0	16.8	62.1	12.7
C 30er 7 Z	20.14	38.36	42.46	98.60	95.2	67.0	63.0	2.6
C 30er 8	-	13.48	7.38	98.30	-	119.5	135.6	2.4
C 30er 9	-	11.09	0.97	90.80	-	132.4	207.5	13.8

4.2. Cordierite Pearl Gneiss

The gneiss samples with a diameter of 50 mm were too sturdy for the 100 kN pressure plate, not failing even under maximum load, except G4. Because of this, the listed compressive strength is simply the maximum load of 99,995 N divided by the support surface area of the sample.

The Syrosonic device [16] takes measurements every 4 s, which causes a delay in the registration of some velocity peaks. This led to small, negative TPPs for the G1 to G6 samples. The bigger, negative TPPs of the 30 mm gneiss partly happened because the sample was still fixed under the hydraulic press, even after the press stopped the test. Through this, some samples remained at their peak velocity until the measuring of the Syrosonic device [16] was manually stopped. For the position of the PPC, I always determined the last peak, or the last data point of the peak, leading to some negative TPPs.

4.2.1. 50 mm Diameter Samples

The 50 mm gneiss samples have an average geometry factor of k = 1.879, with the lowest being 1.621 from G3 and the highest being 1.954 from G5 (see table 4.7). All the geometry factors are very close to the optimal k_{opt} = 2.0, or at least between 1.5 and 2.5, and thus meet the standard of the DIN-18141-1:2014 [1].

The signal strength peaks of the P- and S-waves are lower than the Conduro samples. The weakest signal strength was 1.29 mV from G1 and the strongest was 6.56 mV from G3. They are only listed to be able to be referred to them later for possible explanations of outlier data or unreadable signals.

The P-wave velocity of the 50 mm gneiss samples averaged 5899.26 m/s, with the highest coming from G2 at 6144.76 m/s and the lowest being 5699.93 m/s from G3. The S-wave velocity averaged at 3355.8 m/s, with the highest coming from G4 with 3517.39 m/s and the lowest from G1 with 3051.71 m/s (see table 4.7). The average velocity ratio is 1.763, with the highest coming from G1 with 1.929 and the lowest being 1.648 from G3 (see table 4.7). All velocity ratios are in the expected range and don't give any reason to doubt the measured velocities.

The average compressive strength of all 50 mm gneiss samples was 46.404 MPa, with the lowest being 32.214 MPa from G4 and the highest being 50.282 MPa from G6. Only sample G4 broke during the test, which explains the low compressive strength. All other 50 mm gneiss samples could not be stressed until failure, which resulted in their compressive strength simply being the maximum load of 99,995 N divided by their support surface area (around 2,000 mm^2).

The figures showing the corresponding stress, P-wave and S-waves can be found in the Appendix.

Table 4.7: Sample name and date of testing, geometry factor k, maximum signal strength (mV), maximum velocity (m/s), compressive strength (MPa) and velocity ratio of the gneiss samples G1 to G6.

Sample a. date	k	Signalstr. (mV)		Velocity (m/s)		σ_u (MPa)	VR
		P-wave	S-wave	P-wave	S-wave		
G1 (06.02.23)	1.928	1.29	2.67	5887.54	3051.71	48.936	1.929
G2 (09.02.23)	1.916	1.74	4.13	6144.76	3209.95	48.93	1.914
G3 (08.02.23)	1.621	3.55	6.56	5699.93	3458.09	49.129	1.648
G4 (08.02.23)	1.922	2.92	2.52	5827.13	3517.39	32.214	1.657
G5 (08.02.23)	1.954	3.17	4.89	5843.69	3435.43	48.934	1.701
G6 (09.02.23)	1.931	2.0	4.79	5992.52	3462.2	50.282	1.731

The percentage of the compressive strength at which the velocities of the 50 mm gneiss samples peaked (PPC) is 99.17 % for the P-wave, with all samples except G4 reaching their peak velocity at 100 % of the hydraulic press limit of 99,995 N. The P-wave velocity of G4 peaked at 95.1 % of its compressive strength. The average PPC of the S-wave is 89.09 %, with G3, G5, and G6 reaching their peak velocity at the load limit. G4 reached its S-wave velocity

peak at 46.8 % (see table 4.8).

The average time from the velocity peak to the stress peak (TPP) of the P-wave velocity is 1.85 s, with only G4 having a positive TPP of 12.3 s. The average S-wave velocity TPP of 19.18 s is longer than its P-wave counterpart because G1, G2, and G4 show positive TPP. The highest S-wave TPP is 96.9 s from G4 (see table 4.8).

The 50 mm gneiss samples will not play a big role when discussing velocity peaks as an indicator for sample failure, since only one sample broke.

Table 4.8: Sample name, percentage of compressive strength at which the velocity peak occurred (PPC), and the time that passed from the velocity peak to the stress peak (TPP) in seconds, of the gneiss samples G1 to G6.

Sample	PPC (%)		TPP (s)	
	P-wave	S-wave	P-wave	S-wave
G1	100.0	94.6	-0.2	7.3
G2	100.0	93.2	-0.2	11.7
G3	100.0	100.0	-0.3	-0.3
G4	95.1	46.8	12.3	96.9
G5	100.0	100.0	-0.2	-0.2
G6	100.0	100.0	-0.3	-0.3

The percentage of the compressive strength at which the last inflection points (IP), before the stress peak, in the velocities data from the 50 mm gneiss samples occurred averaged 46.03 % for the P-wave and 53.0 % for the S-wave. With the highest P-wave IP being 78.68 % from G3 and the lowest IP being 24.46 % from G6. The highest S-wave IP is 93 % from G2 and the lowest IP being 25.59 % from G1 (see table 4.9).

The average time from the inflection points to the stress peak (TIP) for the P-wave is 72.2 s, with the longest being 108.5 s from G6 and the shortest being 27.6 s from G2. The average S-wave TIP is 74.5 s, with the longest being 117.3 s from G1 and the shortest being 11.6 s from G2.

Table 4.9: Sample name, percentage of compressive strength at which an inflection point (IP) occurred, of the gneiss samples G1 to G6. For this data set, I chose the penultimate and last inflection points, since those are the relevant ones. The table also shows the time (in seconds) between an inflection point occurring and the peak stress (TIP).

Sample	P-wave IP (%)		S-wave IP (%)		P-wave TIP (s)		S-wave TIP (s)	
G1	-	44.69	-	25.59	-	80.6	-	117.3
G2	-	37.83	-	93.24	-	27.6	-	11.6
G3	53.74	78.68	-	45.86	79.9	31.9	-	93.5
G4	-	50.70	73.25	89.05	-	88.9	48.5	20.3
G5	10.42	39.83	-	37.85	184.5	95.8	-	99.8
G6	-	24.46	2.49	26.64	-	108.5	171.6	104.6

4.2.2. 30 mm Diameter Samples

The 30 mm gneiss samples have an average geometry factor of k = 1.891, with the lowest being 1.244 from G 30er 6.2 and the highest being 2.136 from G 30er 4. All the geometry factors are very close to the optimal k_{opt} = 2.0, except G 30er 6.2, and meet the standard of DIN:18141.1:2014 [1]. How to interpret the data collected from sample G 30er 6.2 will be discussed in chapter 5.

The signal strength peaks of the P- and S-waves are lower than the conduro samples but higher than the 50 mm gneiss samples. The weakest signal strength was 1.57 mV from G 30er 1 and the strongest was 62.33 mV from G 30er 6.2. They are only listed to be able to be referred to them later for possible explanations of outlier data or unreadable signals.

The P-wave velocity of the 30 mm gneiss samples averaged 6031.09 m/s, with the highest coming from G 30er 2 with 6235.42 m/s and the lowest being 5899.07 m/s from G 30er 1.2. The S-wave velocity averaged at 3490.03 m/s, with the highest coming from G 30er 6.2 with 3653.48 m/s and the lowest from G 30er 1.2 with 3166.39 m/s. The average velocity ratio is 1.731, with the highest coming from G 30er 1.2 with 1.863 and the lowest being 1.666 from G 30er 6 (see table 4.10). All velocity ratios are in the expected range and don't give any reason to doubt the measured velocities.

The average compressive strength of all 30 mm gneiss samples was 130.808 MPa, with the lowest being 115.643 MPa from G 30er 1.2 and the highest being 135.042 MPa from G 30er 6.2. Only sample G 30er 1 and G 30er 1.2 broke during the test, which explains the lower compressive strengths (see table 4.10). All other 30 mm gneiss samples could not be stressed until failure, which resulted in their compressive strength simply being the maximum load of 99,995 N divided by their support surface area (around 725 mm^2).

The figures showing the corresponding stress, P-wave and S-wave can be found in Appendix.

Table 4.10: Sample name and date of testing, geometry factor k, maximum signal strength (mV), maximum velocity (m/s), compressive strength (MPa) and velocity ratio of the gneiss samples G 30er 1 to G 30er 6.2.

Sample a. date	k	Signalstr. (mV)		Velocity (m/s)		σ_u (MPa)	VR
		P-wave	S-wave	P-wave	S-wave		
G 30er 1 (16.02.23)	1.97	1.57	5.46	6073.02	3574.92	120.828	1.699
G 30er 1.2 (17.02.23)	1.885	3.37	4.15	5899.07	3166.39	115.643	1.863
G 30er 2 (17.02.23)	1.934	4.09	4.02	6235.42	3576.64	135.03	1.743
G 30er 3 (17.02.23)	1.981	8.28	26.57	6029.03	3402.82	135.038	1.772
G 30er 4 (20.02.23)	2.136	11.03	12.73	6023.19	3585.31	135.038	1.68
G 30er 5 (20.02.23)	1.967	20.62	18.75	5920.79	3393.87	134.816	1.745
G 30er 6 (21.02.23)	2.008	12.09	10.05	5943.58	3566.84	135.031	1.666
G 30er 6.2 (21.02.23)	1.244	15.68	62.33	6124.6	3653.48	135.042	1.676

The percentage of the compressive strength at which the velocities of the 30 mm gneiss peaked (PPC) is 98.125 % for the P-wave, with all samples except G 30er 1 and G 30er 1.2

reaching their peak velocity at 100 % of the hydraulic press limit of 99,995 N. The P-wave velocity of G 30er 1 peaked at 92.68 %, and G 30er 1.2 peaked at 92.34 %. This can be misleading because both samples broke, and both times the P-wave velocity reached its peak after the stress peak, during the nonlinear plastic section (see chapter 2.5.3). This leads to negative TPP for all G 30er samples. The average PPC of the S-wave is 89.37 %, with G 30er 2, G 30er 5, and G 30er 6.2 reaching their peak velocity at the load limit. The velocity peak for these three samples remained after the hydraulic press reached its maximum load, leading to negative TPP (see table 4.11 and figures in the Appendix).

The average time from the velocity peak to the stress peak (TPP) of the P-wave velocity is -19.29 s. The average S-wave velocity TPP of 6.1 s is longer than its P-wave counterpart because G 30er 1, G 30er 3, G 30er 4, and G 30er 6 show positive TPP. The highest S-wave TPP is 90.8 s from G 30er 1 (see table 4.11).

Table 4.11: Sample name, percentage of compressive strength at which the velocity peak occurred (PPC), and the time that passed from the velocity peak to the stress peak (TPP) in seconds, of the gneiss samples G 30er 1 to G 30er 6.2.

Sample	PPC (%)		TPP (s)	
	P-wave	S-wave	P-wave	S-wave
G 30er 1	92.68	45.77	-3.8	90.9
G 30er 1.2	92.34	92.34	-44.7	-44.7
G 30er 2	100.0	100.0	-17.5	-13.5
G 30er 3	100.0	92.22	-7.0	12.7
G 30er 4	100.0	93.66	-29.3	10.3
G 30er 5	100.0	100.0	-21.3	-17.3
G 30er 6	100.0	90.98	-18.1	15.5
G 30er 6.2	100.0	100.0	-12.6	-4.7

The percentage of the compressive strength at which the last inflection points (IP), before the stress peak, in the velocities data from the 30 mm gneiss samples occurred averaged 21.82 % for the P-wave and 40.8 % for the S-wave. Due to the inflection points of all eight samples occurring before the velocity peak, the average P-wave IP is lower (see figures in the Appendix). Whereas for the S-wave IP, only G 30er 1 and G 30er 6 had inflection points before the velocity peak.

The time from the inflection points to the stress peak (TIP) for the P-wave averaged 130.2 s, the longest being 154.0 s from sample G 30er 1 and the shortest being 102.3 s from G 30er 1.2. The average S-wave TIP is 98.19 s, with the longest being 142.2 s from G 30er 6.2 and the shortest being 2.9 s from G 30er 6.

Table 4.12: Sample name, percentage of compressive strength at which an inflection point (IP) occurred, of the gneiss samples G 30er 1 to G 30er 6.2. For this data set, I chose the penultimate and last inflection points, since those are the relevant ones. The table also shows the time (in seconds) between an inflection point occurring and the peak stress (TIP).

Sample	P-wave IP (%)		S-wave IP (%)		P-wave TIP (s)		S-wave TIP (s)	
G 30er 1	-	10.95	7.83	81.14	-	154.0	161.9	35.6
G 30er 1.2	-	35.40	-	35.40	-	102.3	-	102.3
G 30er 2	-	21.76	-	26.04	-	132.8	-	124.9
G 30er 3	-	16.22	-	18.21	-	139.0	-	135.1
G 30er 4	-	27.39	-	27.39	-	117.0	-	117.0
G 30er 5	-	23.60	-	23.60	-	125.6	-	125.6
G 30er 6	-	22.99	22.99	98.38	-	129.0	129.0	2.9
G 30er 6.2	-	16.23	-	16.23	-	142.2	-	142.2

5

Discussion of Errors

5.1. Physical Changes

The hydraulic press only applies vertical force, and the lateral surface of the samples stays unpressured. During the tests, this leads to the height of the samples decreasing and their diameter increasing. I used the starting geometry of the samples to calculate the velocities (v_s and v_p), as well as the compressive strength σ_u. Because the sample height is dynamic during the tests, calculating velocities with the starting heights leads to slight errors. The velocities calculated with the starting geometry will be referred to as static wave velocities, and the ones calculated using the changing sample height will be referred to as dynamic wave velocities.

With the compression data collected by the Z600 software, the shortening of the samples during the experiment is known. Calculating the P- and S-wave velocity with the dynamic length of a sample leads to a slower velocity and slightly different curve behaviour relative to the statically calculated P-wave velocity. This can be seen in the Conduro examples C1 and C 30er 9 in figures 5.1 and 5.2.

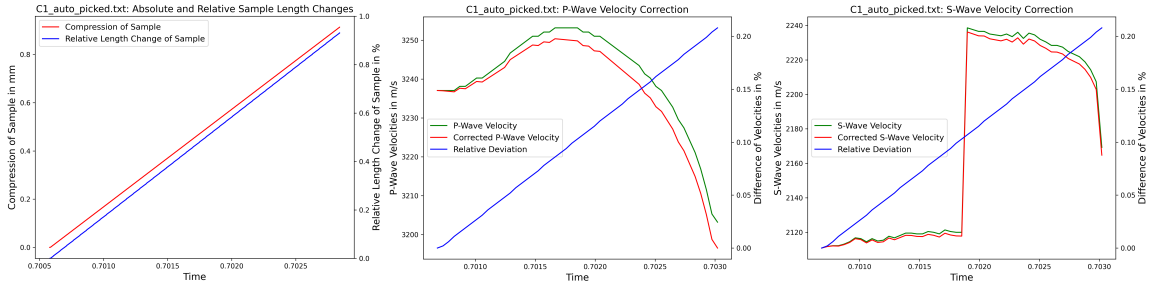

Figure 5.1: (left) The figure shows the absolute and relative compression of the C1 sample during the experiment. The absolute compression of the sample (red), before failure, reaches 0.913 mm. With an initial sample length of 98.05 mm, the relative compression (blue) ends up at 0.931 %. **(middle/right)** The P-/S-wave velocity (green) is plotted together with the corrected P-/S-wave velocity (red), which is calculated using the dynamic sample length. The (blue) line shows the deviation between the two velocities relative to the statically derived P-wave velocity (green). The deviation of both P- and S-wave shows a linear growth, reaching its peak of 0.208 % right before sample failure.

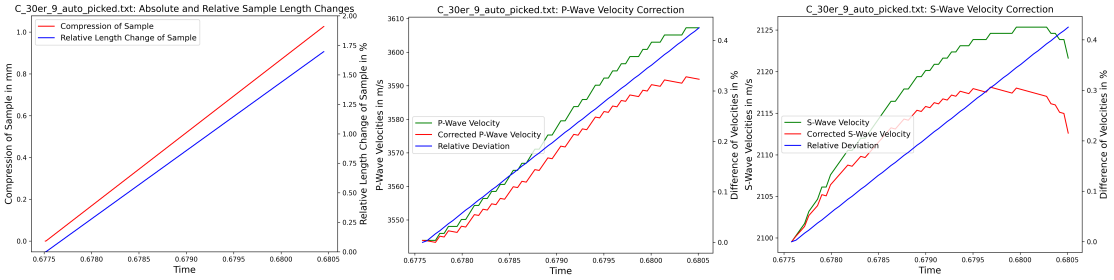

Figure 5.2: (left) The figure shows the absolute and relative compression of the C 30er 9 sample during the experiment. The absolute compression of the sample (red), before failure, reaches 1.03 mm. With an initial sample length of 60.53 mm, the relative compression (blue) ends up at 1.7 %. **(middle/right)** The P-/S-wave velocity (green) is plotted together with the corrected P-/S-wave velocity (red), which is calculated using the dynamic sample length. The blue line shows the deviation of each velocity relative to the statically derived P-wave velocity (green). For the P- and S-wave the deviation experiences a linear growth, reaching its peak of 0.425 % right before sample failure.

Similar behaviour can be seen with examples G1 and G 30er 2 in figures 5.3 and 5.4.

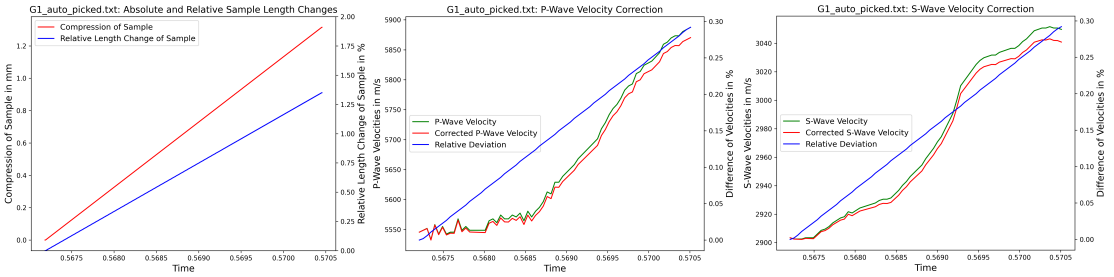

Figure 5.3: (left) The figure shows the absolute and relative compression of the G1 sample during the experiment. The absolute compression of the sample (red), before failure, reaches 1.315 mm. With an initial sample length of 97.38 mm, the relative compression (blue) ends up at 1.35 %. **(middle/right)** The P-/S-wave velocity (green) is plotted together with the corrected P-/S-wave velocity (red), which was calculated by using the dynamic sample length. The blue line shows the deviation of each velocity relative to the statically derived wave velocity. For P- and S-wave the deviation shows a linear growth, reaching its peak of 0.292 % right before sample failure.

Figure 5.4: (left) The figure shows the absolute and relative compression of the G 30er 2 sample during the experiment. The absolute compression of the sample (red), before failure, reaches 0.982 mm. With an initial sample length of 58.8 mm, the relative compression (blue) ends up at 1.67 %. **(middle/right)** The P-/S-wave velocity (green) is plotted together with the corrected P-/S-wave velocity (red) for which the dynamic sample length was used. The blue line shows the deviation of each velocity relative to the statically derived wave velocity. For P- and S-wave the deviation shows a linear growth, reaching its peak of 0.442 % right before sample failure.

These deviations don't impact the values of interest, such as peak position and inflection point position. This can be seen in figure 5.5. The two graphs in the upper row show the calculated inflection points, before (left) and after correction (right), of the C1 sample. The two graphs on the lower row show the calculated inflection point, before (left) and after correction (right), of the G 30er 2 sample. For sample C1, both inflection points stay the same at 16.934 % and 94.305 %, when calculated using the corrected P-wave velocity (see figure 5.5 a) and b)). For sample G 30er 2 the inflection point stays the same at 21.755 % of the maximum stress.

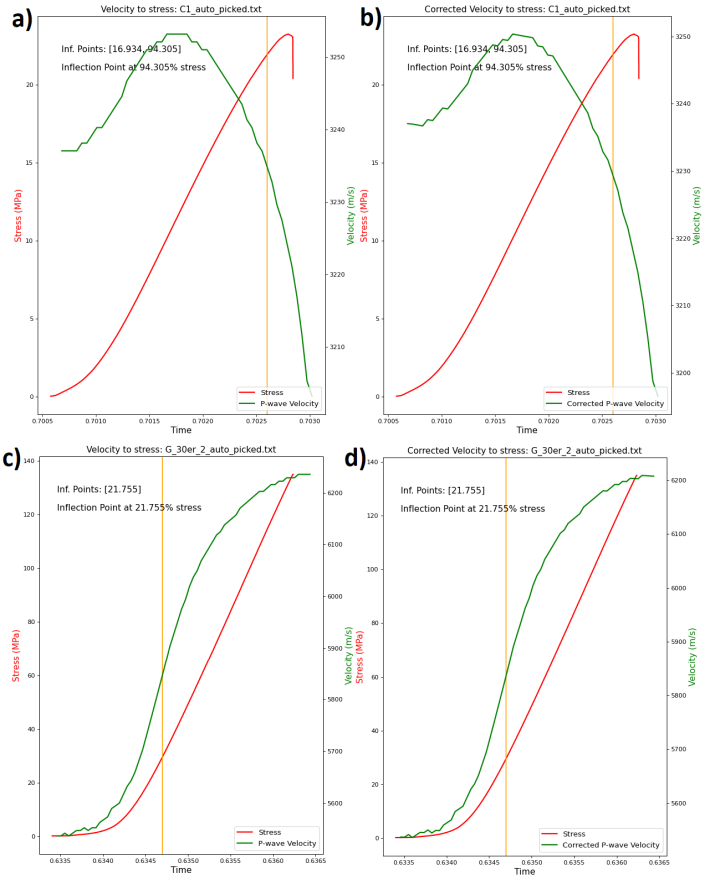

Figure 5.5: a) and b) These two graphs show the stress (red) in MPa and P-wave velocity (green) in m/s over time for the C1 sample, together with the last inflection points of the velocity curves (orange). Both figures indicate the percentage of compressive stress at which the velocity curves have inflection points. a) depicts the static P-wave velocity and b) depicts the corrected, dynamically calculated P-wave velocity. Both velocities show identical inflection points. **c) and d)** These two graphs show the stress (red) in MPa and P-wave velocity (green) in m/s over time for the G 30er 2 sample, together with the last inflection point of the velocity curves (orange). Both figures indicate the percentage of compressive stress at which the velocity curves have inflection points. c) depicts the static P-wave velocity and d) depicts the corrected, dynamically calculated P-wave velocity. Both velocities show identical inflection points.

With these findings, the impact sample shortening has on the velocity and on other values of interest has been deemed negligible and will thus not play a role in the following discussions.

5.2. Outlier and Meaningful Data

During measuring, the sample sometimes moves or shifts slightly to adjust to the increasing stress. Although these moves and shifts are minuscule, in the milli- or sometimes micrometer range, they impact the signal that the Syrosonic [16] detects. Because we measure minute changes in transit times, even small shifts in how the signal travels through the sample, affect the data noticeably. These impacts are visible during data analysis and impact values of interest, such as peak velocity and inflection points.
Sample C1 to give an example, moved during the middle of measuring, leading to a different peak in the signal becoming the dominant one. The signal form stays intact, leading to a static 2.45 s shift (see figure 5.6). This shift is noticeable in the data and changes key values, like velocity peak and inflection points. It can be corrected at the cost of the authenticity of the data.

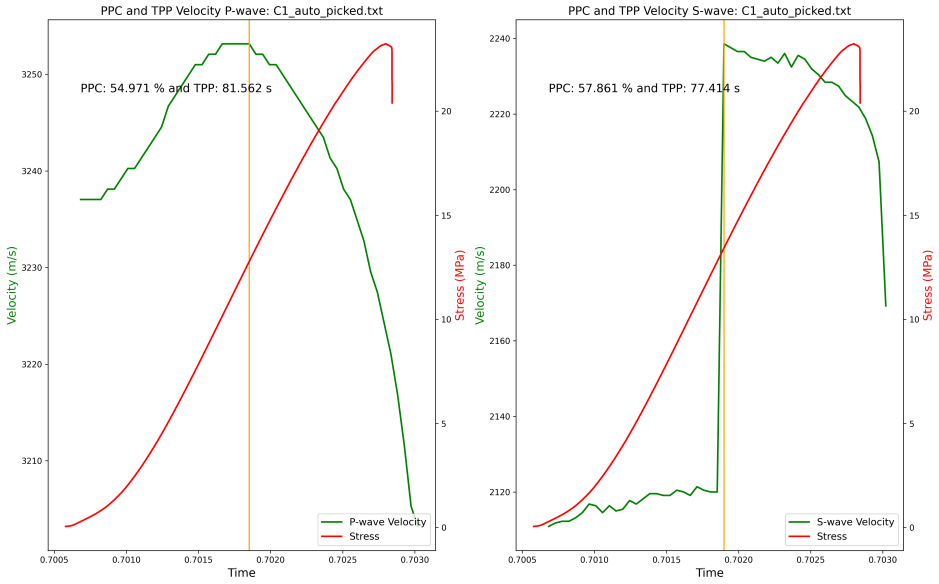

Figure 5.6: These two graphs show the raw C1 data, displaying P-wave velocity and stress over time (left) and S-wave velocity and stress over time (right). As one can see in the middle of measuring the velocity of the S-wave increases immensely and stays around its new peak, before slowly decreasing. The second half of the measuring shows an expected behaviour, slowly decreasing as the sample stability decreases and dropping towards the sample failure.

As one can see in figure 5.6, the dominant peak changed 117 seconds after the test started. This led to the transit times seemingly becoming shorter, making the S-wave speed faster, and creating the visible spike. After a manual correction, the graph looks like 5.7.

The jumps in transit time are affected by a systemic error because even when the `auto_picker.py` code picks a different peak in the signal, the new dominant peak shifts forward and backward, the same as any other peak in the signal. The spikes and jumps that this peak switch causes in the analysis are most often fixed by a simple addition or subtraction of a constant time value between 0.1 and 4 seconds.

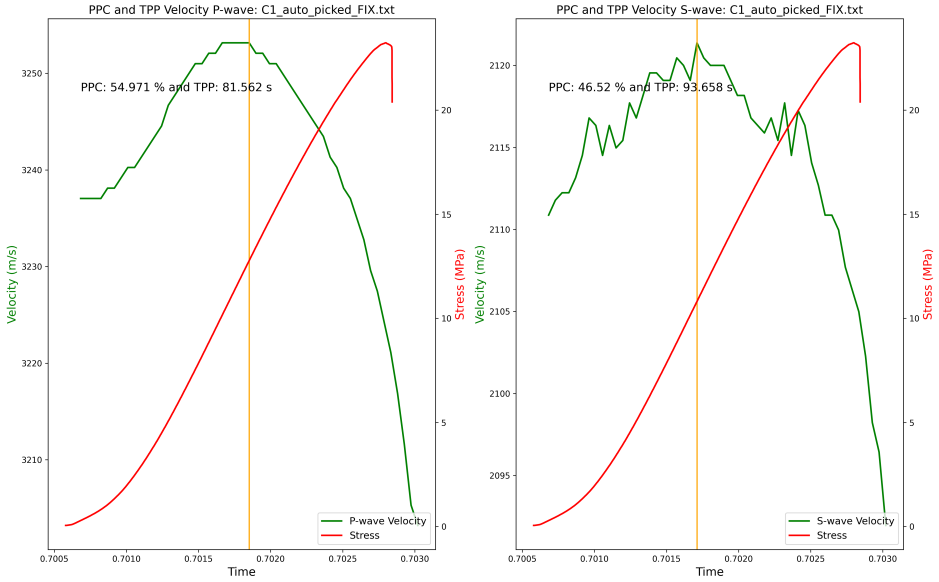

Figure 5.7: Corrected version of the C1 data displaying P-wave velocity and stress over time (left) and S-wave velocity and stress over time (right). The transit times for the S-wave in the first half of measuring shifted down, so the calculated velocity increased.

If the dominant peak switches too often the manual correction can become very elaborate and could lose scientific credibility. An example of this is sample G 30er 1, which can be seen in figure 5.8 with its original version, including multiple spikes and jumps, on the left and the corrected version on the right.

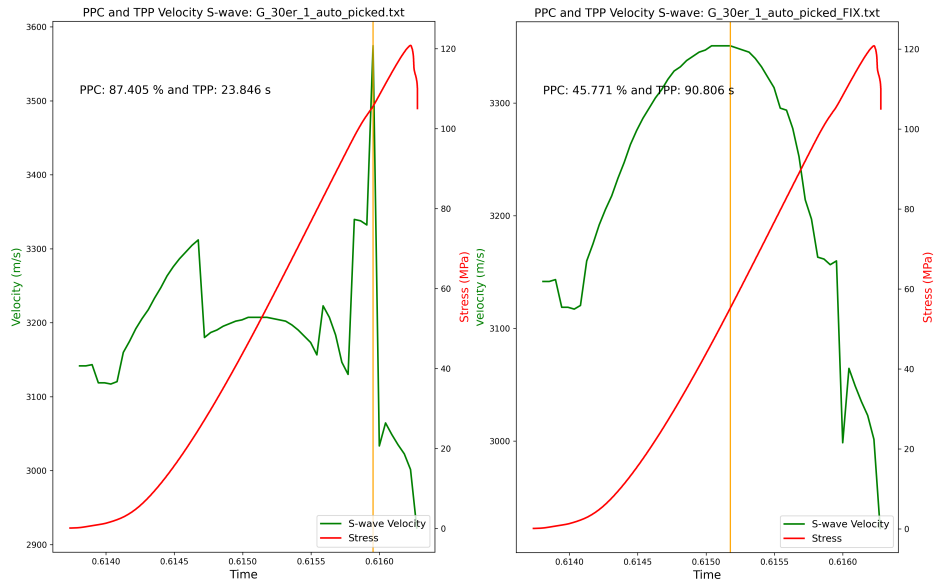

Figure 5.8: Original version of the G 30er 1 data displaying S-wave velocity and stress over time (left) and manually corrected version (right).

Because the mechanisms responsible for lower readability or outlier data are known, such

as problems with finding consistent peaks or the inability to load the sample until failure, we can classify sample data as unusable without losing scientific credibility. This means that data with low readability will be excluded while determining the indicator for sample failure but will be used and referred to while discussing the practical application of the experimental setup and workflow.

5.3. Fault Tree Analysis

Concluding the discussion of errors, I will use the Fault Tree Analysis to give an overview of the causes of the formerly discussed errors and problems.

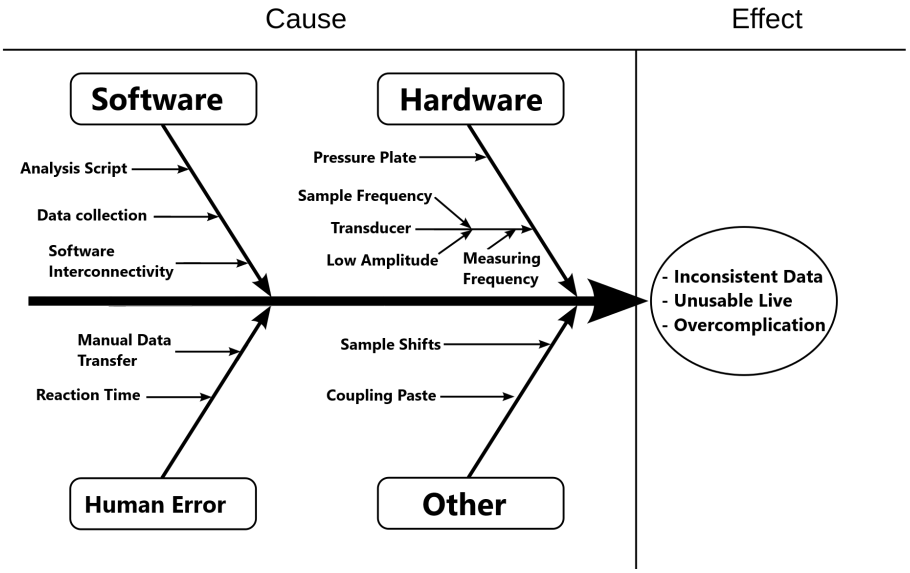

Figure 5.9: Fault tree analysis for the experiments and data analysis. One of the main sources of problems was **Software**, including peak inconsistencies during the arrival times picking, manual corrections and the inability to perform those during the tests. Another problem source was **Hardware**, with problems concerning the transducers such as a high sampling frequency, low signal amplitude and low measuring frequency. **Human Error**, refers to reaction time when starting or stopping tests, and manual inputs or data transfers as sources of error. **Other** causes included sample shifts and the coupling paste. All these problems lead to inconsistent data, an inability to use the analysis live during testing and over-complication.

5.3.1. Software Causes

I wrote the Python script for the semi-automatic picking of arrival times myself (see chapter 3.7). To simplify and accelerate the process, I chose to pick the first dominant peak in the signal as the arrival time. This led to small systemic errors for all velocity values, which was acceptable because the relative changes of velocities are of interest and not the absolute velocities themselves. The simplicity of the picking script caused it to be easily disrupted by shifting signal forms, which would happen when the sample shifted or adjusted itself under the hydraulic press, as discussed in chapter 5.2. The unreliability of the picks prompts manual corrections, which creates an additional workload and introduces new potential sources of error.

As already mentioned in chapter 3.7, the script for the inflection points creates the second derivative, whose zero points are used to determine the inflection point position, based on data that was smoothed using a Gaussian filter. An original data set from a 5-minute long compressive strength test has circa 60 to 70 data points, with the associated smoothed data set and the second derivative having the same amount. With these few data points the second derivative rarely has a data point with the value of 0. Since the zero points of the second derivative indicate the positions of the inflection points, another method was chosen where the script identifies sign switches of the second derivative from one data point to the next, which indicates a zero point between the two data points between which the sign changed. The script then chooses one of the data points as the position of the infection point, creating a small error for the position. This error is between 0 s to 2 s and has no impact on the meaningfulness of the results.

The operational disconnect between the computer running the GL Testsystems Syrosonic software and the computer operating the Z600 hydraulic press and the manner in which the TestXpert exports and saves data made it impossible to perform the manual corrections live during the tests. This would be essential if the premise of this paper, a system to predict sample failure during the experiment itself, were to be put into action. A more sophisticated picking software or script could greatly improve the accuracy and eliminate error sources attached to my picking script for peak and inflection point positions. If the data from the Syrosonic and the Z600 were to be collected and exported together during the experiment, live sample failure predictions would be possible.

5.3.2. Hardware Causes

The GL Testsystem transducers [3] have a sampling frequency of 500 kHz, which was too high for materials with corn sizes over 1 mm, as discussed in chapter 3.6. Also, the shortest measuring interval under which the transducers worked consistently was 4 seconds. When the 3-second interval is chosen in the Syrosonic software, measurement intervals are inconsistent, laying between 3 and 4 seconds. This is a long time relative to the 10 μs measuring intervals of the Z600 and can create situations in which it seems like the velocity reacts to the sample break with a delay of multiple seconds. This can be seen in figure 5.10, with sample C 30er 8 as an example.

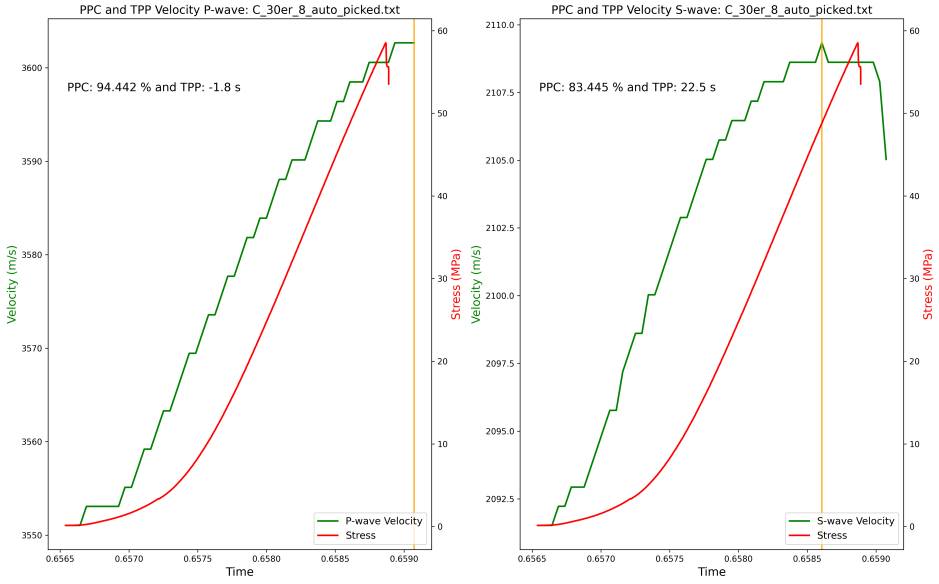

Figure 5.10: The two graphs show the velocity (green) and stress (red) during the test, together with the respective PPC and TPP of the P-wave (left) and S-wave (right) of sample C 30er 8.

The hydraulic press equipped with the 100 kN pressure plate could not produce enough force to break most of the gneiss samples. However, the 600 kN plate, which would be able to apply sufficient force, is connected to the hydraulic press in a way that makes it complicated to create an adapter for the transducers to fit into.

Stronger, more adjustable transducers, with a broader range in both sampling frequency and measuring frequency, would increase the number of potential sample materials and thus make the whole experimental setup more viable.

5.3.3. Human Error

The experimental setup relies on a person starting and stopping the Syrosonic measuring manually after the Z600 test begins and ends. This leads to the velocity data missing the first few seconds of the Z600 test and collecting a few seconds after the Z600 finished its test. Another possible source of error is wrong inputs for the TestXpert software or setting a wrong measuring time window for the Syrosonic software. The current workflow does require too many manual inputs and manual data transfers, each of which is an error source.

The short time periods of unmatched data, created by the start and stop delay, are not a big problem but are easily fixed through a software approach that unifies the two separate processes of the Z600 testing and the Syrosonic measuring. A small library of presets for the TestXpert and Syrosonic software could help minimise the manual input, thus decreasing the error potential.

5.3.4. Other Causes

One of the earliest problems was finding a fitting coupling paste which would support seismic coupling between the transducers and the sample, for both P- and S-wave equally. After multiple tests we decided on the "Echo Shear Wave" couple paste from Echo ultrasonics, since it produced the clearest and most stable signals.

The problem of the sample shifts that lead to different signal forms, which in turn, leads to different dominant peaks, is not easily solved. One possible workaround could be the aforementioned sophisticated picking system, which would pick accurately, unaffected by changing signal forms.

6

Indicator for Sample Failure

It is the goal of this study to find a dependable indicator for impending sample failure during testing. Preferably one that is detectable early enough to stop the experiment and late enough to collect enough data. Enough data means that the stress-strain curve of the uniaxial compressive strength test depicts all or most of the linear section. The more the linear elastic deformation phase is measured, the more accurate the calculated material properties of the sample are (see chapter 2.5.3). The samples would be driven to failure after the sensors are dismantled. Since uniaxial compressive data from one uninterrupted test is valuable, the goal becomes to collect as much data as possible before the test is stopped.

Since determining the ideal stopping point on the stress-strain curve exceeds the scope of this study, I chose a time window based on experiences made during the experiments. 10 s to 30 s should allow the operating human enough time to react and stop the test while also allowing for satisfactory data collection. If a software-based stop is used, shorter times might be possible.

To judge the results of the indicators, the optimal time for the indicator to appear would be between 10 s and 30 s. An example of what 10 s to 30 s as a warning time window looks like can be seen in figure 6.1.

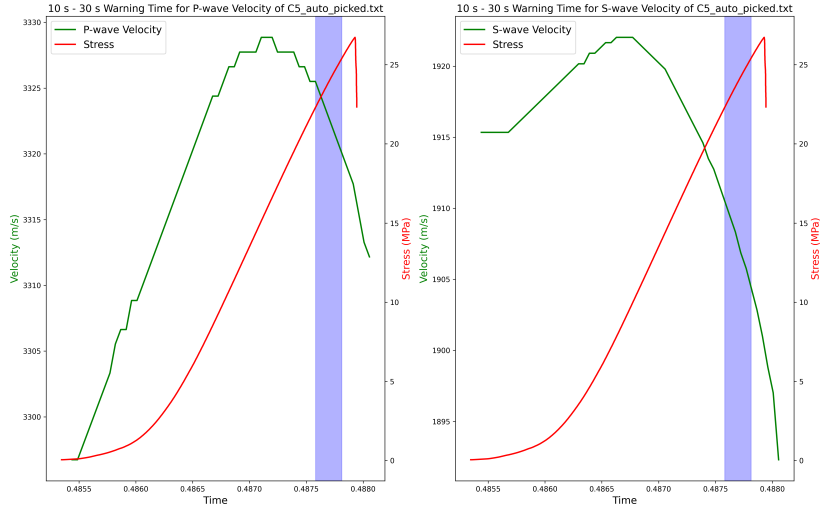

Figure 6.1: The figure shows the P-wave velocity (green) **(left)** and the S-wave velocity (green) **(right)** together with the applied stress (red) over time for sample C5. The opaque blue stripe visualizes the 10 s to 30 s time window before the stress peak, in which the indicator would ideally be located.

To simplify later explanations and discussions, I will establish different velocity behaviour forms to cover all tests. The **first-form** can be seen in figure 6.2, where the velocity increased monotonously reaching its maximum at the same time as, or shortly after, the stress peak. This led to an early inflection point that occurred before the velocity peak.

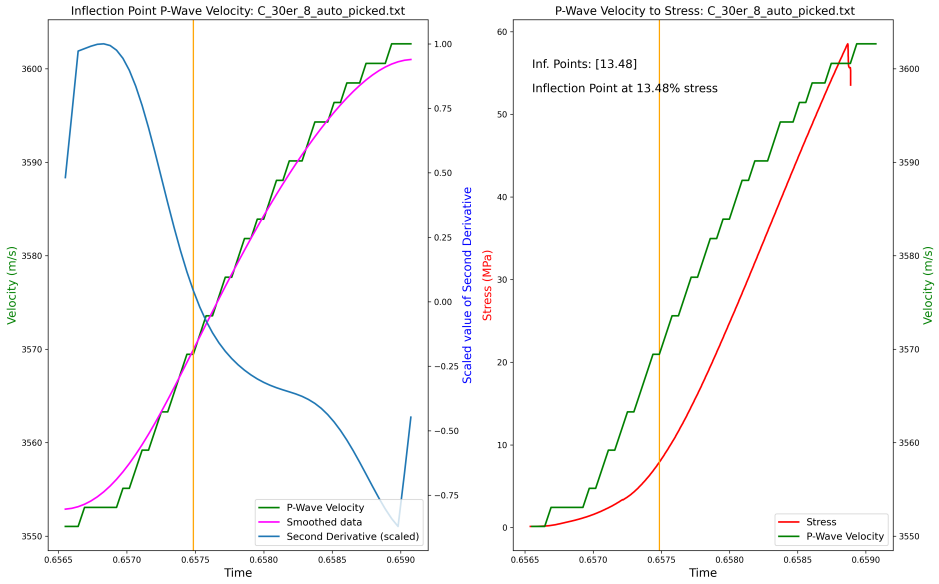

Figure 6.2: The **left** graph shows the P-wave velocity of the C 30er 8 sample (green), the velocity data smoothed by a Gaussian filter (magenta), the second derivative of the smoothed data (blue), and the inflection point of the smoothed data (orange vertical line).
The **right** graph shows stress (red) and velocity (green) over the time of the test. The inflection point is indicated by the orange line, together with text, displaying at what percentage of the maximum load the inflection point is located.

The **second-form** happens when the velocity does show behaviour resembling a parabola, but the inflection point after the velocity peak is located after the stress peak. This led to a negative time from the inflection point to the stress peak (TIP). This behaviour can be seen in figure 6.3, where the second inflection point happened shortly after the sample failure. Because the stress already decreased at this point, the script indicated an inflection point at 86.94 % of compressive strength but with a negative TIP. The first inflection point before the velocity peak was detected at 32.66 %.

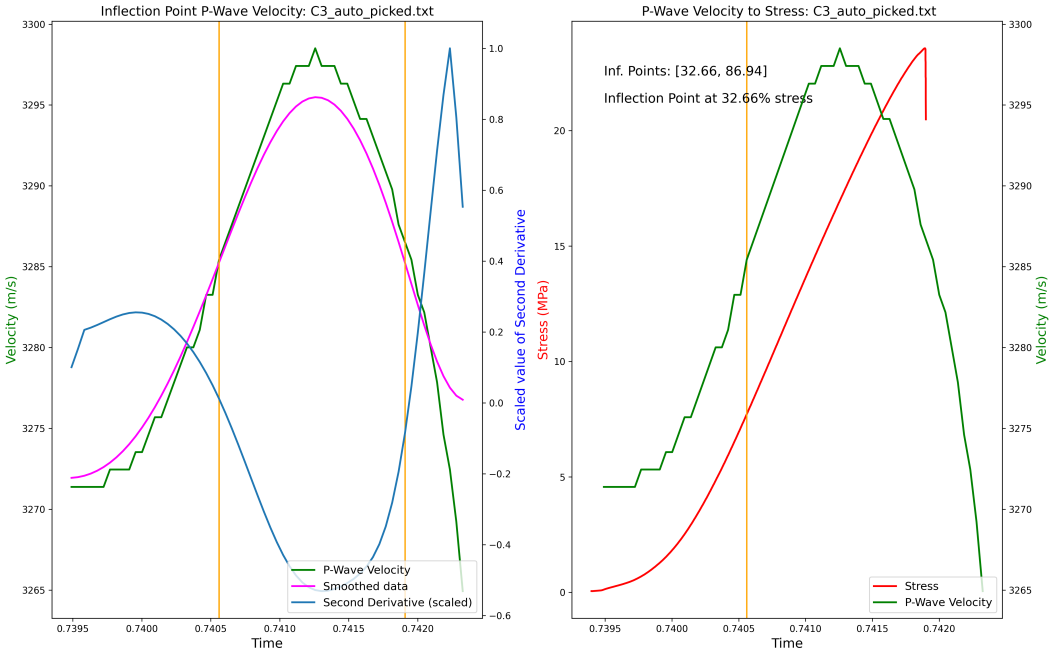

Figure 6.3: The left graph shows the P-wave velocity of the C3 sample (green), the velocity data smoothed by a Gaussian filter (magenta), the second derivative of the smoothed data (blue), and the inflection points of the smoothed data (orange vertical lines).
The right graph shows stress (red) and velocity (green) over the time of the test. The inflection point is indicated by the orange line, together with text, displaying at what percentage of the maximum load the inflection point is located.

The **third-form**, that can be seen in figure 6.4, is a velocity behaviour similar to a parabola, where the inflection point after the velocity occurs before the stress peak. This is the ideal case because this behaviour gives IP with a high percentage and TIP within the desired time frame of 10 s to 30 s.

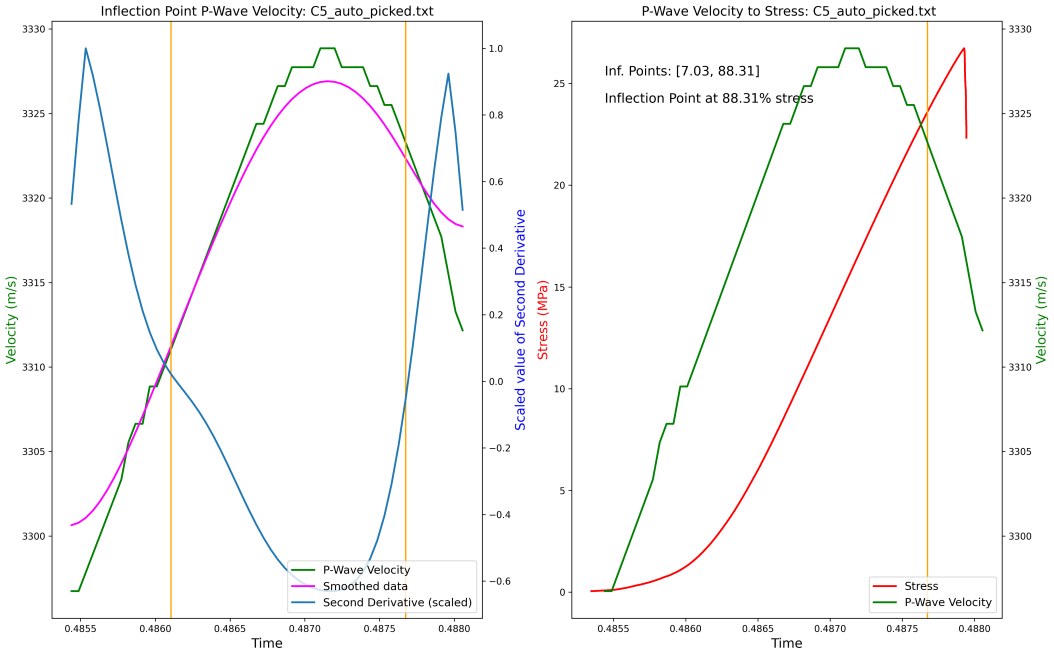

Figure 6.4: The left graph shows the P-wave velocity of the C5 sample (green), the velocity data smoothed by a Gaussian filter (magenta), the second derivative of the smoothed data (blue), and the inflection point of the smoothed data (orange vertical line).
The right graph shows stress (red) and velocity (green) over the time of the test. The inflection point (orange vertical line) of the velocity data is also shown, together with text, displaying at what percentage of the maximum load the inflection point is located.

6.1. Velocity Peak

One option is to use the velocity peak as an indicator. To evaluate the indicator the time between the velocity peak and the stress peak is determined and analysed. For each sample, the "Peak Percent of Compressive Strength" or **PPC** and the "Time from Peak to Peak" or **TPP** of P- and S-waves are assessed and visualized in the following tables and figures.

6.1.1. Peak Percentage Compressive Strength (PPC)

When looking at the PPC of the 50 mm Conduro plaster samples (see figure 6.5) it becomes apparent that the S-wave velocity reaches its peak at a lower stress level than the P-wave velocity. Not only is the average P-wave PPC of 80.46 % substantially higher than the average S-wave PPC of 47.82 % but also for each sample. This coincides with the findings of (Mittelbach, Konietzky, and Baumgarten [8]).

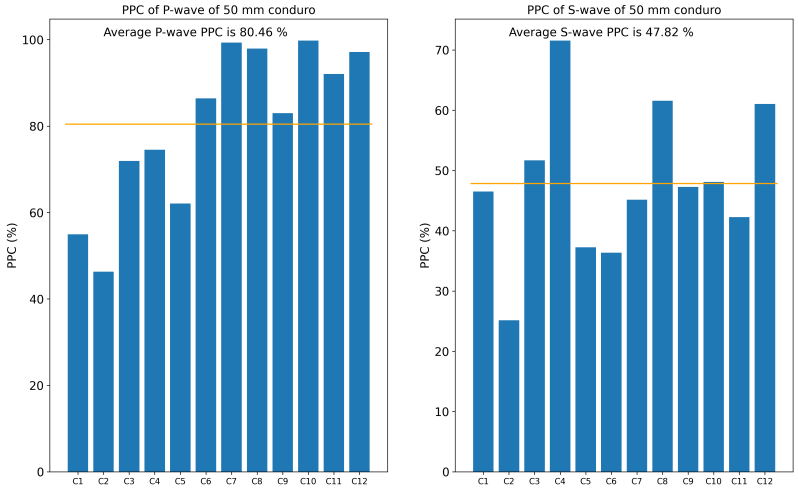

Figure 6.5: Shows at what percentage of the compressive strength the velocity had its peak (PPC) for every Conduro plaster sample with a diameter of 50 mm (see Appendix).

This phenomenon of the S-wave velocity, on average, changing faster and reaching its peak under lower stress, can be observed for every sample type, as can be seen in the figures 6.6, 6.7, and 6.8. The average PPC for the 30 mm Conduro samples are 90.1 % for the P-wave velocity and 84.55 % for the S-wave velocity (see figure 6.6).

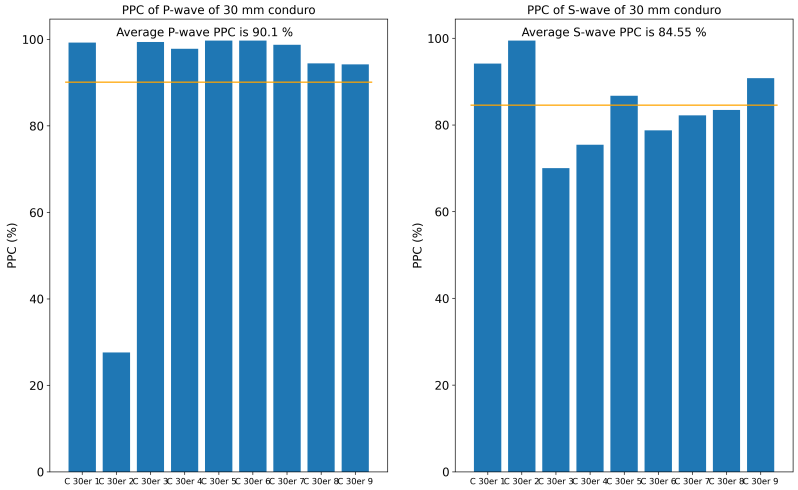

Figure 6.6: Shows at what percentage of the compressive strength the velocity hat its peak (PPC) for every Conduro plaster sample with a diameter of 30 mm (see Appendix).

For the 50 mm Gneiss samples, the average PPC of the P-wave velocity is 99.17 %, and the average S-wave velocity PPC is 89.09 % (see figure 6.7). Since these Gneiss samples did not break, except for G4, the data collected for the velocity peak as an indicator for sample failure for 50 mm Gneiss samples is insufficient. However, it can be mentioned that G4 behaved as expected, with the P-wave velocity reaching its peak at 95.1 % and thus under significantly more stress than the S-wave velocity, which reached its peak under 46.8 % of the compressive strength.

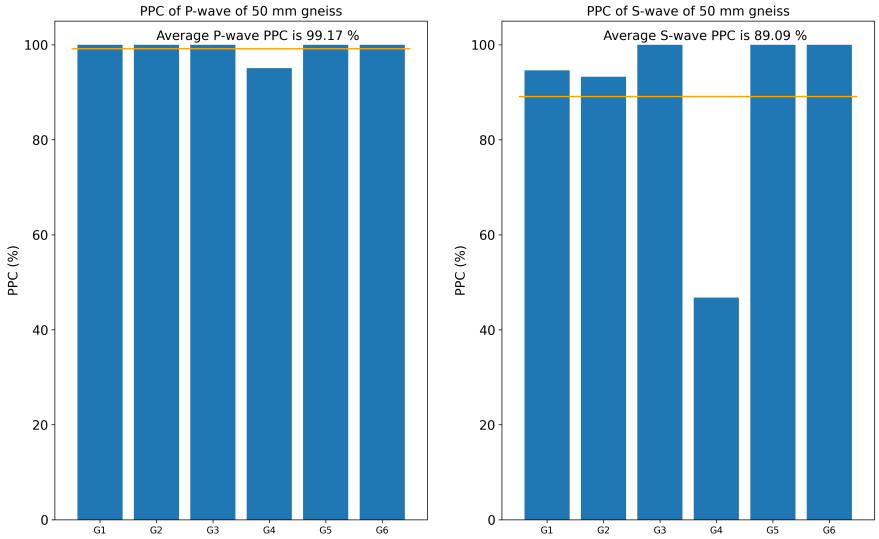

Figure 6.7: Shows at what percentage of the compressive strength the velocity had its peak (PPC) for every Cordierite Pearl Gneiss sample with a diameter of 50 mm (see Appendix).

For the 30 mm Gneiss samples, the average PPC of the P-wave velocity is 98.13 %, and the average S-wave velocity PPC is 89.37 % (see figure 6.8). From the eight Gneiss samples with 30 mm diameter only G 30er 1.2 and G 30er 1 broke. G 30er 1.2 showed unexpected behaviour, reaching its P- and S-wave velocity peak after the sample failure. Although it looks like the time scale for the wave velocities was shifted, after multiple evaluations I could confirm that the time scales are indeed accurate. They represent the sample staying intact after the break and having enough contact with both transducers to allow for seismic wave transversal.

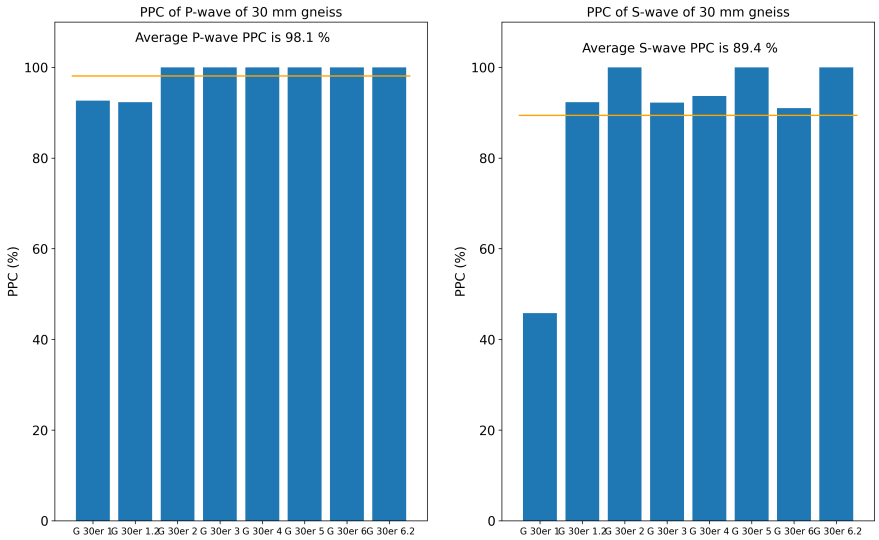

Figure 6.8: Shows at what percentage of the compressive strength the velocity had its peak (PPC) for every Cordierite Pearl Gneiss sample with a diameter of 30 mm (see Appendix).

6.1.2. Time from Velocity Peak to Stress Peak (TPP)

The time between the velocity peak and the stress peak (TPP) is the measurement that will be used to decide if the velocity peak is suited as an indicator for sample failure.

The P-wave velocity of the 50 mm Conduro samples had an average TPP of 34.5 s, with the shortest being -4.4 s from sample C8 and the longest being 97.9 s from C2. The P-wave velocity shows inconsistent TPP, with 33 %, or 4 out of 12 of the samples having a TPP under 2 s, while 50 % or 6 out of 12 samples have a TPP of over 30 s (see figure 6.9).

The S-wave velocity has an average TPP of 92.1 s, with the shortest being 43.1 s from sample C4 and the longest being 130.6 s from C2. 67 %, or 8 out of the 12 samples had a TPP of 100 s ± 15 s, with none being shorter than the desired 30 s, and thus not meeting the set requirements for a usable indicator.

The Conduro samples are the most meaningful, since they broke during the tests, and nearly all of them show the expected parabola form for the velocity. If these samples do not meet the requirements, the Gneiss samples can only reinforce the hypotheses of the velocity peak being unsuitable as an indicator for sample failure.

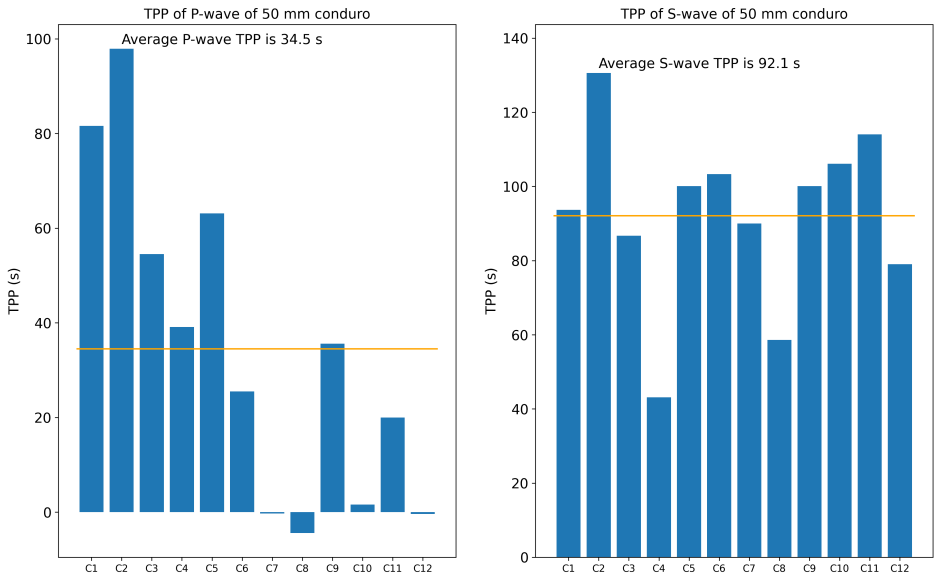

Figure 6.9: Shows time from peak velocity to peak of stress (TPP) in seconds for every Conduro plaster sample with a diameter of 50 mm (see Appendix).

The P-wave velocity of the 30 mm Conduro samples had an average TPP of 5.8 s, with the shortest being -2.0 s from sample C 30er 7 and the longest being 56.5 s from C 30er 2 (see figure 6.10). Sample C 30er 2 is the only sample that has a TPP longer than 10 s, but with its 56.5 s, it is still outside the desired time window. All other P-wave velocities peaked around ±2 s of the stress peak, which does not meet the indicator requirements.

The S-wave velocity has an average TPP of 19.5 s, with the longest being 38.7 s from

C 30er 3 and the shortest being -0.3 s from sample C 30er 2. 67 %, or 6 out of the 9 samples had a TPP that was within the desired time window of 10 s to 30 s. Additionally, C 30er 1 and C 30er 3 are close to the time window with TTPs of 9.2 s and 38.7 s respectively.

Figure 6.10 shows that the S-wave TPP is more consistent than the P-wave TPP and overall shows TPP closer or within the desired time window, to a larger degree than the P-wave velocity.

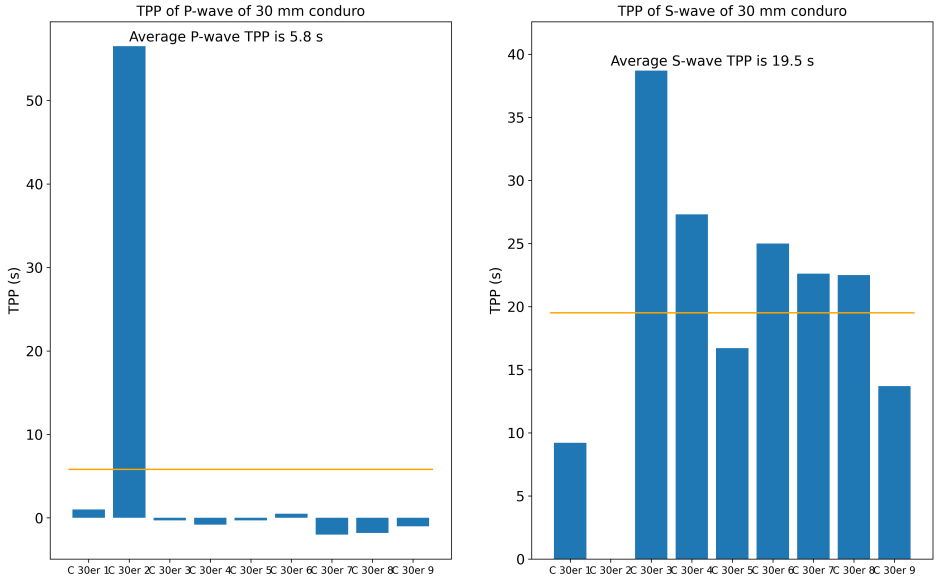

Figure 6.10: Shows time from peak velocity to peak of stress (TPP) in seconds for every Conduro plaster sample with a diameter of 30 mm (see Appendix).

The P-wave velocity of the 50 mm Gneiss samples had an average TPP of 1.9 s, with the longest being 12.3 s from G4 and the shortest being -0.3 s by G3 and G6 (see figure 6.11). Sample G4 is the only sample that shows a TPP within the time window, with all other samples reaching their peak P-wave velocity around the time of the stress peak. This correlates strongly with sample failure, seeing how G4 was the only sample that broke during the test, while all other samples kept their structural integrity over the whole experiment.

The S-wave velocity has an average TPP of 19.2 s, with the longest being 96.9 s from G4 and the shortest being -0.3 s by G3 and G6. G1, G2, and G4 show positive S-wave TPP, with only the TPP of G2 with 11.7 s meeting the indicator requirements.

Due to all but one 50 mm Gneiss samples not breaking during the tests, none, except G4, showed velocity behaviour resembling a parabola.

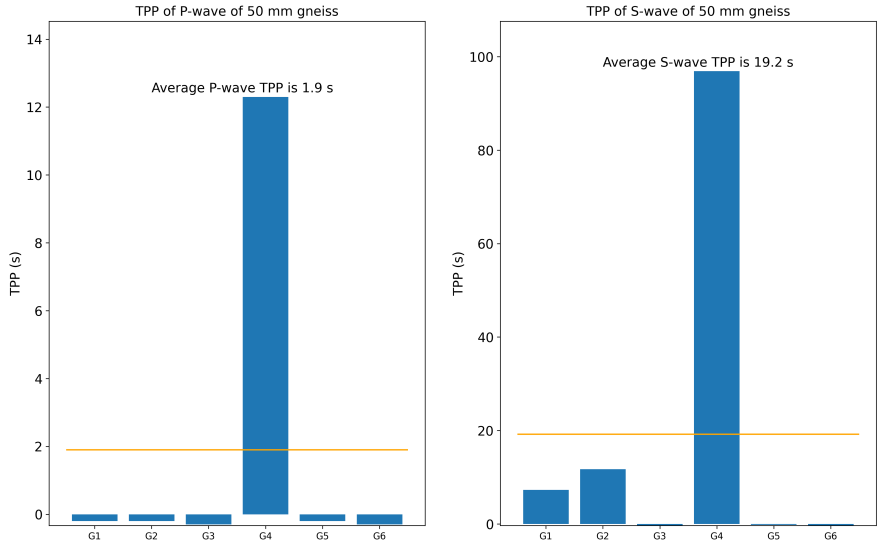

Figure 6.11: Shows time from peak velocity to peak of stress (TPP) in seconds for every Cordierite Pearl Gneiss sample with a diameter of 50 mm (see Appendix).

Only G 30er 1 and G30er 1.2, out of all the 30 mm Gneiss samples, broke during the tests. But the applied pressure was enough for all the S-wave velocities to show enough of a parabola form, for velocity peaks to be determined. On the other hand, all of the P-wave velocities reached their peak after the stress peaked, which led to all negative TPP.

The P-wave velocity of the 30 mm Gneiss samples had an average TPP of -19.3 s, with only G 30er 1.2 showing velocity behaviour in a parabola similar form. The S-wave velocity has an average TPP of 6.1 s, with the longest being 90.8 s from G 30er 1 and the shortest being -44.7 s from sample G 30er 2. 50 % or 4 out of the 8 samples had a positive TPP (see figure 6.12).

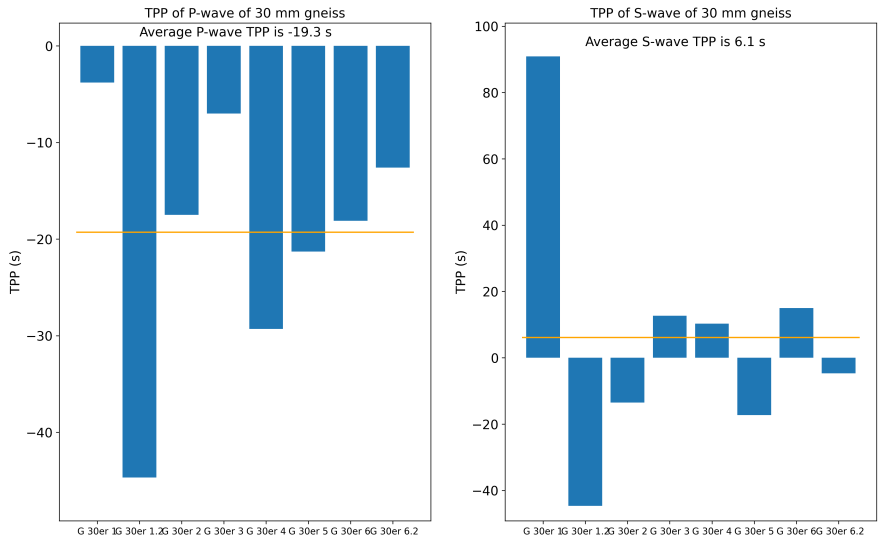

Figure 6.12: Shows time from peak velocity to peak of stress (TPP) in seconds for every Cordierite Pearl Gneiss sample with a diameter of 30 mm (see Appendix)

Assessment of Viability

For the assessment of the velocity peak, I will exclude the Gneiss samples, since they were not tested until failure and showed mostly first-form velocity behaviour for both wave types (see chapter 6.1.1). The distribution of TPPs of Gneiss samples can be seen in figure 6.13, but it will not be referenced in the following.

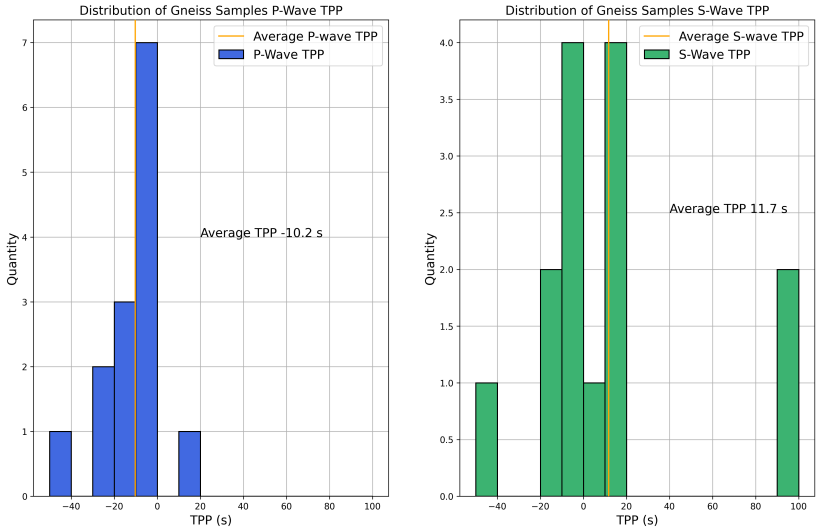

Figure 6.13: This figure shows the TPP distribution of the P-wave velocity **(left)** and the S-wave velocity **(right)**, of all Gneiss samples. The P-wave TPPs are scattered between -44.7 s and 12.3 s with an average TIP of -10.2 s. The S-wave TPPs are spread wide, between -44.7 s s and 96.9 s, with an average TPP of 11.7 s.

The P-wave velocity peak is not viable as an indicator for sample failure since the P-wave has been shown to frequently peak after the stress peak (see figures 6.9 and 6.10). The times at which the peak occurs are inconsistent, with the TPP for the 50 mm Conduro spanning from -4.4 s to 97.9 s with a wide variety of times (see figure 6.9). 57 % or 12 out of the 21 Conduro samples showed TPP with under 10 s, which does not meet the desired indicator requirements.

Table 6.1: Percentage at which the velocity peak occurred (PPC) and time between said velocity peak and the stress peak (TPP) for all samples.

Samples	PPC (%)		TPP (s)	
	P-wave	S-wave	P-wave	S-wave
Conduro 50 mm	46.31 % - 99.80 %	25.13 % - 71.56 %	-4.4 s - 97.9 s	43.1 s - 130.6 s
C 50 Averages	80.46 %	47.82 %	34.5 s	92.1 s
Conduro 30 mm	27.61 % - 99.73 %	70.00 % - 99.46 %	-2.0 s - 56.5 s	-0.3 s - 38.7 s
C 30 Averages	90.10 %	84.55 %	5.8 s	19.5 s
Gneiss 50 mm	95.07 % - 100.00 %	46.77 % - 100.00 %	-0.3 s - 12.3 s	-0.3 s - 96.9 s
G 50 Averages	99.17 %	89.09 %	1.9 s	19.2 s
Gneiss 30 mm	92.34 % - 100.00 %	45.77 % - 100.00 %	44.7 s - -3.8 s	-44.7 s - 90.8 s
G 30 Averages	98.13 %	89.37 %	-19.3 s	6.1 s

The S-wave velocity peak is not viable as an indicator for sample failure, but showed that the S-wave velocity is impacted differently than the P-wave velocity, under increasing load. The PPCs of the Conduro samples S-wave are overall lower, not only the averages but also for each sample, as discussed in chapter 6.1.1. This led to longer S-wave TPPs for all Conduro samples, except C 30er 2. For the 30 mm Conduro samples, the TPPs showed times that mostly fit into the desired time window, but for the 50 mm Conduro samples, the TPPs show an equally large spread as the P-wave TPPs, being between 43.1 s and 130.6 s.

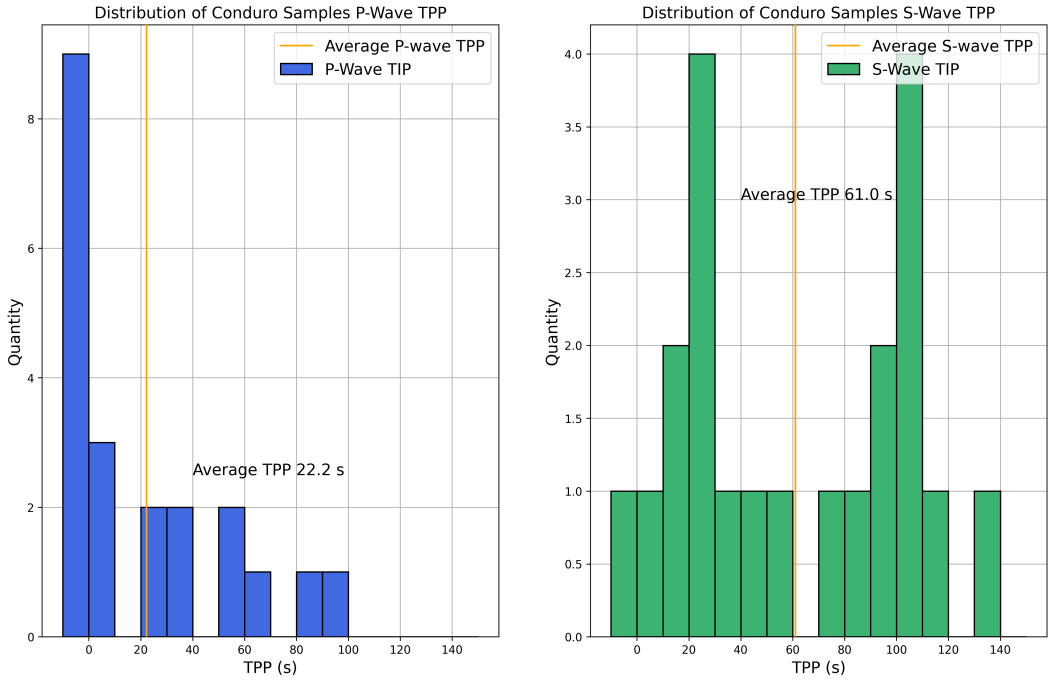

Figure 6.14: This figure shows the TPP distribution of the P-wave velocity **(left)** and the S-wave velocity **(right)**, of all Conduro samples. The P-wave TPPs are scattered between -4.4 s and 97.9 s with an average TIP of 22.2 s. The S-wave TPPs are spread wide, between -0.3 s s and 130.6 s, with an average TPP of 61.0 s.

The target time window was missed by the majority of P-wave and S-wave velocities of the Conduro samples, with only 19 % or 8 out of 42 TPPs being between 10 s and 30 s. Overall, the velocity peak can be discarded as a reliable indicator for sample failure.

6.2. Velocity Inflection Point

Because the 100 kN pressure plate of the hydraulic press was unable to break the Gneiss samples or produce a sufficient velocity peak, a different form of indicator has to be found. The increase in velocity is always associated with an increase in stability, density or sample shortening. This means that during the compressive strength test, certain microcracks are closing, the sample structure aligns itself to optimally handle the increasing load and, or the sample gets compressed, shortening the transit time ([7]).

The shortening of the sample has a negligible impact on the peak and inflection point position, as discussed in chapter 5.1, and will not be taken into account. The main focus of

this chapter will be the percentage of stress at which the inflection points occur and how much time lies between the detected inflection points and the stress peaks. The stress peak has been chosen over the breakpoint because the sample breaks are too different in length and process, to allow a consistent comparison of the samples.

Inflection points that occurred after the stress peak, will be excluded if at least one occurred before the peak. All velocity data gained from non-cyclic testing was smoothed using the same Gaussian one-dimensional filter with a standard deviation of $\sigma = 6$. Data gained during cyclic testing was smoothed using the same filter but with a $\sigma = 2$. To create an analysis workflow that is as streamlined and reproducible as possible, the filters were not changed, even if a slight adjustment would fit one sample better.

Figures 6.15 and 6.16 show how different filters can lead to different inflection points. When using a $\sigma = 6$, the inflection point for C 30er 1 is located at 6.55 %, resulting in a TIP of 136.1 s. When using $\sigma = 4$, the smoothed data more accurately represents the dip in velocity at the end of the data set, leading to an inflection point at 90.48 % with a TIP of 6.1 s.

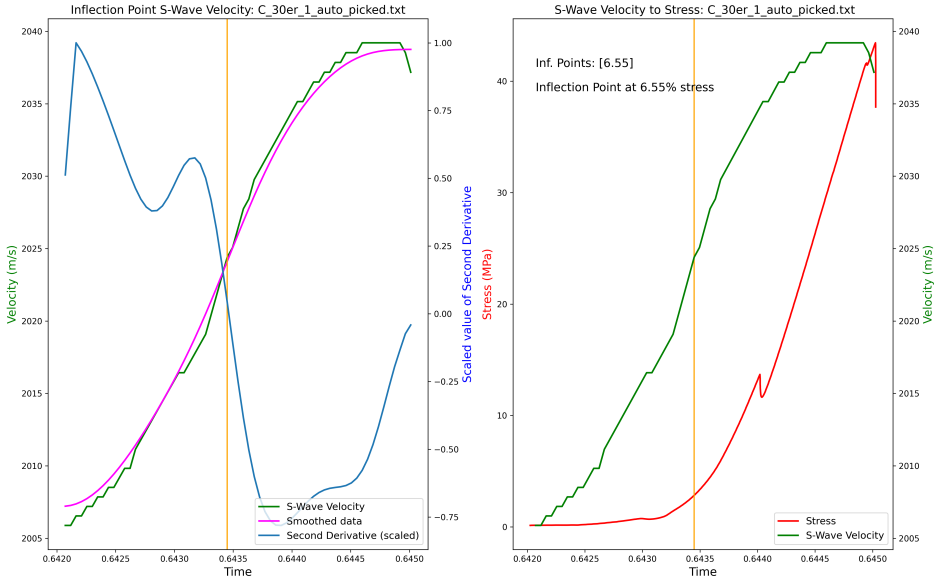

Figure 6.15: (left) The figure shows the velocity of the S-wave over time for sample C 30er 1. The velocity data (green) gets smoothed (pink) using a Gaussian one-dimensional filter with standard deviation $\sigma = 6$ and the second derivative (blue) is determined. The zero points of the second derivative are the positions of the inflection points (orange). **(right)** The figure shows the velocity (green) and stress data (red) of C 30er 1 over time. The (orange) vertical line indicates the inflection point at 6.55 % resulting in a TIP of 136.1 s.

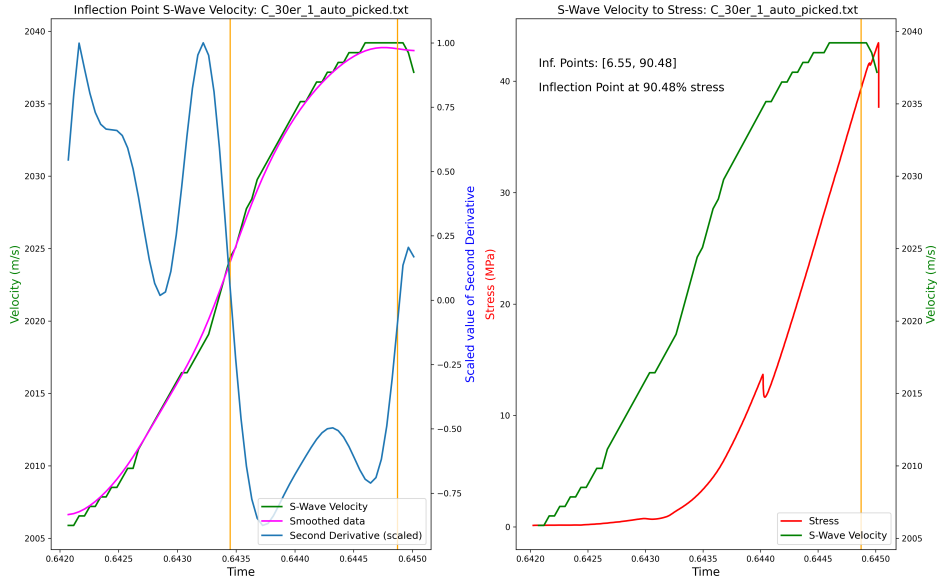

Figure 6.16: (left) The figure shows the velocity of the S-wave over time for sample C 30er 1. The velocity data (green) gets smoothed (pink) using a Gaussian one-dimensional filter with standard deviation $\sigma = 4$ and the second derivative (blue) is determined. The zero points of the second derivative are the positions of the inflection points (orange). **(right)** The figure shows the velocity (green) and stress data (red) of C 30er 1 over time. The (orange) vertical lines indicate the inflection points at 6.55 % and 90.48 % resulting in a TIP of 13.1, which is substantially different to the 136.1 s seen in figure 6.15, when using a $\sigma = 6$.

The following analysis of the inflection points was made using the Gaussian one-dimensional filter with a $\sigma = 6$ for non-cyclic data collection and $\sigma = 2$ for cyclic data collection.

6.2.1. Inflection Point Position (IP)

None of the 50 mm Gneiss samples, except G4, broke during the tests. Because of this, they all show first-form velocity behaviour with low IPs and long TIPs. Thus they are far from optimal for assessing the viability of the inflection point as an indicator for sample failure.

The P-wave velocity of the 50 mm Conduro samples had an average IP of 61.2 %, with the highest being 99.23 % from C11 and the lowest being 12.57 % from C12. 42 %, or 5 out of 12 samples (C3, C7, C8, C10, and C12), have a IP of under 85 % (see figure 6.17). 33 %, or 4 out of 12 samples (C7, C8, C10, and C12), showed first-form velocity behaviour. 9 %, or only sample C3, showed second-form velocity behaviour and 58 %, or 7 out of 12 samples (C1, C2, C4, C5, C6, C9, and C11), showed third-form velocity behaviour (see in the Appendix). The first and second-form of velocity behaviour correlate with IP under 85 %.

The S-wave velocity has an average IP of 89.1 %, with the highest being 99.3 % from C3 and the lowest being 83.41 % from C5 (see figure 6.17). All samples show third-form velocity behaviour with the IP located after the velocity peak, but before the stress peak (see in the Appendix). This correlates strongly with all S-wave IPs being over 83 %.

The P-wave velocity of the 30 mm Conduro samples had an average IP of 46.3 %, with the

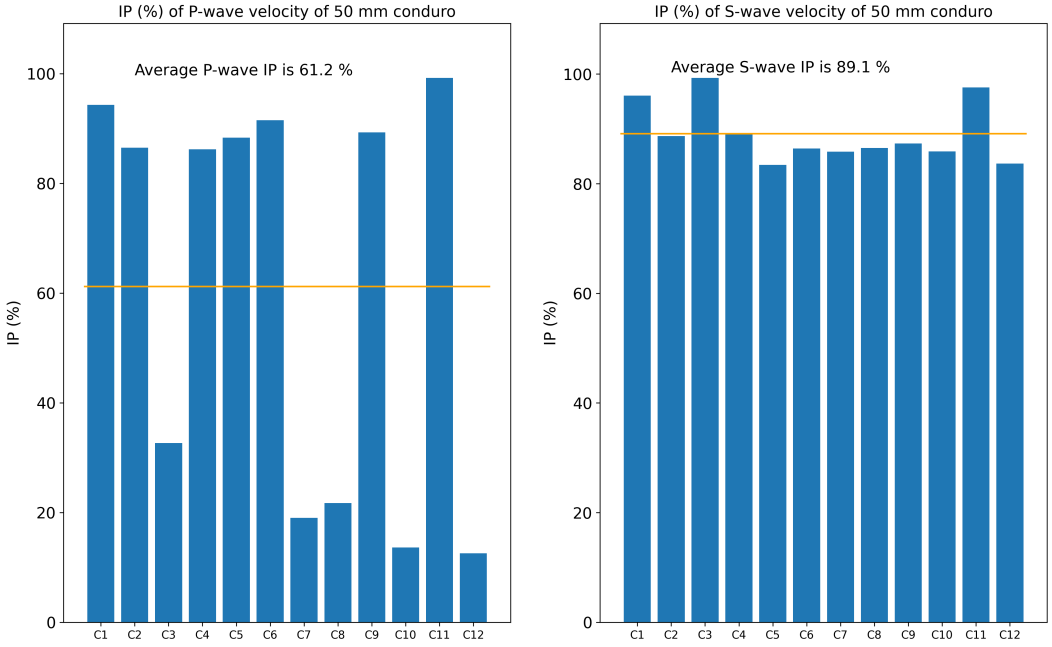

Figure 6.17: Shows at what percentage of the compressive strength the velocity hat its inflection point (IP) in percent for every Conduro sample with a diameter of 50 mm (see in Appendix).

highest being 92.66 % from C 30er 3 and the lowest being 1.76 % from C 30er 1. 67 %, or 6 out of 9 samples, have an IP of under 85 % (see figure 6.19). While all samples show first-form velocity behaviour, the three samples C 30er 2, C 30er 3, and C 30er 6, that have IP over 85 %, show very distinct velocity behaviours. C 30er 3 and C 30er 6 have small spikes at the end of the test, leading to two inflection points that are very close together and close to the stress peak (see figure 6.18). C 30er 2s P-wave velocity reacted delayed to changing load during the cyclic testing, leading to an inflection point from a small increase in velocity at the end of testing, very close to the maximum stress (see figure C 30er 2 in Appendix).

The S-wave velocity has an average IP of 79.7 %, with the highest being 98.6 % from C 30er 7 and the lowest being 6.57 % from C 30er 1 (see figure 6.19). 22 %, or 2 out of 9 samples (C 30er 1 and C 30er 2), show the first form of velocity behaviour and have IPs under 85 %. All other samples show first-form behaviour and have an average IP of 94.47 % with no IP under 90 %.

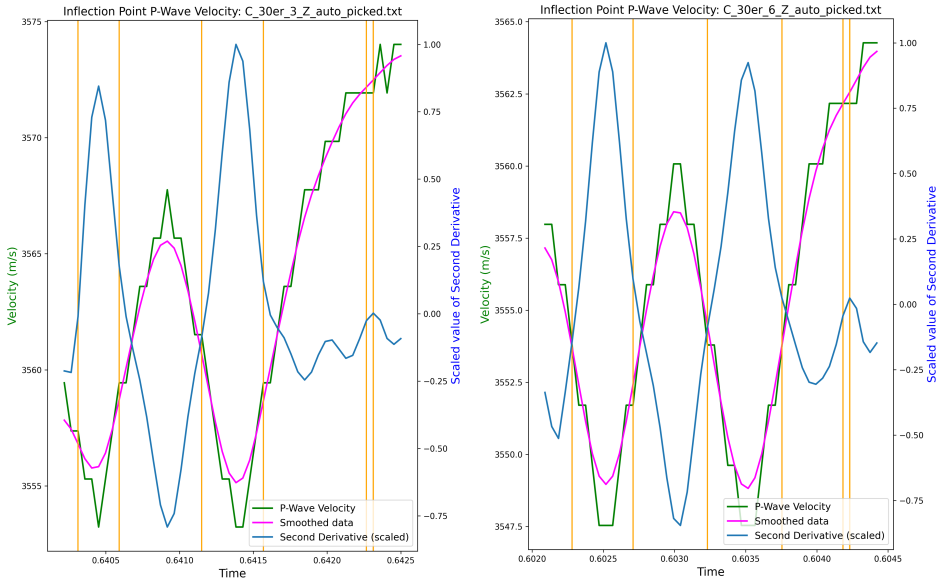

Figure 6.18: The figure shows the velocity of the P-wave over time for samples C 30er 3 **(left)** and C 30er 6 **(right)**. The velocity data (green) gets smoothed (pink) using a Gaussian filter and the second derivative (blue) is determined. The zero points of the second derivative are the positions of the inflection points (orange).

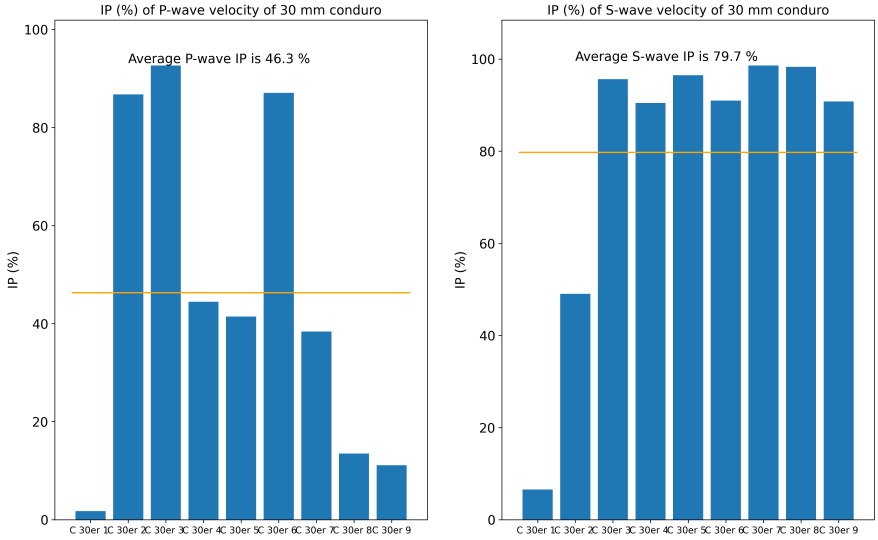

Figure 6.19: Shows at what percentage of the compressive strength the velocity hat its inflection point (IP) in percent for every Conduro sample with a diameter of 30 mm (see in Appendix).

The P-wave velocity of the 50 mm Gneiss samples had an average IP of 46.0 %, with the highest being 78.68 % from G3 and the lowest being 24.46 % from G6. All samples have an IP of under 85 % (see figure 6.21). All samples show first-form velocity behaviour, although G4 is a unique case, where the smoothed data, created by the chosen Gaussian filter, does not have an inflection point after the velocity peak (see figure 6.20).

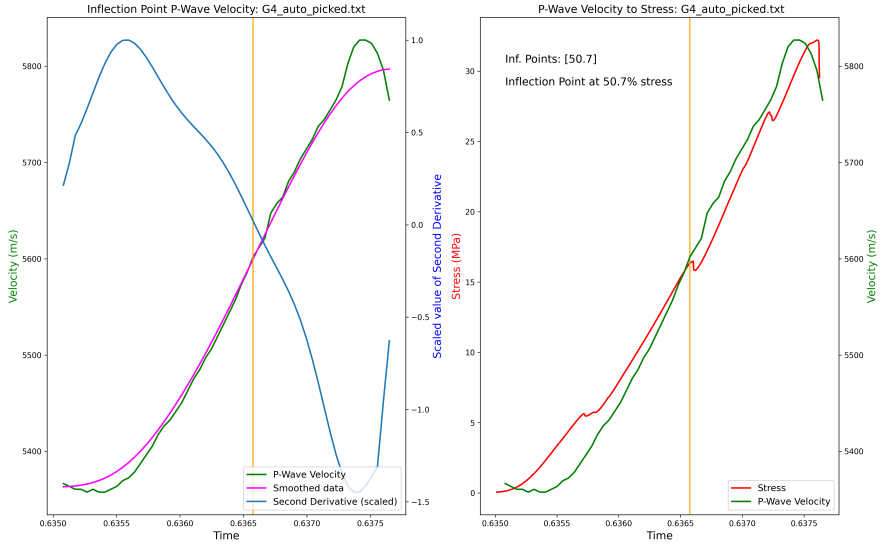

Figure 6.20: (left) The figure shows the velocity of the P-wave over time for sample G4. The velocity data (green) gets smoothed (pink) using a Gaussian filter and the second derivative (blue) is determined. The zero point of the second derivative is the position of the inflection point (orange). **(right)** The figure shows the velocity (green) and stress data (red) of G4 over time. The (orange) vertical line indicates the inflection point at 50.7 %.

The S-wave velocity of the 50 mm Gneiss has an average IP of 53.0 %, with the highest being 93.0 % from G2 and the lowest being 25.59 % from G1 (see figure 6.21). 67 % or 4 out of 6 samples show first-form velocity behaviour (G1, G3, G5, and G6), while G2 and G4 show third-form behaviour.

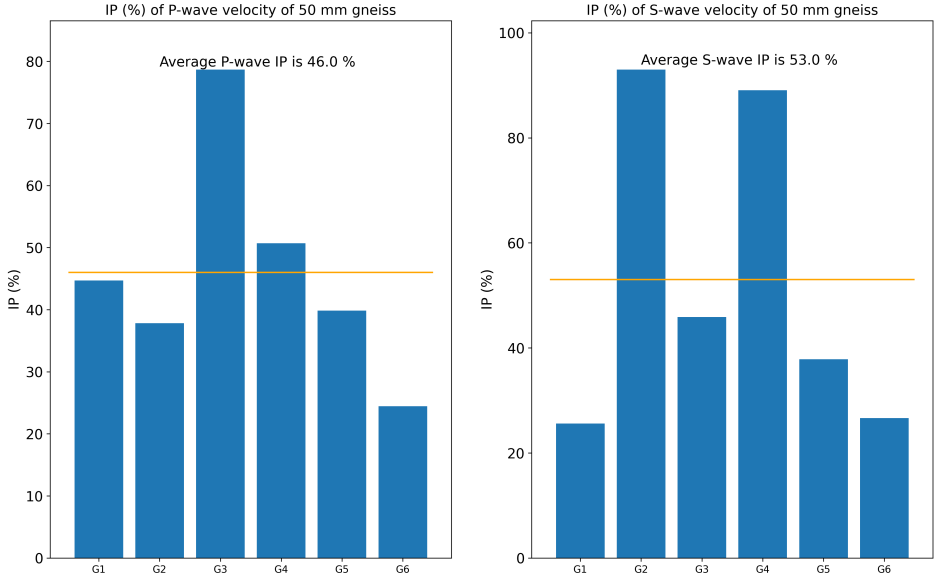

Figure 6.21: Shows at what percentage of the compressive strength the velocity hat its inflection point (IP) in percent for every Cordierite Pearl Gneiss sample with a diameter of 50 mm (see in Appendix).

The P-wave velocity of the 30 mm Gneiss samples had an average IP of 21.8 %, with the highest being 35.4 % from G 30er 1.2 and the lowest being 10.95 % from G 30er 1 % (see figure

6.23). 13 %, or only G 30er 1.2 showed second form velocity behaviour (see figure 6.22), with the rest of the samples showing first form behaviour.

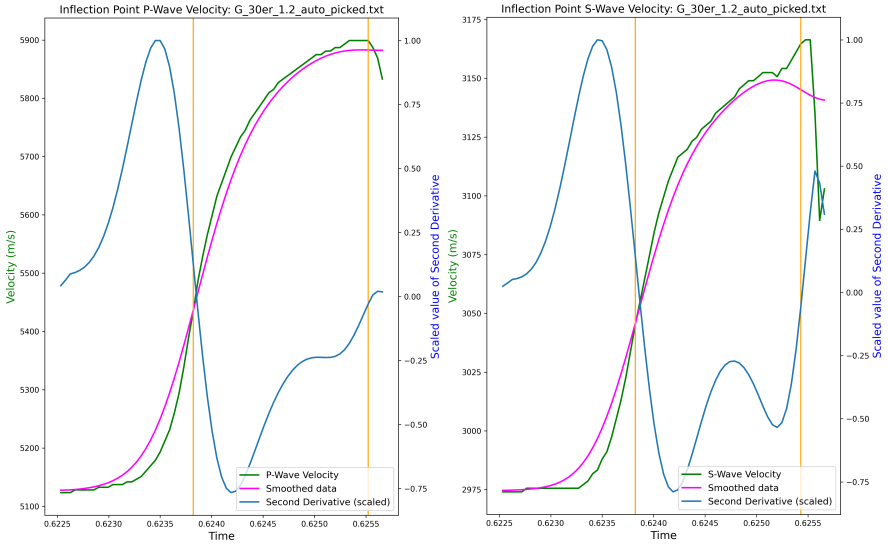

Figure 6.22: (left) The figure shows the velocity of the P-wave over time for sample G 30er 1.2. The velocity data (green) gets smoothed (pink) using a Gaussian filter and the second derivative (blue) is determined. The zero point of the second derivative is the position of the inflection point (orange). **(right)** The figure shows the velocity of the S-wave over time for sample G 30er 1.2. The velocity data (green) gets smoothed (pink) using a Gaussian filter and the second derivative (blue) is determined. The zero point of the second derivative is the position of the inflection point (orange).

The S-wave velocity on the other hand has an average IP of 40.8 %, with the highest being 98.38 % from G 30er 6 and the lowest being 16.23% from G 30er 6.2 (see figure 6.23).

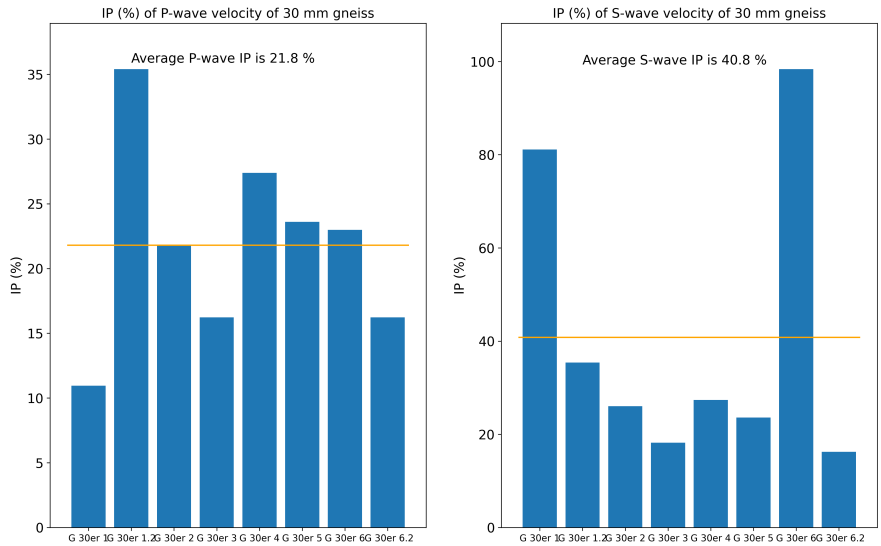

Figure 6.23: Shows at what percentage of the compressive strength the velocity hat its inflection point (IP) in percent for every Cordierite Pearl Gneiss sample with a diameter of 30 mm (see in Appendix).

6.2.2. Time from Inflection Point to Peak of Stress (TIP)

The identified IP phenomenon with the S-wave velocity reacting faster to stress changes and reaching its peak under lower stress than the P-wave leads to more third-form velocity behaviour from the S-wave. The P-wave on the other hand shows more first-form velocity behaviour, which results in longer TIPs for the P-wave velocities. This holds for samples that showed second and third-form velocities behaviour, which excludes most Gneiss samples.

The P-wave velocity of the 50 mm Conduro samples had an average TIP of 72.4 s, with the longest being 184.2 s from C12 and the shortest being 2.9 s from C11 (see figure 6.24). 33 %, or 4 out of 12 samples (C7, C8, C10, and C12) showed first-form and only C3 showed second-form velocity behaviour (see figure 6.3 in chapter 6.2.1). The rest of the samples showed third-form behaviour, which strongly correlates with the TIP.

The sample with first and second-form velocity behaviour have an average TIP of 146.3 s, with the highest being 184.2 s from C12 and the lowest being 115.4 s from C3, while the samples with third-form behaviour have an average TIP of just 19.7 s, with the highest being 32.2 s from C2 and the lowest being 2.9 s from C11 (see figure 6.24).

The S-wave velocity of the 50 mm Conduro samples had an average TIP of 22.5 s, with the longest being 35.1 s from C10 and the shortest being 2.9 s from C3 (see figure 6.24). All of the samples showed third-form behaviour, which strongly correlates with the average TIP.

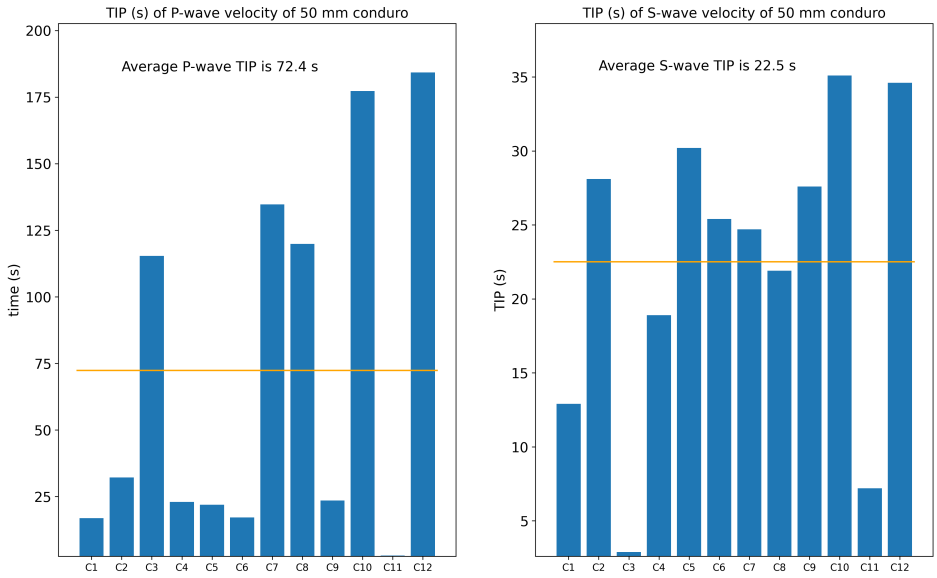

Figure 6.24: Shows time from inflection point to peak of stress (TPP) in seconds for every Conduro sample with a diameter of 50 mm (see in Appendix).

The P-wave velocity of the 30 mm Conduro samples had an average TIP of 71.5 s, with the longest being 163.9 s from C 30er 1 and the shortest being 10.5 s from C 30er 3 (see figure 6.25). All of the samples showed first-form velocity behaviour, which strongly correlates with the long average TIP.

The S-wave velocity of the 30 mm Conduro samples had an average TIP of 25.6 s, with the longest being 136.1 s from C 30er 1 and the shortest being 2.4 s from C 30er 8 (see figure 6.25). 22 %, or 2 out of 9 samples (C 30er1 and C 30er 2), showed first-form velocity behaviour, while the rest showed third-form behaviour. This strongly correlates with the TIP length, seeing how the first-form samples' average TIP of 88.3 s is substantially longer than the average TIP of the third-form samples of 7.7 s.

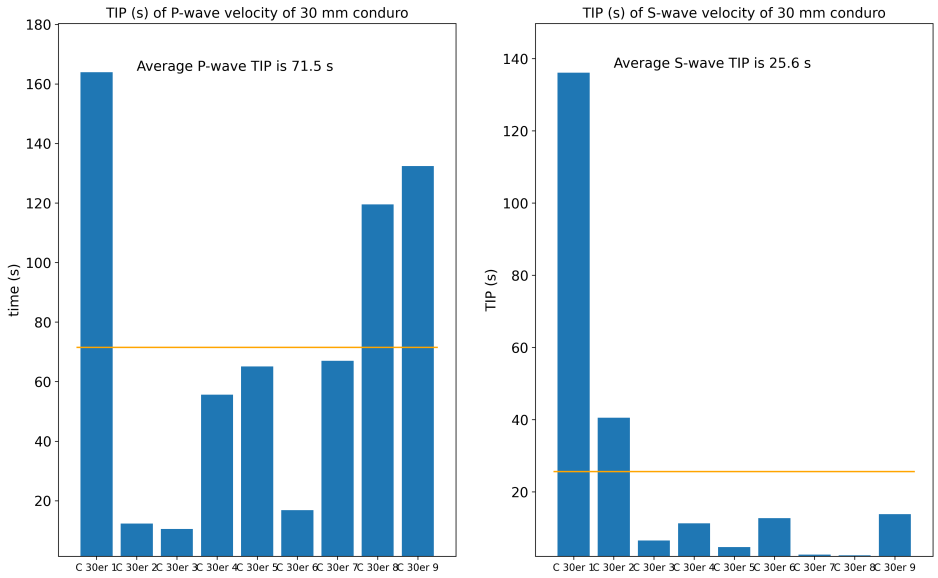

Figure 6.25: Shows time from inflection point to peak of stress (TPP) in seconds for every Conduro sample with a diameter of 30 mm (see in Appendix).

The P-wave velocity of the 50 mm Gneiss samples had an average TIP of 72.2 s, with the longest being 108.5 s from G6 and the shortest being 27.6 s from G2 (see figure 6.26). All of the samples showed first-form velocity behaviour, which strongly correlates with the long average TIP.

The S-wave velocity of the 50 mm Gneiss samples had an average TIP of 74.5 s, with the longest being 117.3 s from G1 and the shortest being 11.6 s from G2 (see figure 6.26). 33 %, or 2 out of 6 samples (G2 and G4), showed third-form velocity behaviour, while the rest showed first-form behaviour. This again strongly correlates with the TIP length, seeing how the first-form samples' average TIP of 103.8 s is substantially longer than the average TIP of the third-form samples of 16.0 s.

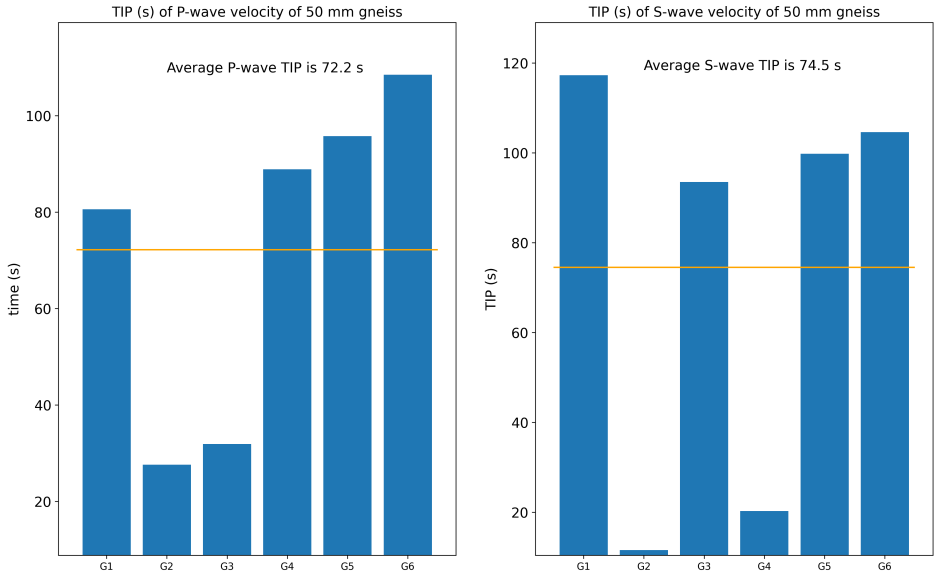

Figure 6.26: Shows time from inflection point to peak of stress (TPP) in seconds for every Cordierite Pearl Gneiss sample with a diameter of 50 mm (see in Appendix).

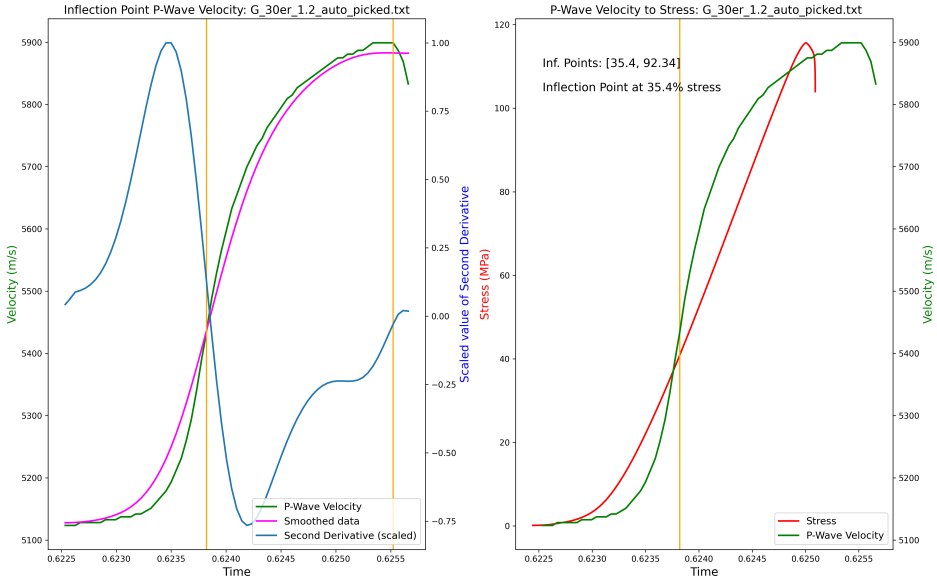

Figure 6.27: (left) The figure shows the velocity of the P-wave over time for sample G 30er 1.2. The velocity data (green) gets smoothed (pink) using a Gaussian filter and the second derivative (blue) is determined. The zero points of the second derivative are the positions of the inflection points (orange). **(right)** The figure shows the velocity (green) and stress data (red) of G 30er 1.2 over time. The (orange) vertical line indicates the inflection point before the stress peak at 35.4 %.

The P-wave velocity of the 30 mm Gneiss samples had an average TIP of 130.2 s, with the longest being 154.0 s from G 30er 1 and the shortest being 102.3 s from G 30er 1.2 (see figure 6.28). All samples, except G 30er 1.2, showed first-form velocity behaviour, which strongly correlates with the long average TIP. G 30er 1.2 has an inflection point after the stress peak, as

figure 6.27 shows.

The S-wave velocity of the 30 mm Gneiss samples had an average TIP of 98.2 s, with the longest being 142.2 s from G 30er 6.2 and the shortest being 2.9 s from G 30er 6 (see figure 6.28). 25 %, or 2 out of 8 samples (G 30er 1 and G 30er 6), showed third-form velocity behaviour, G 30er 1.2 showed second-form behaviour, while the rest showed first-form behaviour. This again strongly correlates with the TIP length, seeing how the first and second-form samples' average TIP of 124.5 s is substantially longer than the average TIP of the third-form samples of 19.3 s.

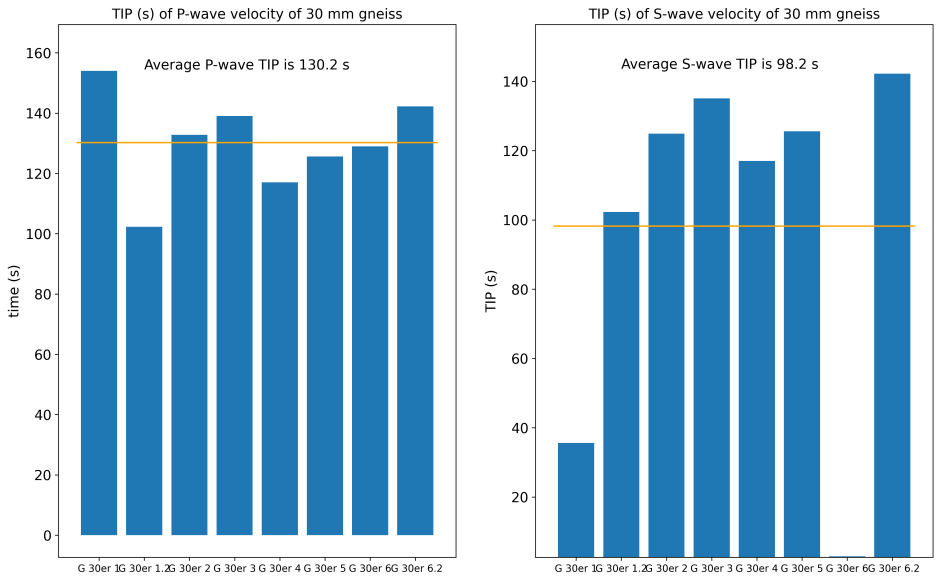

Figure 6.28: Shows time from inflection point to peak of stress (TPP) in seconds for every Cordierite Pearl Gneiss sample with a diameter of 30 mm (see in Appendix).

Assessment of Viability

Regarding the P-wave of 67 %, or 14 out of 21, Conduro samples showed first- or second-form velocity behaviour with TIP between 10.5 s and 184.2 s with an average TIP of 72.0 s (see figure 6.29). The P-wave is unreliable in producing third-form velocity behaviour during a compressive strength test and in producing TIPs in the desired time window, of 10 s to 30 s. Because of this, the inflection points of the P-wave velocity are unfit to be used as an indicator of sample failure.

The S-wave of all the 50 mm Conduro samples showed third-form velocity behaviour with warning times between 2.9 s and 35.1 s. 10 out of these 12 samples, or 83 %, have a warning time between 12.9 s and 35.1 s, which is nearly ideal. The S-wave of the 30 mm Conduro samples showed third-form velocity behaviour for 78 % or 7 out of the 9 samples, together with TIPs between 2.4 s and 13.8 s for these samples.

Table 6.2: Percentage at which the last velocity inflection point before the stress peak occurred (IP) and time between said inflection point and the stress peak (TIP) for all samples.

Samples	IP (%)		TIP (s)	
	P-wave	S-wave	P-wave	S-wave
Conduro 50 mm	12.57 % - 99.23 %	83.41 % - 99.3 %	2.9 s - 184.2 s	2.9 s - 35.1 s
C 50 Averages	61.25 %	89.14 %	72.4 s	22.4 s
Conduro 30 mm	1.76 % - 92.66 %	6.56 % - 98.6 %	10.5 s - 163.9 s	2.4 s - 136.1 s
C 30 Averages	46.34 %	79.65 %	71.4 s	25.6 s
Gneiss 50 mm	24.46 % - 78.68 %	25.59 % - 93.00 %	27.6 s - 108.5 s	11.6 s - 117.3 s
G 50 Averages	46.03 %	53.00 %	72.2 s	74.5 s
Gneiss 30 mm	10.95 % - 35.40 %	16.23 % - 98.38 %	102.3 s - 154.0 s	2.9 s - 142.2 s
G 30 Averages	21.82 %	40.8 %	130.2 s	98.2 s

If taken together, the Conduro samples show third-form behaviour for 90 % or 19 out of 21 samples and have TIPs between 2.4 s and 136.1 s (see figure 6.29). The samples with third-form velocity behaviour have TIPs between 2.4 s and 35.1 s. The two outliers C 30er 1 and C 30er 2, show first-form behaviour and have TIPs of 136.1 s and 40.5 s respectively.

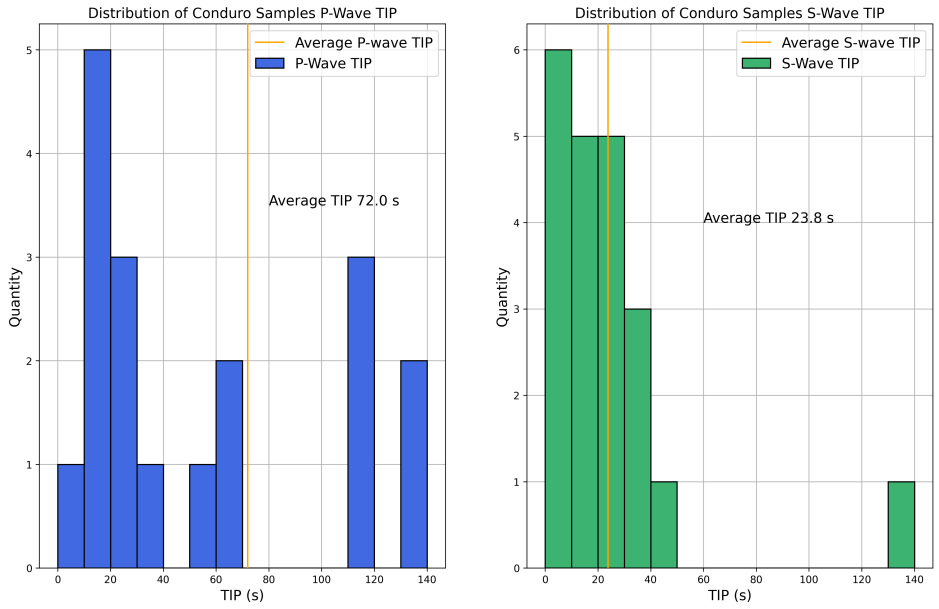

Figure 6.29: This figure shows the TIP distribution of the P-wave velocity **(left)** and the S-wave velocity **(right)**, of all Conduro samples. The P-wave TIP is scattered between 2.9 s and 184.2 s with an average TIP of 72.0 s. The S-wave TIP is concentrated between 2.4 s s and 40.5 s, with one outlier at 136.1 s and an average TIP of 23.8 s.

Chapter 6.2.2 showed a strong correlation between the samples that were tested until failure, the samples of which the S-wave velocity showed third-form behaviour, and samples with high IP and with TIP in the desired time window. From this, we can assume that, if a Conduro sample is about to be tested until failure, the S-wave velocity will most likely show third-form behaviour. The inflection point after the velocity peak will most likely occur at a

time of 2.4 s to 35.1 s before the stress peak.

With the Gneiss samples, a clear divide can be seen between samples that showed first- or second-form velocity behaviour and samples that showed third-form behaviour. The P-wave velocities all showed first- or second-form behaviour, leading to widespread TIPs between 80.6 s and 154.0 s, with two outliers (G2 and G3) at 27.6 s and 31.9 s. These two outliers have some drops and spikes in their velocity data, which led to inflection points with shorter TIPs.

For the S-wave, all samples that showed third-form velocity behaviour (G 30er 1, G 30er 6, G2, and G4) have TIPs between 2.9 s and 35.6 s (see figure 6.30). The samples with first- and second-form behaviour are substantially longer, laying between 93.5 s and 142.2 s.

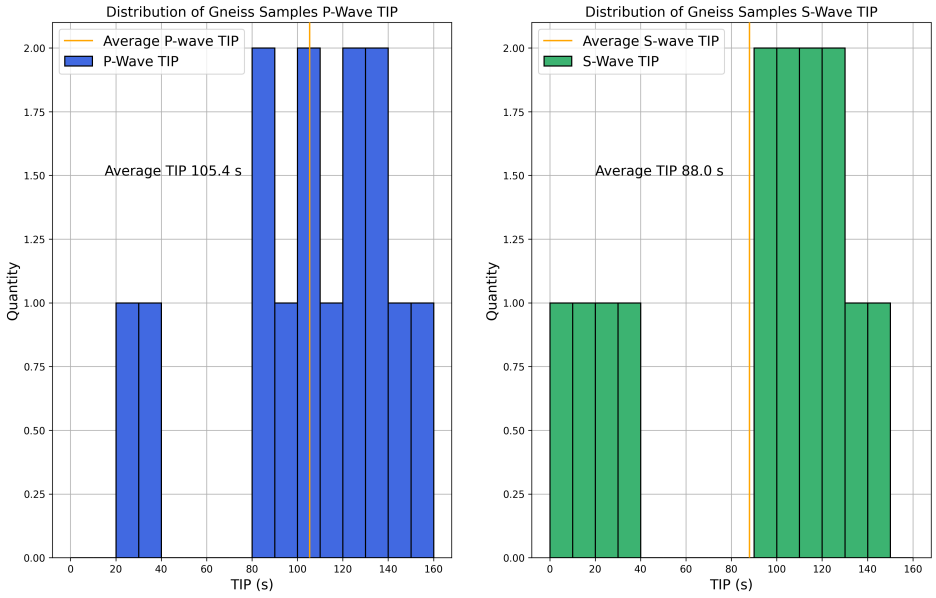

Figure 6.30: This figure shows the TIP distribution of the P-wave velocity **(left)** and the S-wave velocity **(right)**, of all Gneiss samples. The P-wave TIPs have a wide spread, between 27.6 s and 154.0 s with an average TIP of 105.4 s. The S-wave TIPs are spread similarly wide between 2.9 s and 142.2 s, with an average TIP of 88.0 s.

After analysing the results of both Conduro and Gneiss samples, it becomes apparent that the only possible indicator for sample failure, out of the ones we tested, is the inflection point of the S-wave velocity. It has the potential to indicate sample failure with a warning time between 2.9 s and 35.6 s. If the measuring intervals of the transducers were made shorter, longer warning times might be possible, shifting the warning time window to a manageable 5 s to 40 s.

The amount of data collected is still lacking and thus I would suggest the S-wave inflection point as an indicator for sample failure, only for plaster or similarly homogeneous samples.

7
Conclusion

The main objective of this thesis was to evaluate the seismic wave velocities as indicators for sample failure during uniaxial compressive strength tests to allow the lab assistant enough time to stop the test and remove sensors attached to the sample. It is important that the indicator in the velocity behaviour occurs at a late stage of the compressive strength test to allow for as much of the linear elastic section of the stress-strain graph to be uninterrupted. The preferred time window in which the indicator should fall was set to 10 s to 30 s before the stress peak. The tested indicators were the peaks of the P- and S-wave velocity, and the last inflection points before the stress peak of the P- and S-wave velocity.

We performed compressive strength tests following the DIN 18141-1:2014 [1] and DIN EN ISO 17892-7:2018 [2] while measuring P- and S-wave velocities, with 35 cylindrical samples. Of those, 21 were Conduro plaster, with 12 having a 50 mm diameter and 9 having a 30 mm diameter. The other 14 samples were Cordierite Pearl Gneiss, with 6 having a 50 mm diameter and 8 having a 30 mm diameter. The Gneiss samples could not be pressured until failure, leading to the data gained during the Gneiss compressive strength tests being less meaningful.

After analysing the percentage of compressive strength at which the velocity peaked (PPC) and the time from the velocity peak to the stress peak (TPP) (see table 6.1), both the velocity peak of P- and S-wave are deemed unsuitable as an indicator for sample failure. Neither P-wave nor S-wave velocity showed consistent TPP within the chosen time window of 10 s to 30 s for both Conduro and Gneiss samples (see table 6.1).

The percentage of compressive strength at which the last velocity inflection point before the stress peak occurred (IP) and the associated time from the inflection point to the stress speak (TIP) have proven to be far more consistent than the velocity peaks (see table 6.2). The inflection point of the P-wave velocity occurs at inconsistent times, showing TIP between 2.9 s and 184.2 s for the Conduro samples and 27.6 s and 154.0 s for the Gneiss samples (see table 6.2). For this reason, the P-wave velocity inflection point is deemed unsuitable as an indicator for sample failure.

The inflection point of the S-wave velocity showed promising TIP for Conduro samples with times between 2.9 s and 40.5 s, except for one outlier with 136.1 s, for the Conduro samples and 2.9 s and 142.2 s for the Gneiss samples. The data from the Gneiss samples is less

meaningful because most samples were not driven to failure. But at times when the velocity showed third-form behaviour, the TIPs were between 2.9 s and 35.6 s.

The one outlier for the Conduro samples occurred due to the smoothed data that did not accurately represent the raw data. With a more sophisticated analysis script, all Conduro samples would fall very close or right into the set time window. For these reasons, the S-wave velocity inflection point is deemed a potentially suitable indicator for sample failure under certain conditions. With the current hydraulic press setup, I can only recommend the S-wave velocity inflection point as an indicator for sample failure for samples that can be driven to failure with a 100 kN pressure plate. The data collected during this thesis only supports the application of the S-wave velocity inflection point as an indicator for very homogeneous materials, such as the used Conduro plaster.

To widen the range of testable samples with the presented experimental setup and to improve the accuracy and amount of data gained during experiments, I suggest using transducers with a broader frequency range, a higher sampling rate, and higher amplitudes. Furthermore, I would recommend an adapter that connects these transducers with the 600 kN pressure plate of the Z600 hydraulic press, which would allow more samples to be driven until failure and to show third-form velocity behaviour.

These hardware changes, paired with a data exporting and analysing workflow that functions during the measurements, would allow for the practical application of the derived indicator for sample failure. An experimental setup that allows for the Syrosonic software and the Z600s TestXperts software to be used from one computer with presets for different samples and a more sophisticated analysing script would decrease the human inputs and improve the usability of the setup and the indicator. An automated analysing and stopping system would allow for a shorter time window since the human reaction time doesn't have to be taken into account.

These changes could allow for the S-wave velocity inflection point to be used as an indicator for sample failure without condition. However, more research with different materials is needed to support that claim.

Acknowledgement

First, I like to thank Prof. Dr. Thomas Bohlen for giving me the opportunity to write an external Bachelors Thesis at the BAW.

Thanks to my supervisors Eberhard Kunz and Dr.-Ing. Julia Götz, for not only guiding me through the intricacies of this interesting thesis topic but also for their unwavering support throughout the experimental and writing phases. They were always ready to answer my questions and assist with any challenges during the experiments and the writing phase. A special thank you to Julia for her meticulous proofreading of my Thesis and her help in navigating the bureaucratic aspects.

Thanks to Alexander Heuser and Florian Keller for all the insights into working with the Z600 Hydraulic Press and handling samples, and thanks to Ralf Anzböck for his instructions regarding sample preparation.

I would like to extend my gratitude to the entire BAW staff for creating a welcoming and supportive working environment, where I always felt at ease.

And last but not least, thanks to my family and friends for supporting me during my studies.

References

[1] *Baugrund - Untersuchung von Gesteinsproben -Teil 1: Bestimmung der einaxial Druckfestigkeit, DIN 18141-1 Normenausschuss Bauwesen (NABau) des Deutschen Institut für Normung e.V.* May 2014.

[2] Normenausschuss Bauwesen (NABau) des Deutschen Institut für Normung e.V. *Geotechnische Erkundung und Untersuchung - Laborversuche an Bodenproben - Teil 1 Deutsche Fassung EN ISO 18892-7:2018*. May 2018.

[3] *Electro-Acoustic Transducer - GL Testsystems*. 2023. URL: `http://www.gl-testsystems.com/de/Syrosonic/articles/Syrosonic_TecDaten.html`.

[4] G. Gottstein. *Materialwissenschaft und Werkstofftechnik Physikalische Grundlagen*. 4th ed. 2014. ISBN: 978-3-642-36603-1.

[5] L. Griffiths et al. "Quantification of microcrack characteristics and implications for stiffness and strength of granite". In: *International Journal of Rock Mechanics and Mining Sciences* 100 (2017).

[6] Z. D. Jastrzebski. *Nature and properties of engineering materials*. 1959.

[7] R. L. Kranz. "Microcracks in rock: A review". In: *International Journal of Rock Mechanics and Mining Sciences & Geomechanics Abstracts* 100 (June 1983), pp. 449–480.

[8] L. Mittelbach, H. Konietzky, and L. Baumgarten. "Ultraschallmessungen bei Triaxialversuchen - Laborversuche und numerische Simulation". In: *BAW Mitteilung Nr. 95 2012* (2012), pp. 70–78.

[9] T. Mutschler. *Neufassung der Empfehlung Nr. 1 des Arbeitskreises „Versuchstechnik Fels" der Deutschen Gesellschaft für Geotechnik e. V.: Einaxiale Druckversuche an zylindrischen Gesteinsprüfkörpern*. 2004, pp. 825–834.

[10] W. H. Prosser. "Stress dependence of ultrasonic velocity in unidirectional graphite/epoxy composites for longitudinal waves propagating along the direction of stress". In: *Review of Progress in Quantitative Nondestructive Evaluation* 9 (June 1990), pp. 1701–1707.

[11] S. I. Rokhlin. *Determination of residual stress in composite materials using ultrasonic waves*. Tech. rep. 1997.

[12] P. M. Shearer. *Introduction to Seismology: The wave equation and body waves*. University of California, San Diego, June 2010.

[13] G. Simmons et al. "Microcracks in rock". In: *The Physics and Chemistry of Minerals and Rocks* (1976).

[14] S. Stein and M. Wysession. *An Introduction to Seismology, Earthquakes, and Earth Structure*. 2003. ISBN: 0 865 42078 5.

[15] J. A. Studer and M. G. Koller. *Bodendynamik - Grundlagen, Kennziffern, Probleme*. Vol. 2. 1997. ISBN: 3-540-62446-5.

[16] *Syrosonic - ultrasonic device*. 2023. URL: https://www.gl-testsystems.com/en/Syrosonic_EN.html.

[17] *Vorteile und Merkmale der Z600*. 2023. URL: https://www.zwickroell.com/de/produkte/statische-material%20pruefmaschinen/universalpruefmaschinen-fuer-statische-anwendungen/materialpruefmaschine-mit-hydraulikantrieb/.

Eidesstattliche Versicherung

Hiermit versichere ich an Eides statt, dass ich die vorliegende Arbeit im Studiengang Geophysik selbstständig verfasst und keine anderen als die angegebenen Hilfsmittel – insbesondere keine im Quellenverzeichnis nicht benannten Internet-Quellen – benutzt habe. Alle Stellen, die wörtlich oder sinngemäß aus Veröffentlichungen entnommen wurden, sind als solche kenntlich gemacht. Ich versichere weiterhin, dass ich die Arbeit vorher nicht in einem anderen Prüfungsverfahren eingereicht habe und die eingereichte schriftliche Fassung der auf dem elektronischen Speichermedium entspricht.

Einer Veröffentlichung der vorliegenden Arbeit in der zuständigen Fachbibliothek des Fachbereichs stimme ich zu.

Karlsruhe, den _____ Unterschrift: _____

Anhang

Conduro Plaster 50 mm Diameter

PPC and TPP

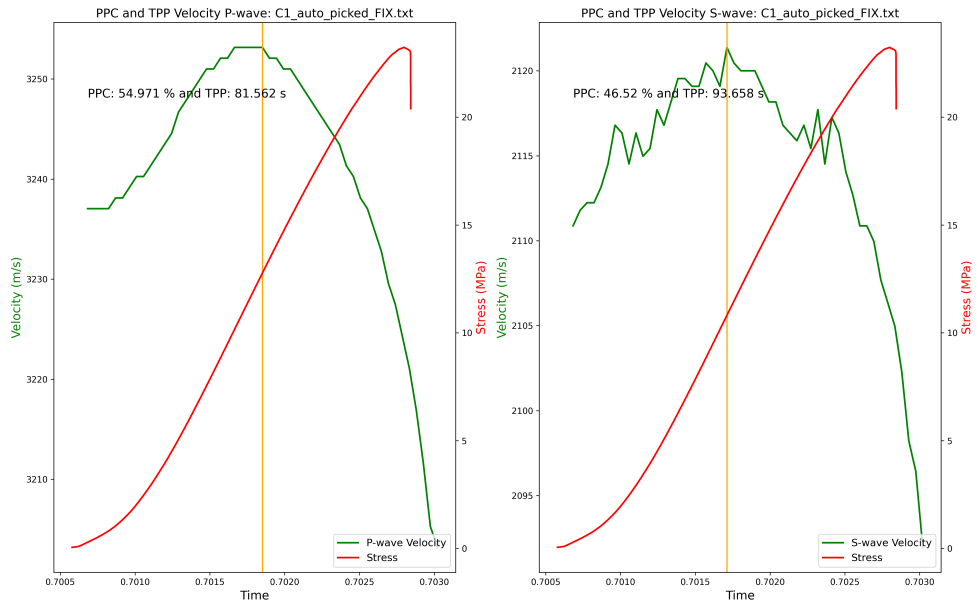

Figure 1: P- and S-wave velocity (green) and stress (red) plotted over the time of the "C1" test. With the PPC being P-wave: 54.971 % and S-wave: 46.52 % and the TPP being P-wave: 81.562 s and S-wave: 93.658 s.

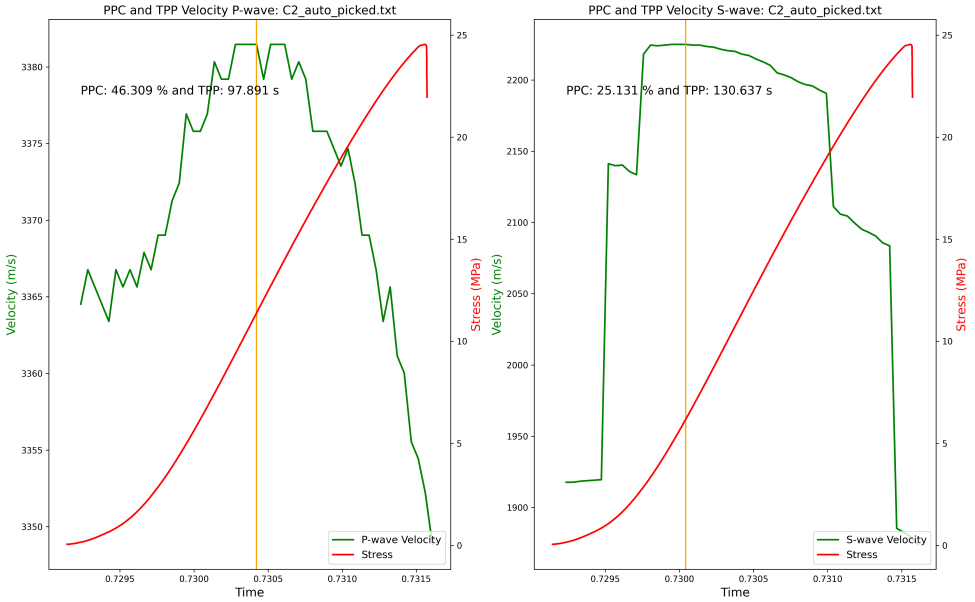

Figure 2: P- and S-wave velocity (green) and stress (red) plotted over the time of the "C2" test. With the PPC being P-wave: 46.309 % and S-wave: 25.131 % and the TPP being P-wave: 97.891 and S-wave: 130.637 s.

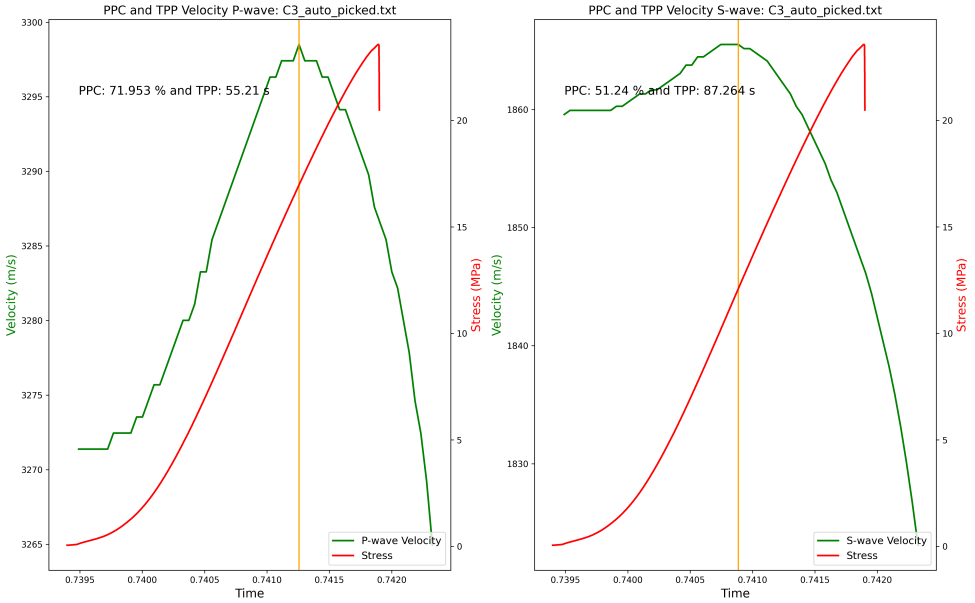

Figure 3: P- and S-wave velocity (green) and stress (red) plotted over the time of the "C3" test. With the PPC being P-wave: 71.953 % and S-wave: 51.24 % and the TPP being P-wave: 55.21 s and S-wave: 87.264 s.

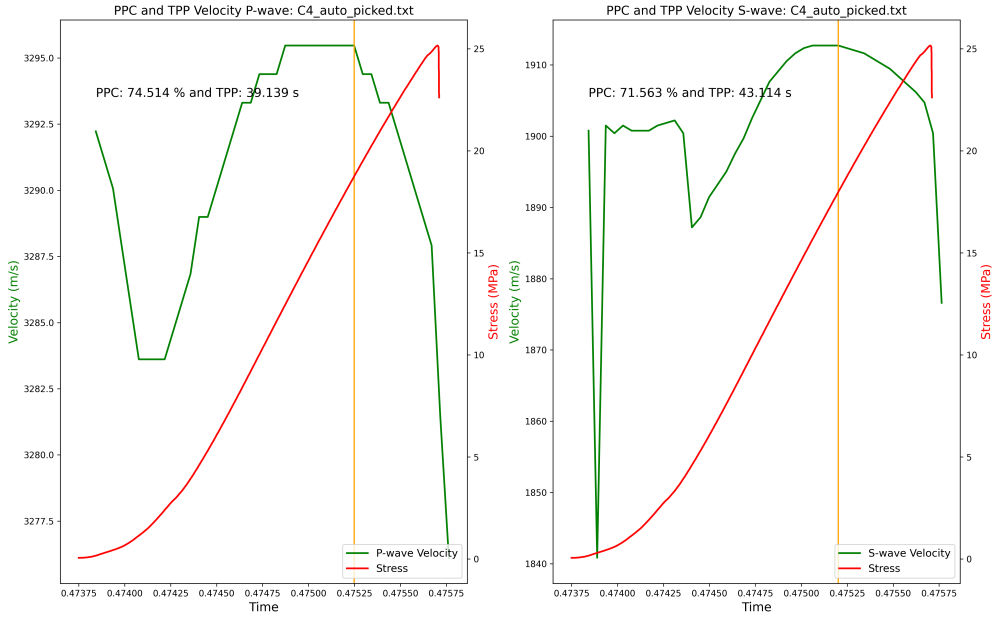

Figure 4: P- and S-wave velocity (green) and stress (red) plotted over the time of the "C4" test. With the PPC being P-wave: 74.514 % and S-wave: 71.563 % and the TPP being P-wave: 39.139 s and S-wave: 43.114 s.

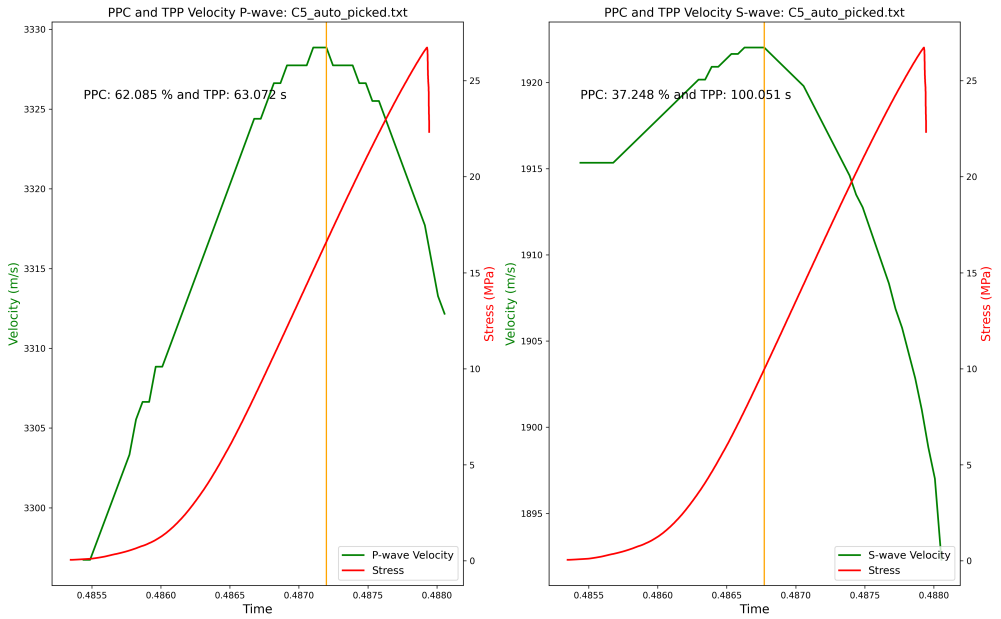

Figure 5: P- and S-wave velocity (green) and stress (red) plotted over the time of the "C5" test. With the PPC being P-wave: 62.085 % and S-wave: 37.248 % and the TPP being P-wave: 63.072 s and S-wave: 100.051 s.

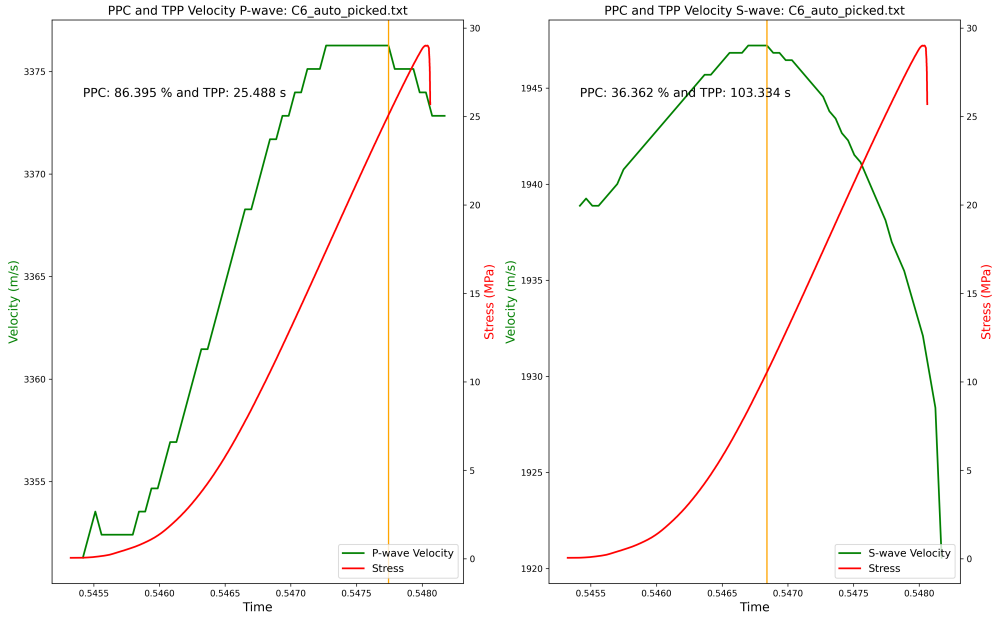

Figure 6: P- and S-wave velocity (green) and stress (red) plotted over the time of the "C6" test. With the PPC being P-wave: 86.395 % and S-wave: 36.362 % and the TPP being P-wave: 25.488 s and S-wave: 103.334 s.

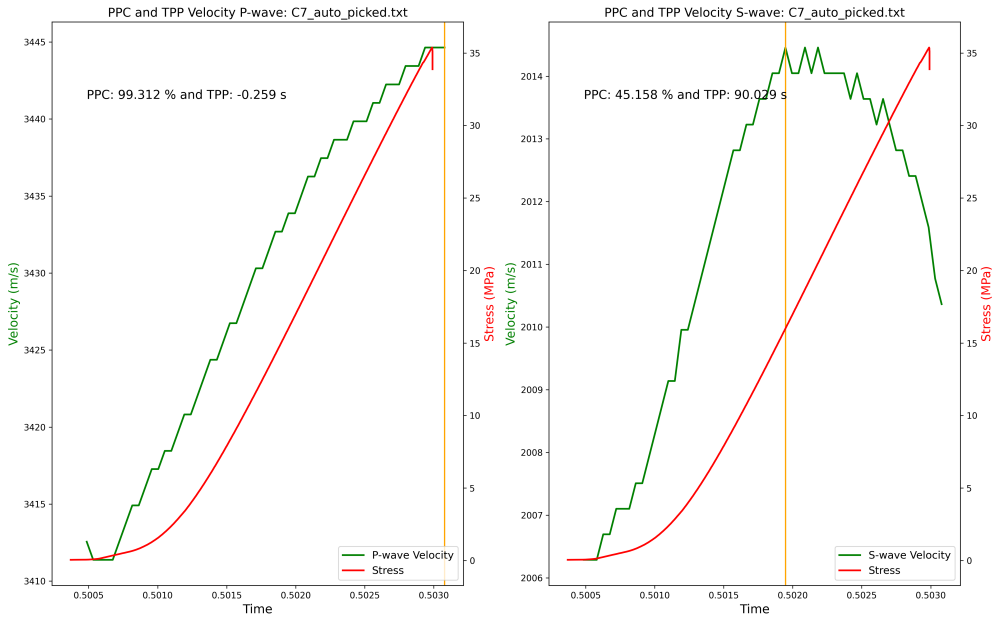

Figure 7: P- and S-wave velocity (green) and stress (red) plotted over the time of the "C7" test. With the PPC being P-wave: 99.312 % and S-wave: 45.158 % and the TPP being P-wave: -0.259 s and S-wave: 90.029 s.

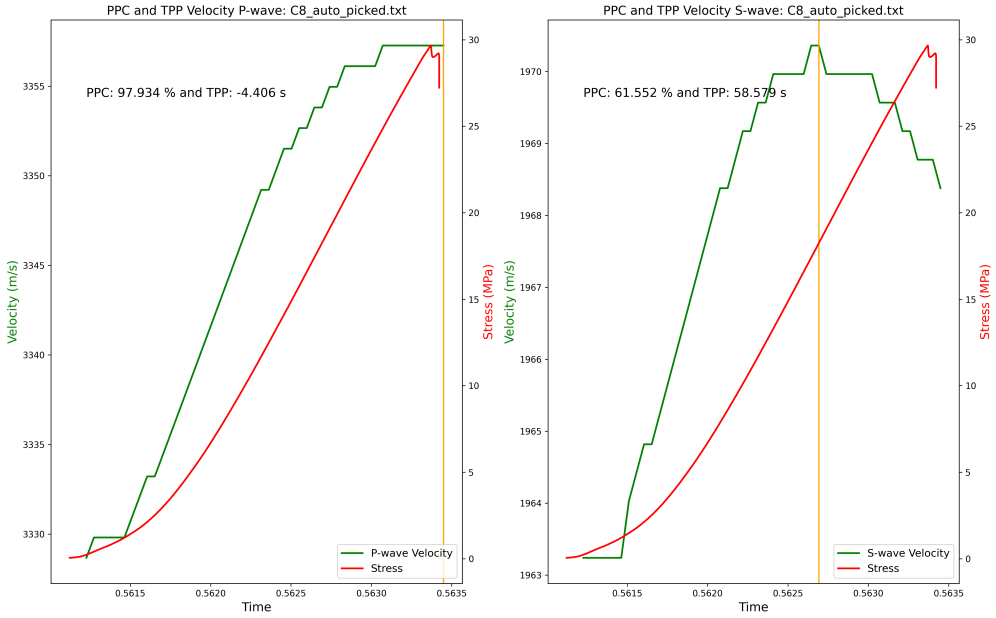

Figure 8: P- and S-wave velocity (green) and stress (red) plotted over the time of the "C8" test. With the PPC being P-wave: 97.934 % and S-wave: 61.552 % and the TPP being P-wave: -4.406 s and S-wave: 58.579 s.

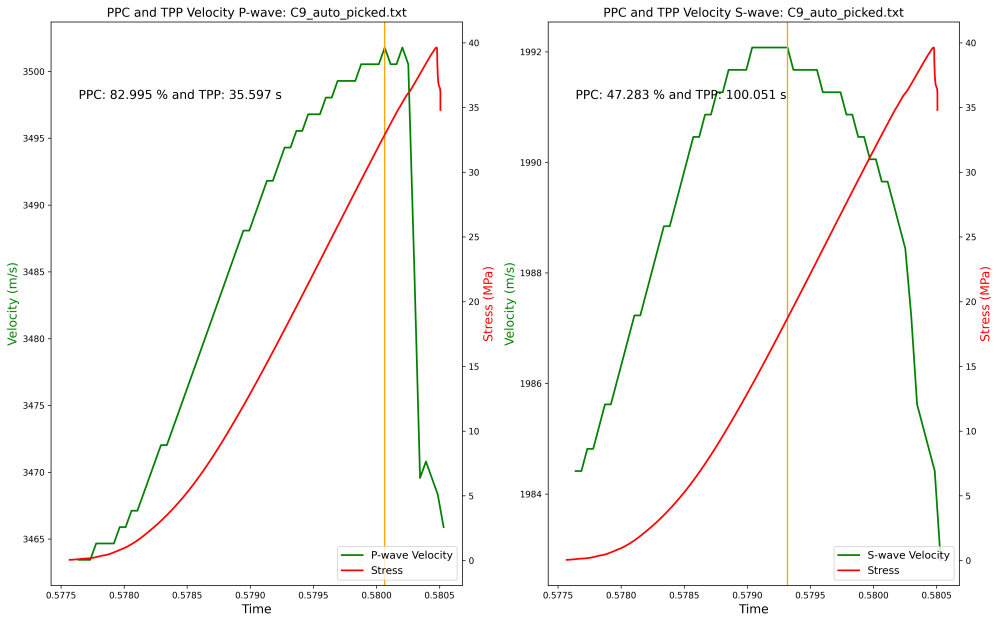

Figure 9: P- and S-wave velocity (green) and stress (red) plotted over the time of the "C9" test. With the PPC being P-wave: 82.995 % and S-wave: 47.283 % and the TPP being P-wave: 35.597 s and S-wave: 100.051 s.

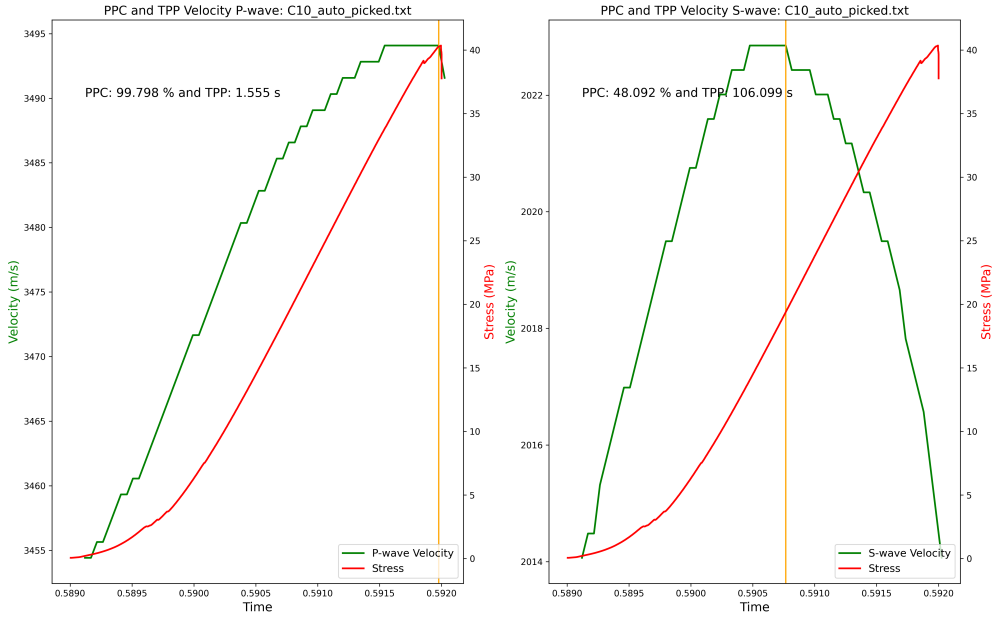

Figure 10: P- and S-wave velocity (green) and stress (red) plotted over the time of the "C10" test. Last two ticks were cut due to them corrupting the data. With the PPC being P-wave: 99.798 % and S-wave: 48.092 % and the TPP being P-wave: 1.555 s and S-wave: 106.099 s.

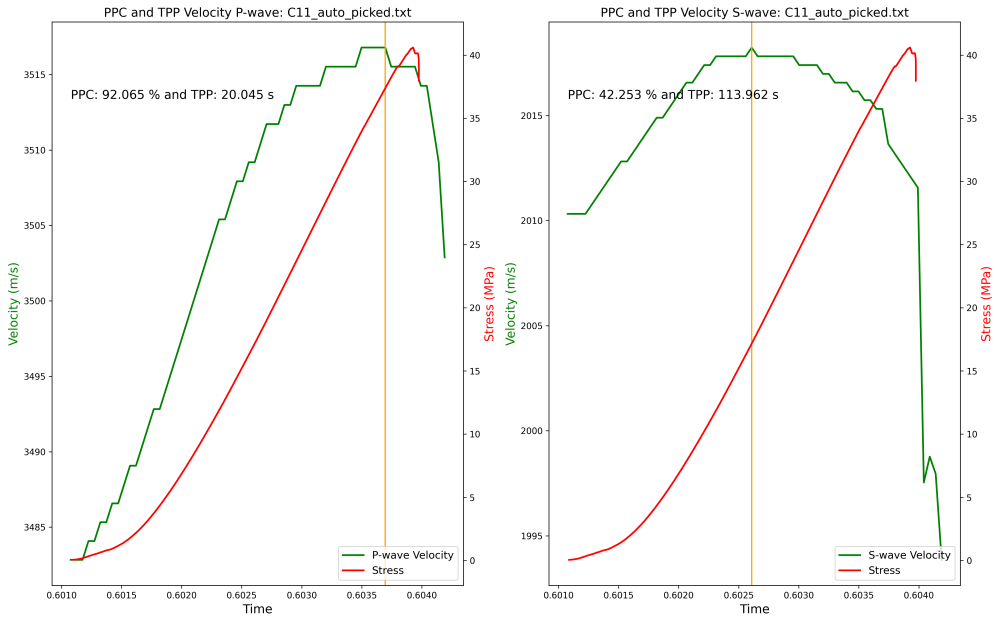

Figure 11: P- and S-wave velocity (green) and stress (red) plotted over the time of the "C11" test. With the PPC being P-wave: 92.065 % and S-wave: 42.253 % and the TPP being P-wave: 20.045 s and S-wave: 113.962 s.

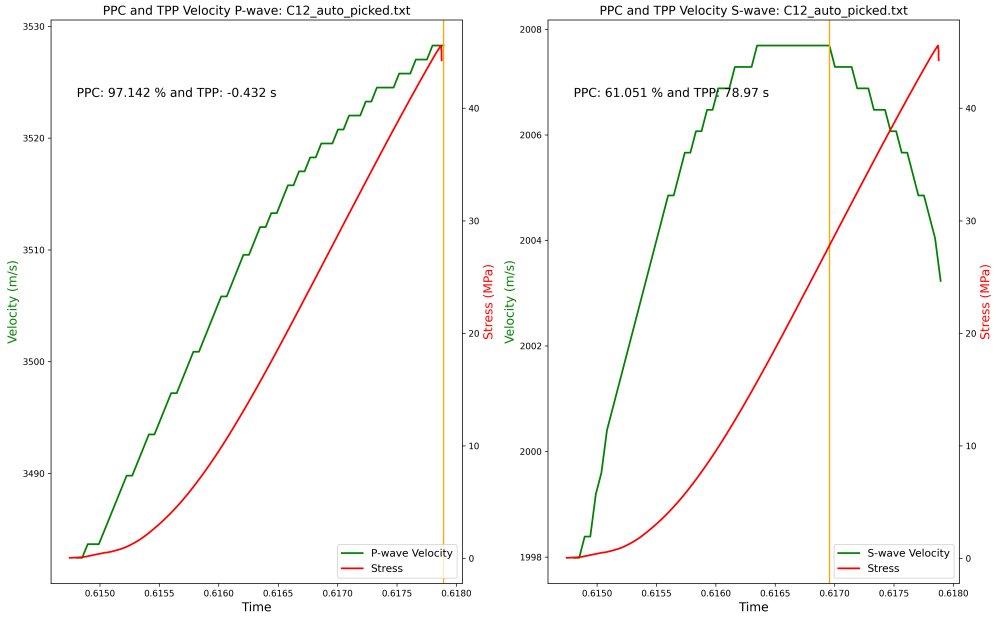

Figure 12: P- and S-wave velocity (green) and stress (red) plotted over the time of the "C12" test. With the PPC being P-wave: 97.142 % and S-wave: 61.051 % and the TPP being P-wave: -0.432 s and S-wave: 78.97 s.

IP and TIP

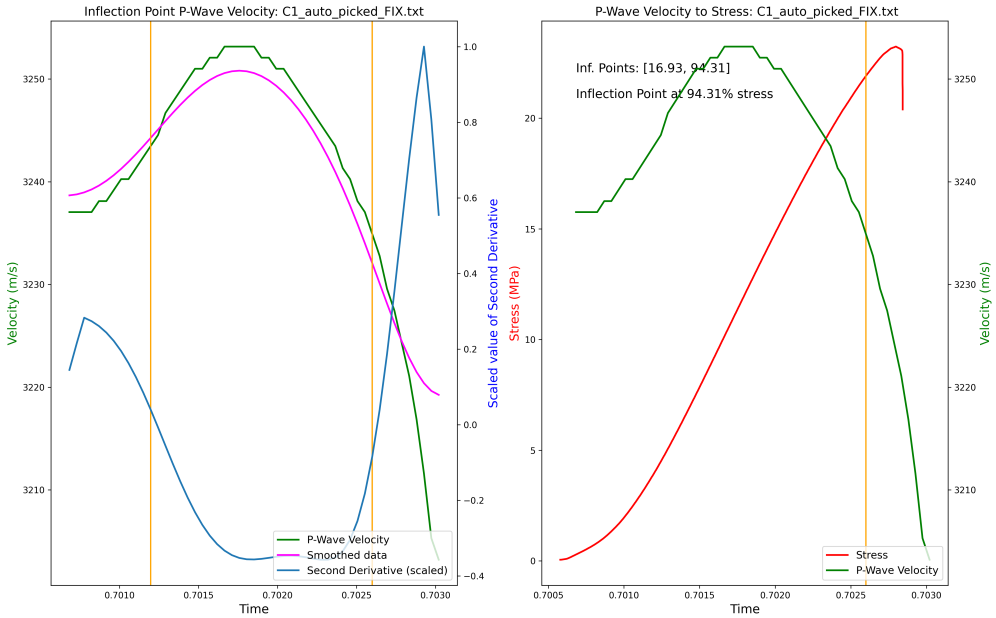

Figure 13: The **left** graph shows the P-wave velocity of the "C 1" sample (green), the velocity data smoothed by a Gaussian filter (magenta), the second derivative of the smoothed data (blue), and the inflection point of the smoothed data (orange vertical line). The **right** graph shows stress (red) and velocity (green) over the time of the test. The last IP is at 94.31 % with a TIP of 16.9 s.

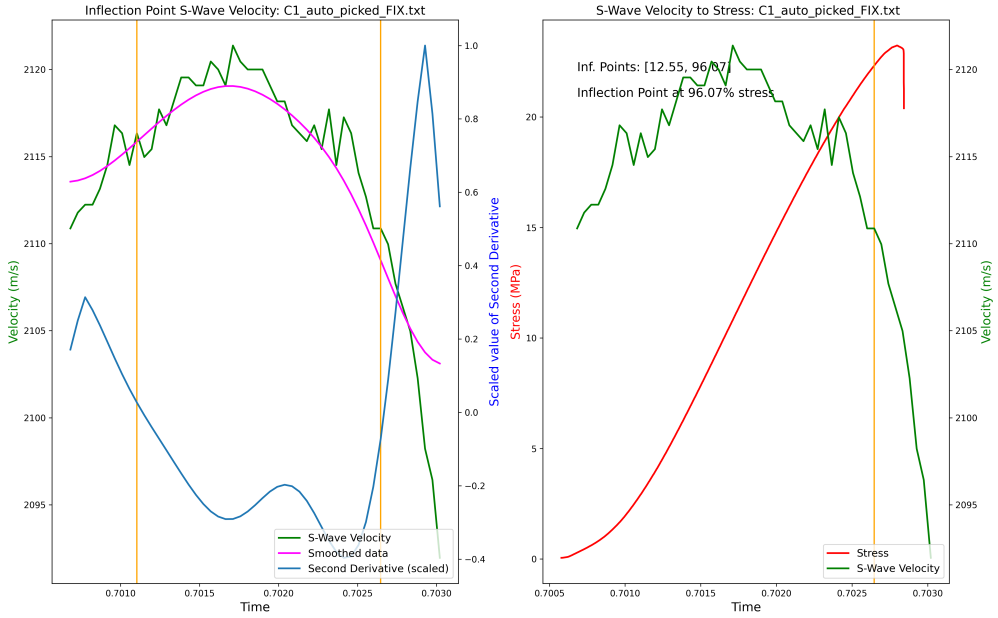

Figure 14: The **left** graph shows the S-wave velocity of the "C 1" sample (green), the velocity data smoothed by a Gaussian filter (magenta), the second derivative of the smoothed data (blue), and the inflection point of the smoothed data (orange vertical line). The **right** graph shows stress (red) and velocity (green) over the time of the test. The last IP is at 96.07 % with a TIP of 12.9 s.

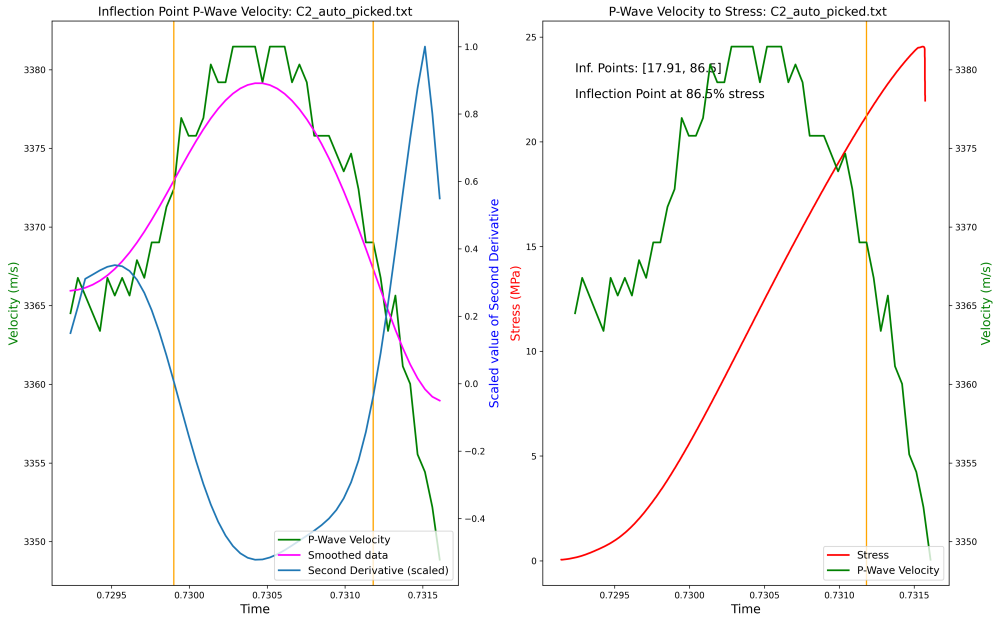

Figure 15: The **left** graph shows the P-wave velocity of the "C 2" sample (green), the velocity data smoothed by a Gaussian filter (magenta), the second derivative of the smoothed data (blue), and the inflection point of the smoothed data (orange vertical line). The **right** graph shows stress (red) and velocity (green) over the time of the test. The last IP is at 86.5 % with a TIP of 32.2 s.

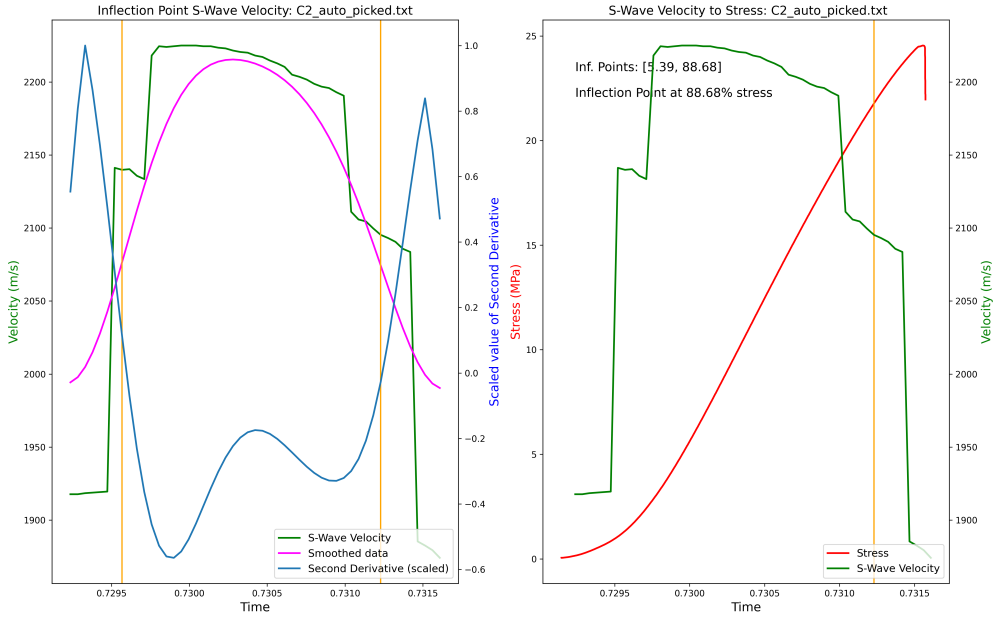

Figure 16: The **left** graph shows the S-wave velocity of the "C 2" sample (green), the velocity data smoothed by a Gaussian filter (magenta), the second derivative of the smoothed data (blue), and the inflection point of the smoothed data (orange vertical line). The **right** graph shows stress (red) and velocity (green) over the time of the test. The last IP is at 88.69 % with a TIP of 28.1 s.

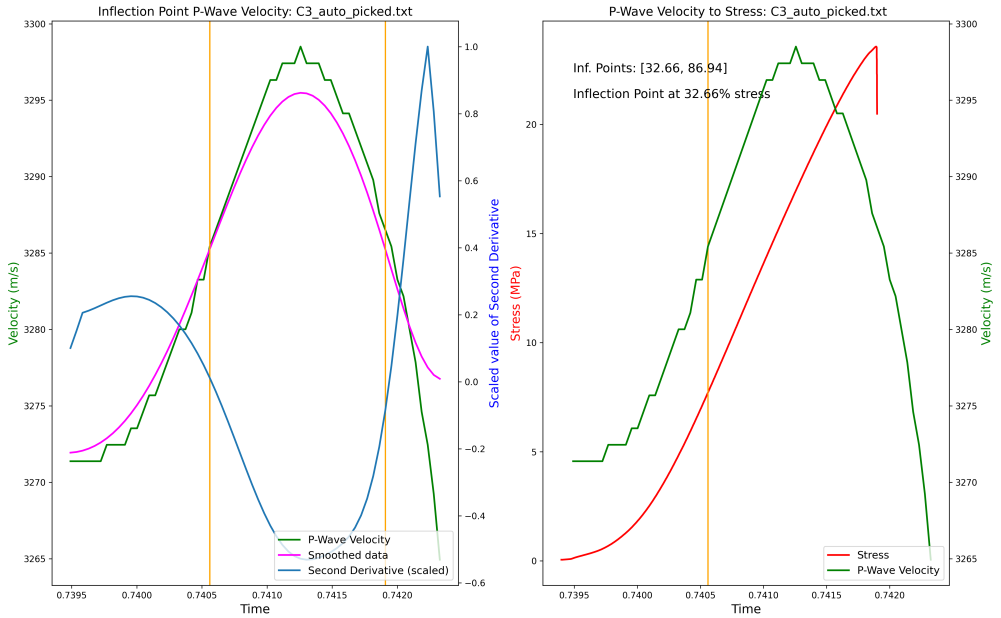

Figure 17: The **left** graph shows the P-wave velocity of the "C 3" sample (green), the velocity data smoothed by a Gaussian filter (magenta), the second derivative of the smoothed data (blue), and the inflection point of the smoothed data (orange vertical line). The **right** graph shows stress (red) and velocity (green) over the time of the test. The last IP is at 32.66 % with a TIP of 115.4 s.

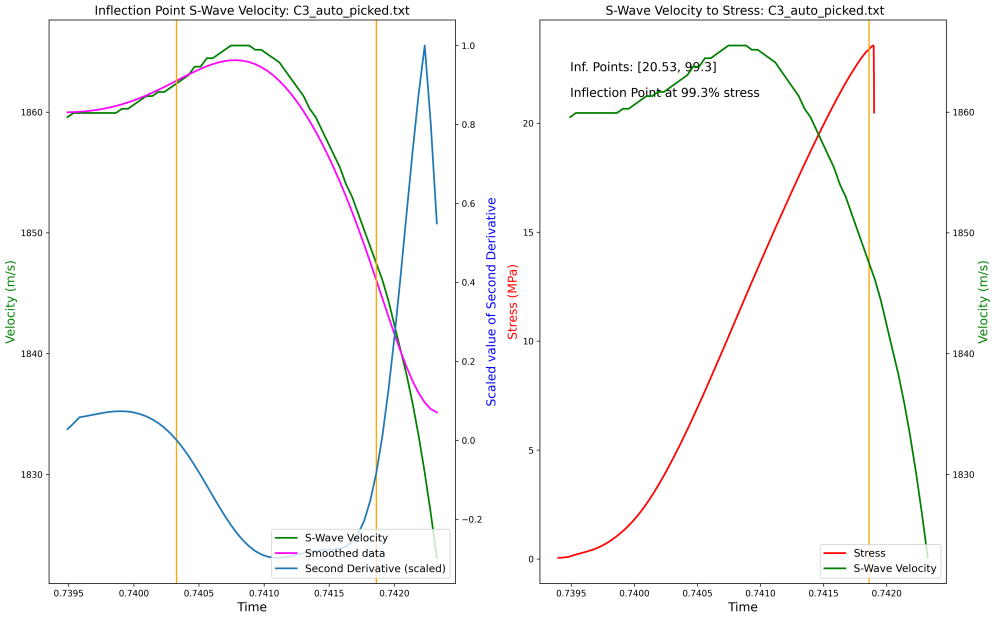

Figure 18: The **left** graph shows the S-wave velocity of the "C 3" sample (green), the velocity data smoothed by a Gaussian filter (magenta), the second derivative of the smoothed data (blue), and the inflection point of the smoothed data (orange vertical line). The **right** graph shows stress (red) and velocity (green) over the time of the test. The last IP is at 99.3 % with a TIP of 2.9 s.

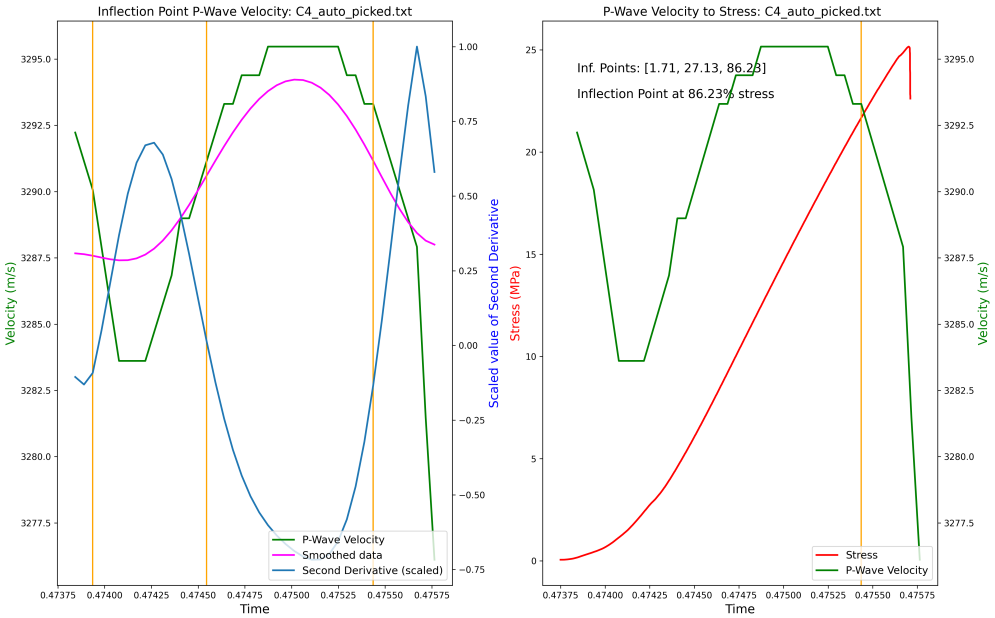

Figure 19: The **left** graph shows the P-wave velocity of the "C 4" sample (green), the velocity data smoothed by a Gaussian filter (magenta), the second derivative of the smoothed data (blue), and the inflection point of the smoothed data (orange vertical line). The **right** graph shows stress (red) and velocity (green) over the time of the test. The last IP is at 86.23 % with a TIP of 23.0 s.

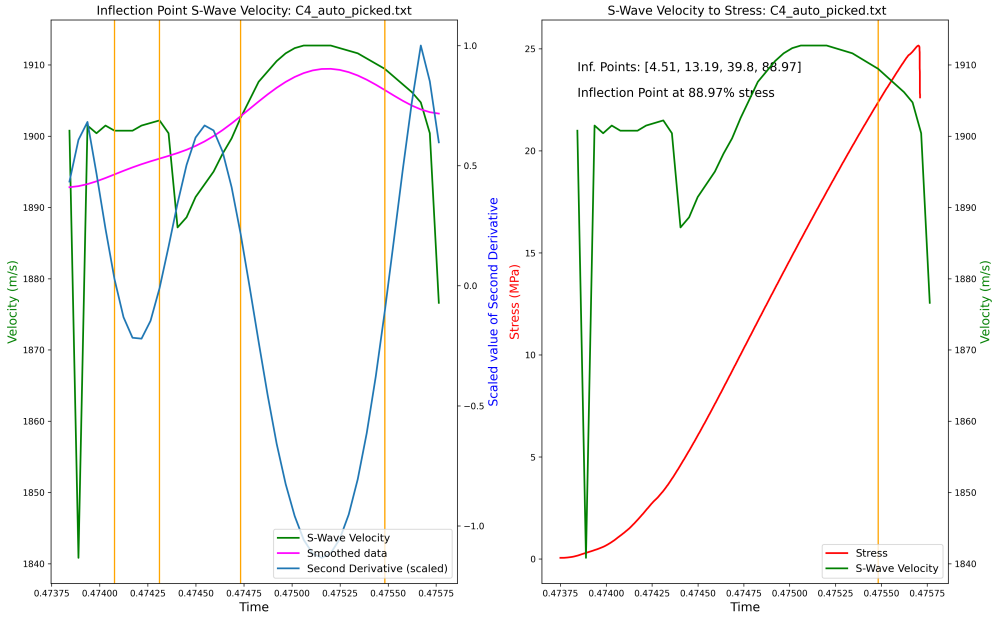

Figure 20: The **left** graph shows the S-wave velocity of the "C 4" sample (green), the velocity data smoothed by a Gaussian filter (magenta), the second derivative of the smoothed data (blue), and the inflection point of the smoothed data (orange vertical line). The **right** graph shows stress (red) and velocity (green) over the time of the test. The last IP is at 88.97 % with a TIP of 18.9 s.

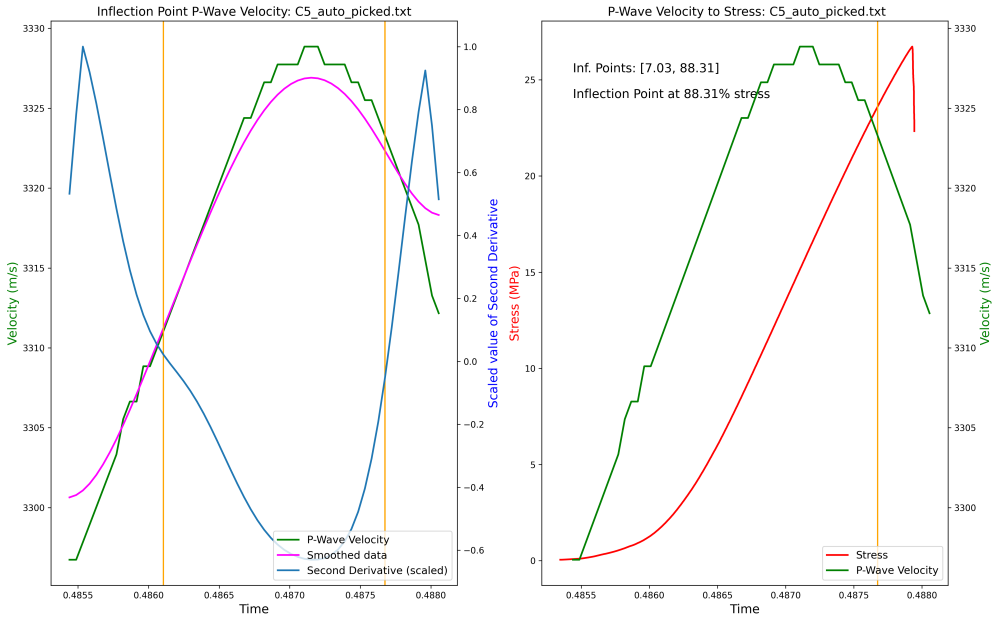

Figure 21: The **left** graph shows the P-wave velocity of the "C 5" sample (green), the velocity data smoothed by a Gaussian filter (magenta), the second derivative of the smoothed data (blue), and the inflection point of the smoothed data (orange vertical line). The **right** graph shows stress (red) and velocity (green) over the time of the test. The last IP is at 88.31 % with a TIP of 21.9 s.

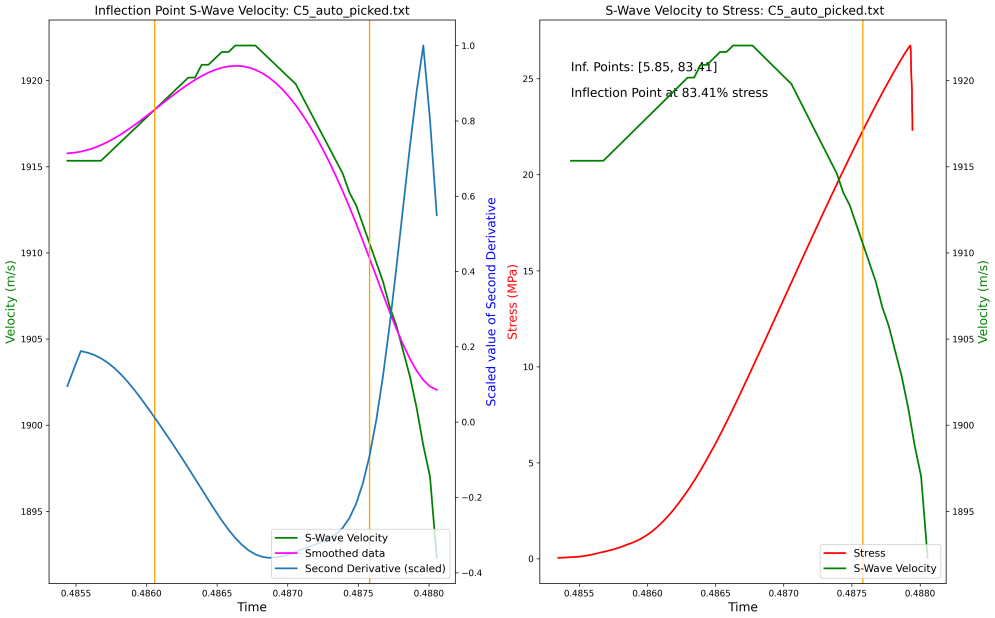

Figure 22: The **left** graph shows the S-wave velocity of the "C 5" sample (green), the velocity data smoothed by a Gaussian filter (magenta), the second derivative of the smoothed data (blue), and the inflection point of the smoothed data (orange vertical line). The **right** graph shows stress (red) and velocity (green) over the time of the test. The last IP is at 83.41 % with a TIP of 30.2 s.

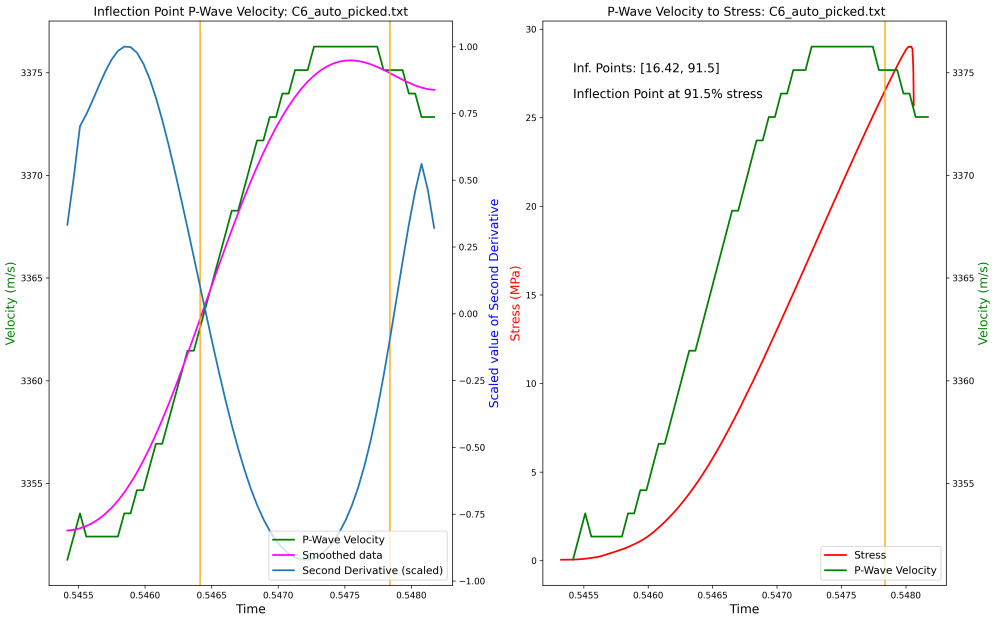

Figure 23: The **left** graph shows the P-wave velocity of the "C 6" sample (green), the velocity data smoothed by a Gaussian filter (magenta), the second derivative of the smoothed data (blue), and the inflection point of the smoothed data (orange vertical line). The **right** graph shows stress (red) and velocity (green) over the time of the test. The last IP is at 91.5 % with a TIP of 17.2 s.

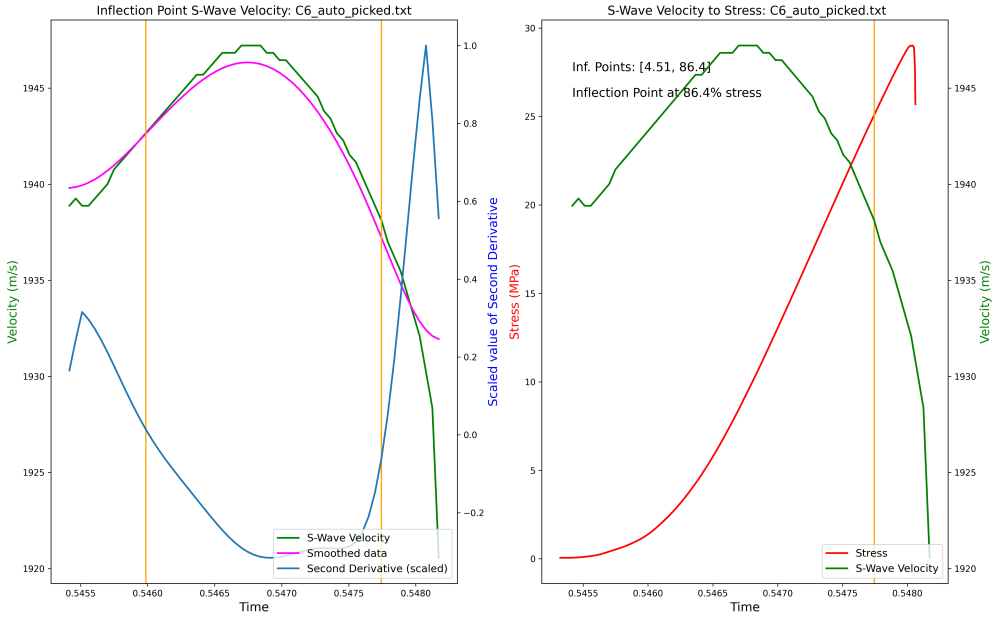

Figure 24: The **left** graph shows the S-wave velocity of the "C 6" sample (green), the velocity data smoothed by a Gaussian filter (magenta), the second derivative of the smoothed data (blue), and the inflection point of the smoothed data (orange vertical line). The **right** graph shows stress (red) and velocity (green) over the time of the test. The last IP is at 86.4 % with a TIP of 25.4 s.

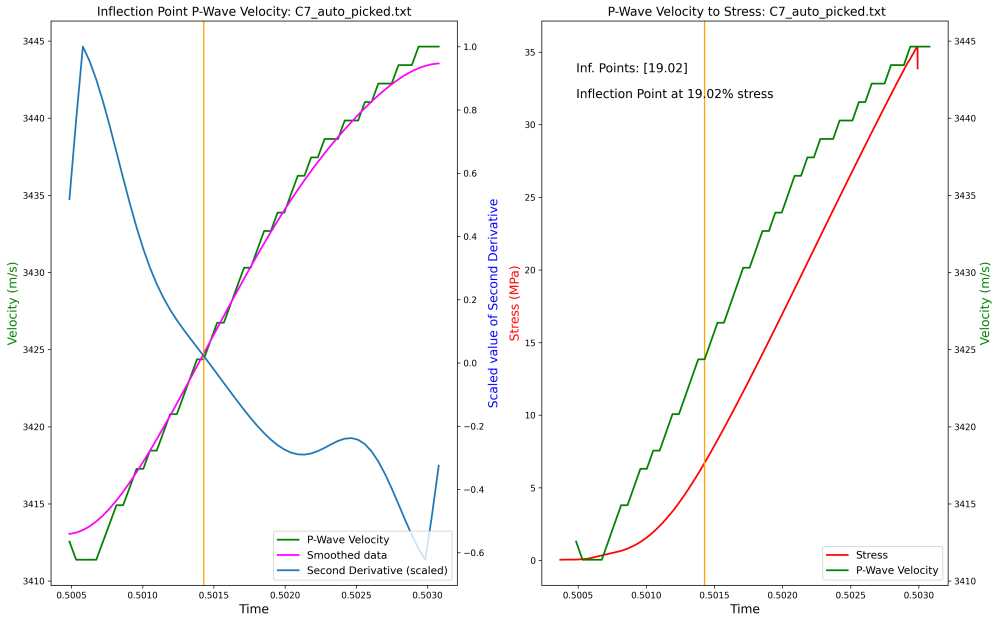

Figure 25: The **left** graph shows the P-wave velocity of the "C 7" sample (green), the velocity data smoothed by a Gaussian filter (magenta), the second derivative of the smoothed data (blue), and the inflection point of the smoothed data (orange vertical line). The **right** graph shows stress (red) and velocity (green) over the time of the test. The last IP is at 19.02 % with a TIP of 134.7 s.

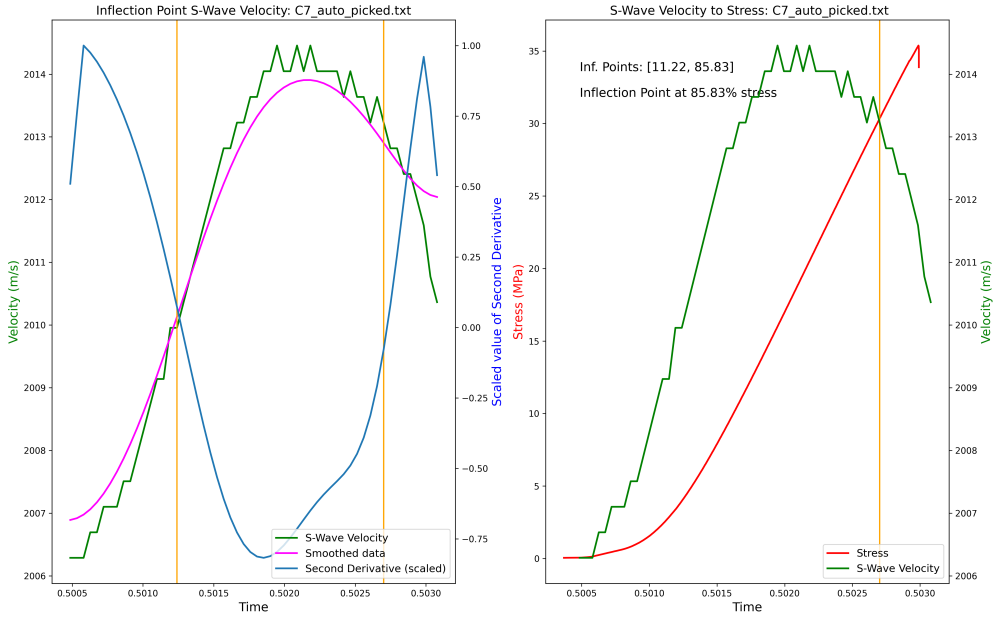

Figure 26: The **left** graph shows the S-wave velocity of the "C 7" sample (green), the velocity data smoothed by a Gaussian filter (magenta), the second derivative of the smoothed data (blue), and the inflection point of the smoothed data (orange vertical line). The **right** graph shows stress (red) and velocity (green) over the time of the test. The last IP is at 85.83 % with a TIP of 24.7 s.

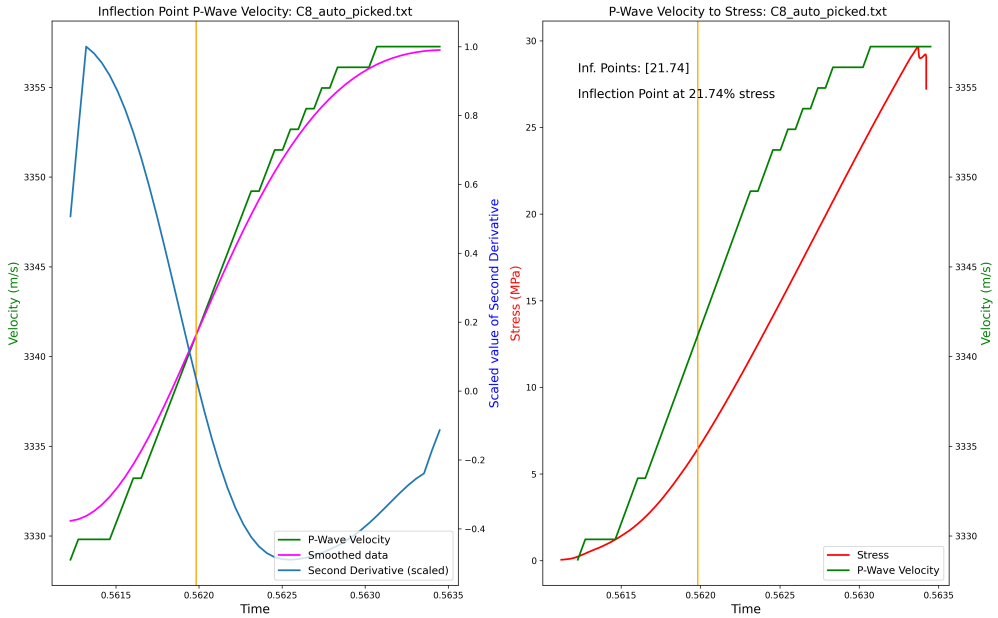

Figure 27: The **left** graph shows the P-wave velocity of the "C 8" sample (green), the velocity data smoothed by a Gaussian filter (magenta), the second derivative of the smoothed data (blue), and the inflection point of the smoothed data (orange vertical line). The **right** graph shows stress (red) and velocity (green) over the time of the test. The last IP is at 21.74 % with a TIP of 119.9 s.

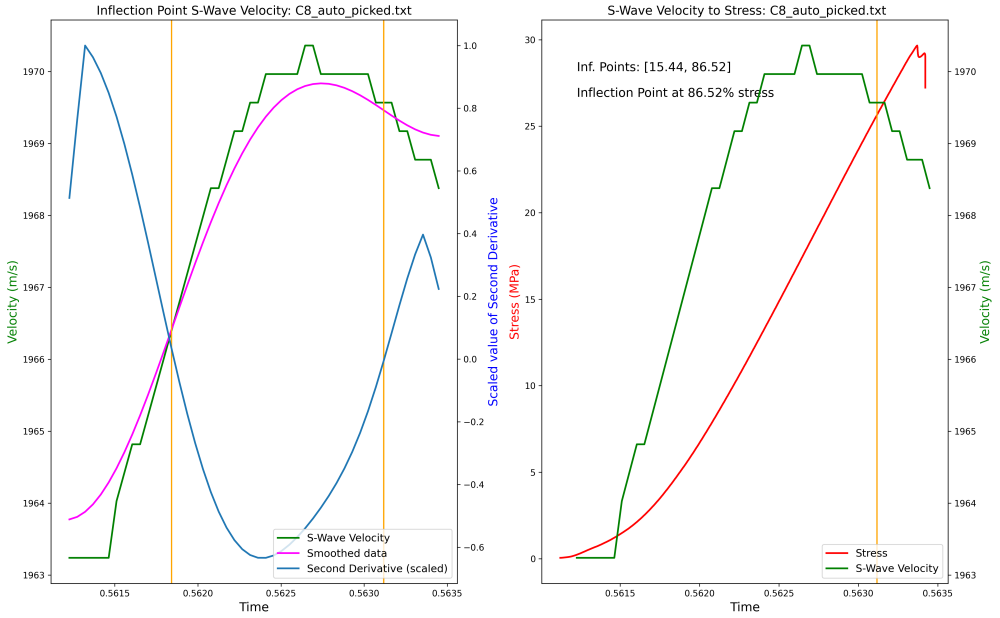

Figure 28: The **left** graph shows the S-wave velocity of the "C 8" sample (green), the velocity data smoothed by a Gaussian filter (magenta), the second derivative of the smoothed data (blue), and the inflection point of the smoothed data (orange vertical line). The **right** graph shows stress (red) and velocity (green) over the time of the test. The last IP is at 86.52 % with a TIP of 21.9 s.

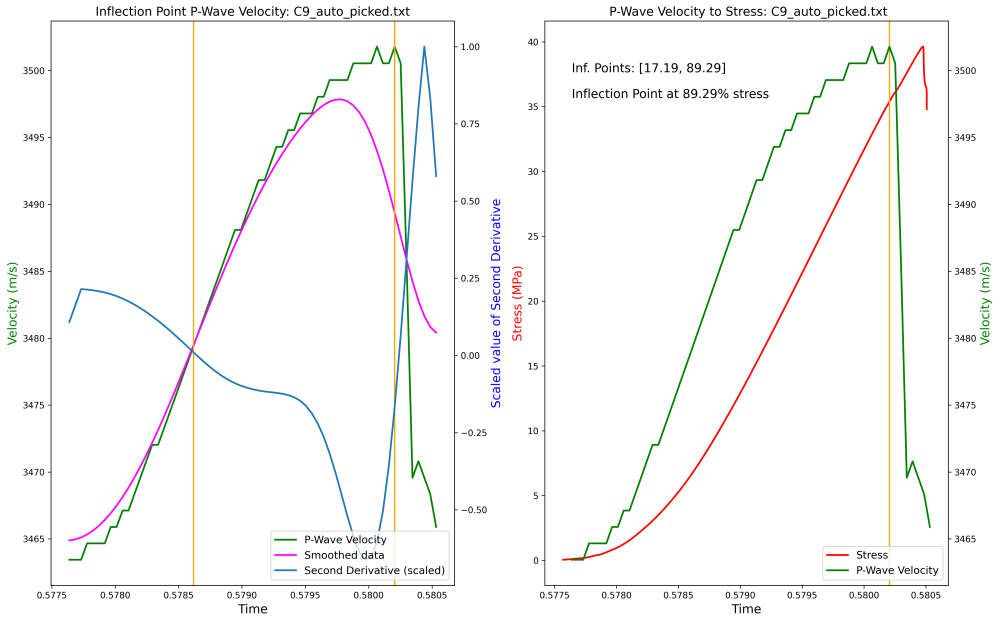

Figure 29: The **left** graph shows the P-wave velocity of the "C 9" sample (green), the velocity data smoothed by a Gaussian filter (magenta), the second derivative of the smoothed data (blue), and the inflection point of the smoothed data (orange vertical line). The **right** graph shows stress (red) and velocity (green) over the time of the test. The last IP is at 89.29 % with a TIP of 23.5 s.

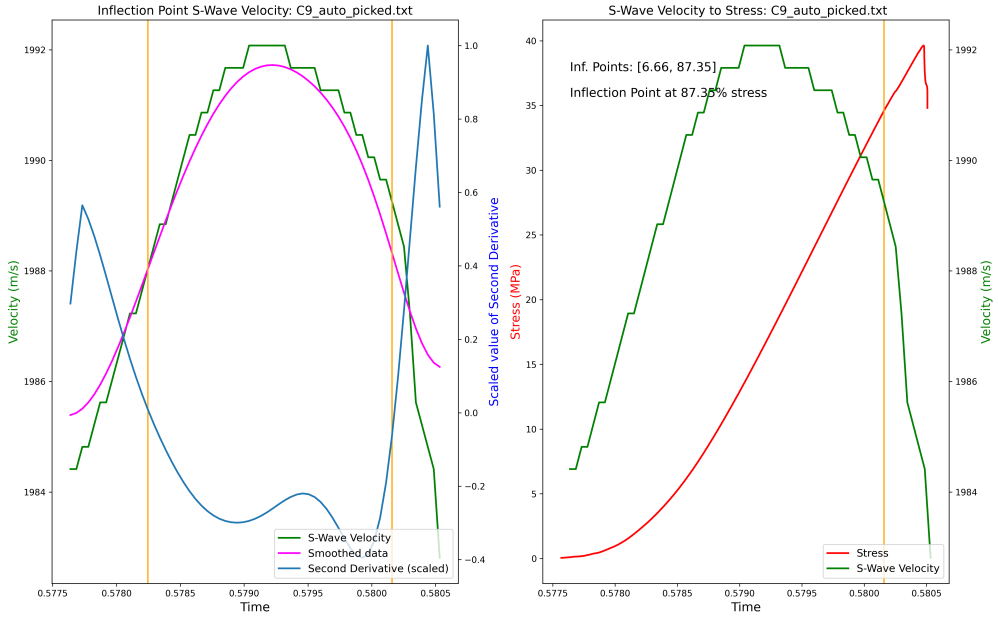

Figure 30: The **left** graph shows the S-wave velocity of the "C 9" sample (green), the velocity data smoothed by a Gaussian filter (magenta), the second derivative of the smoothed data (blue), and the inflection point of the smoothed data (orange vertical line). The **right** graph shows stress (red) and velocity (green) over the time of the test. The last IP is at 87.35 % with a TIP of 27.6 s.

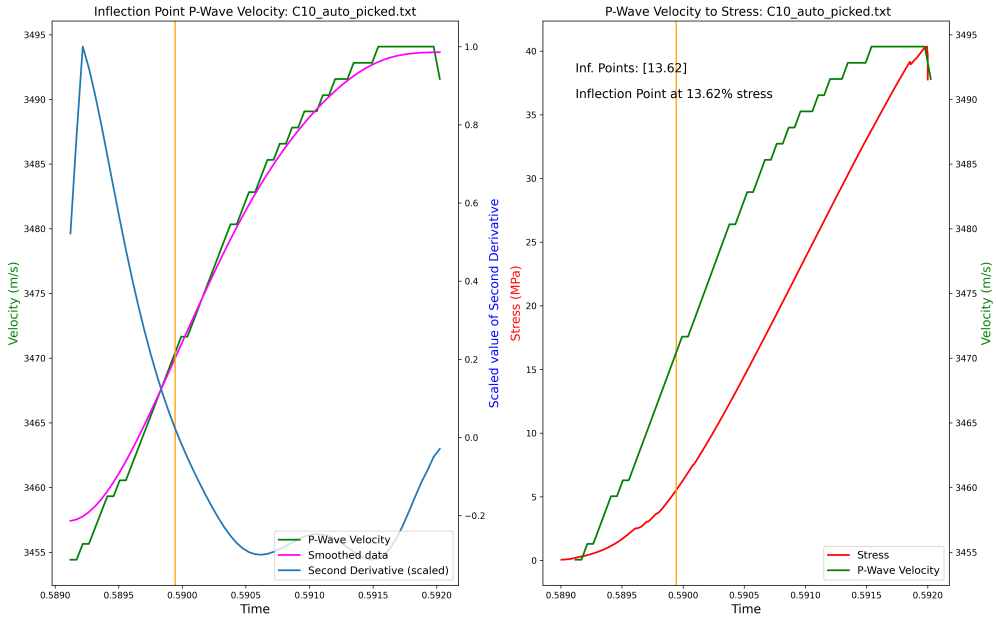

Figure 31: The **left** graph shows the P-wave velocity of the "C 10" sample (green), the velocity data smoothed by a Gaussian filter (magenta), the second derivative of the smoothed data (blue), and the inflection point of the smoothed data (orange vertical line). The **right** graph shows stress (red) and velocity (green) over the time of the test. The last IP is at 13.62 % with a TIP of 177.3 s.

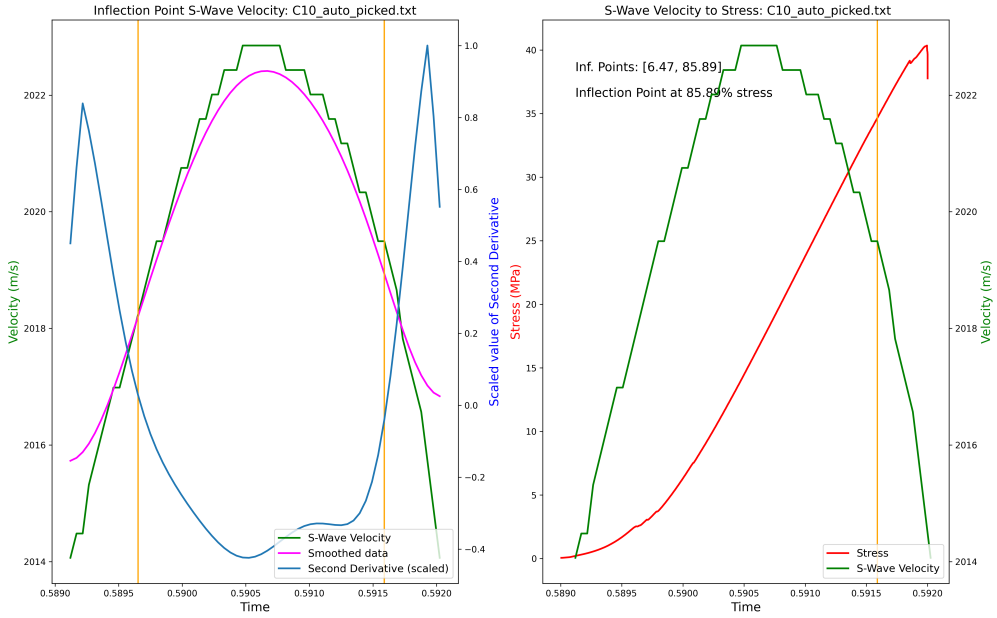

Figure 32: The **left** graph shows the S-wave velocity of the "C 10" sample (green), the velocity data smoothed by a Gaussian filter (magenta), the second derivative of the smoothed data (blue), and the inflection point of the smoothed data (orange vertical line). The **right** graph shows stress (red) and velocity (green) over the time of the test. The last IP is at 85.89 % with a TIP of 35.1 s.

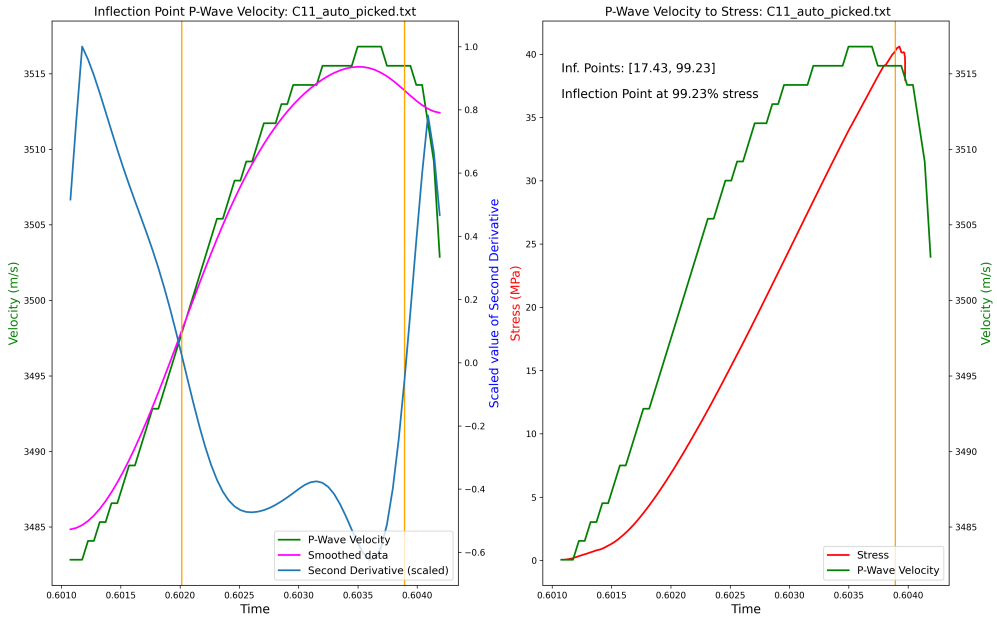

Figure 33: The **left** graph shows the P-wave velocity of the "C 11" sample (green), the velocity data smoothed by a Gaussian filter (magenta), the second derivative of the smoothed data (blue), and the inflection point of the smoothed data (orange vertical line). The **right** graph shows stress (red) and velocity (green) over the time of the test. The last IP is at 99.23 % with a TIP of 2.9 s.

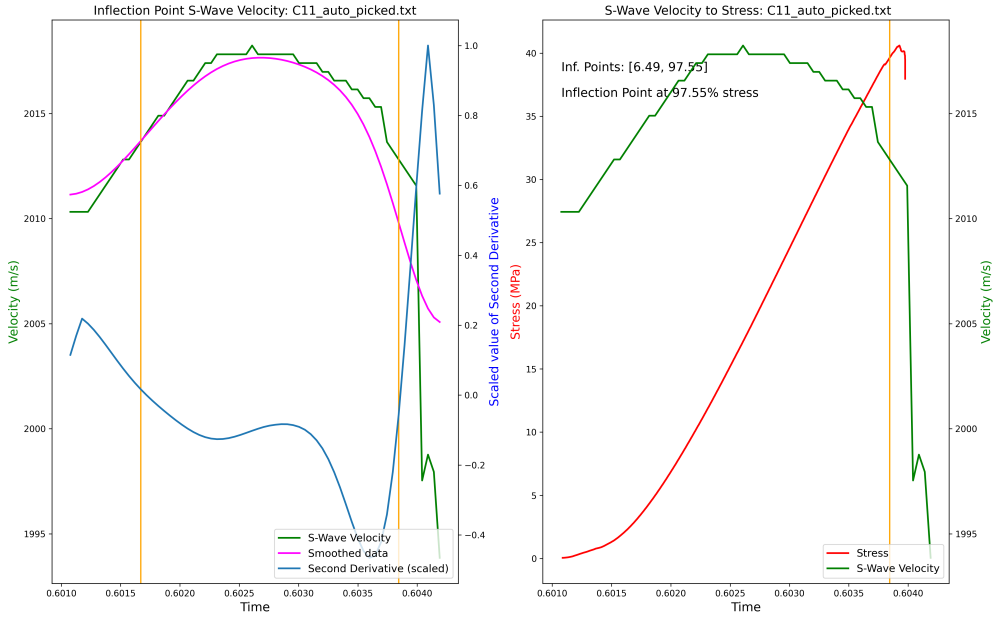

Figure 34: The **left** graph shows the S-wave velocity of the "C 11" sample (green), the velocity data smoothed by a Gaussian filter (magenta), the second derivative of the smoothed data (blue), and the inflection point of the smoothed data (orange vertical line). The **right** graph shows stress (red) and velocity (green) over the time of the test. The last IP is at 97.55 % with a TIP of 7.2 s.

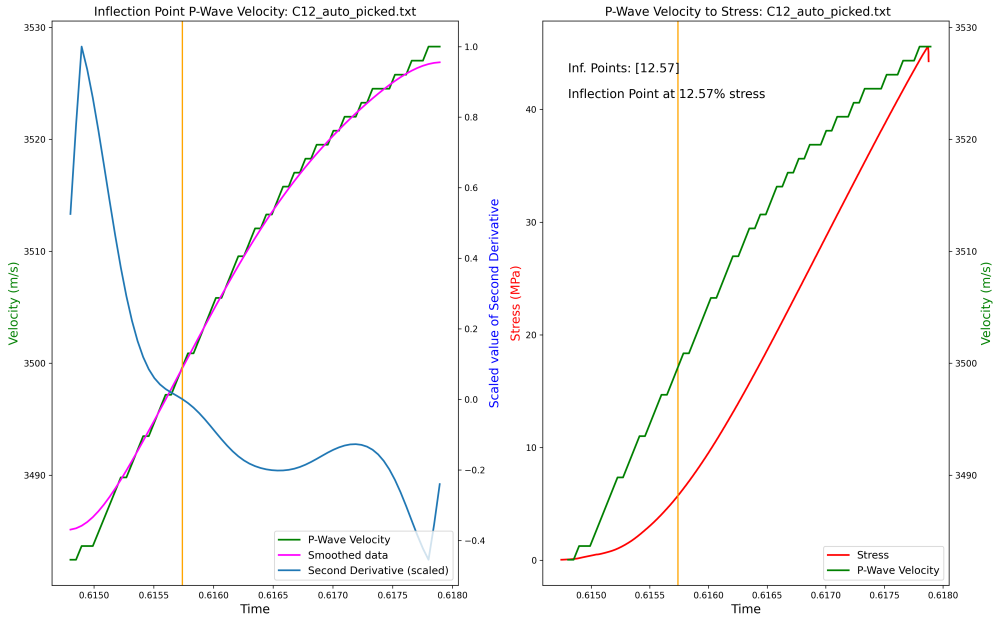

Figure 35: The **left** graph shows the P-wave velocity of the "C 12" sample (green), the velocity data smoothed by a Gaussian filter (magenta), the second derivative of the smoothed data (blue), and the inflection point of the smoothed data (orange vertical line). The **right** graph shows stress (red) and velocity (green) over the time of the test. The last IP is at 12.57 % with a TIP of 184.2 s.

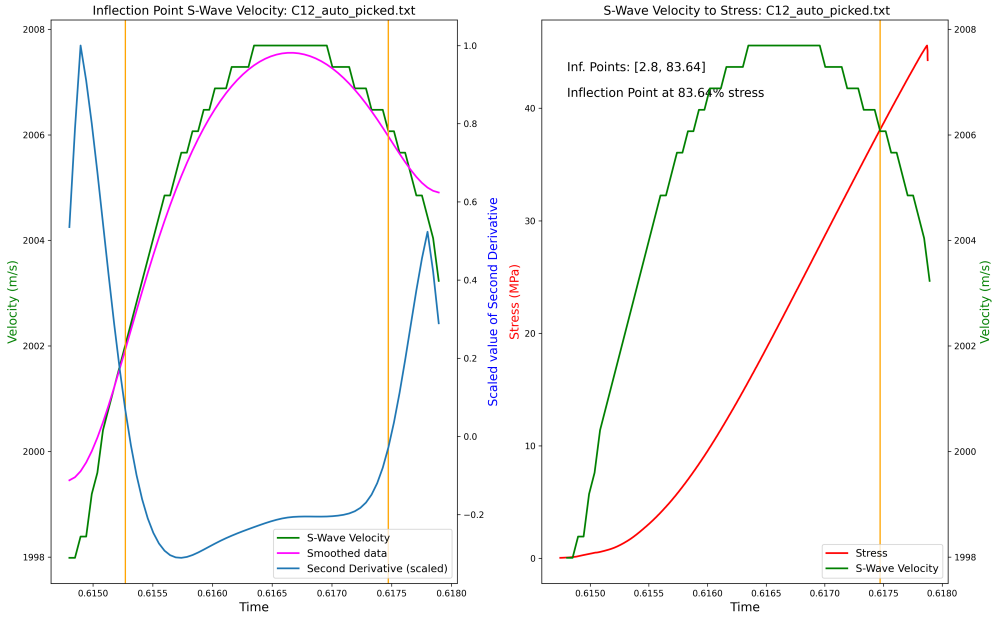

Figure 36: The **left** graph shows the S-wave velocity of the "C 12" sample (green), the velocity data smoothed by a Gaussian filter (magenta), the second derivative of the smoothed data (blue), and the inflection point of the smoothed data (orange vertical line). The **right** graph shows stress (red) and velocity (green) over the time of the test. The last IP is at 83.64 % with a TIP of 34.6 s.

Conduro Plaster 30 mm Diameter

PPC and TPP

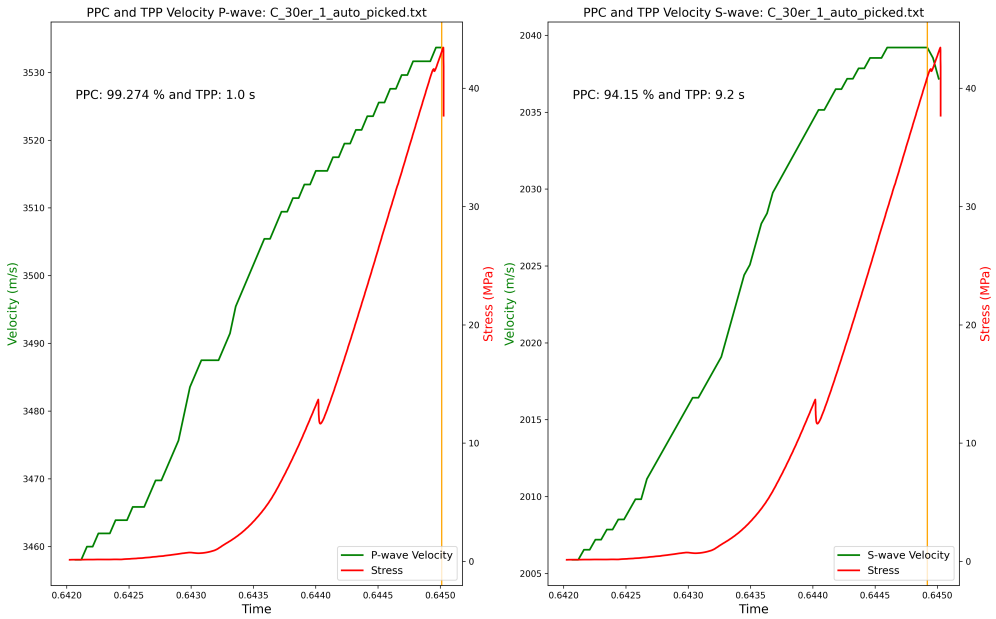

Figure 37: P- and S-wave velocity (green) and stress (red) plotted over the time of the "C 30er 1" test. With the PPC being P-wave: 99.27 % and S-wave: 94.15 % and the TPP being P-wave: 1.0 s and S-wave: 9.2 s.

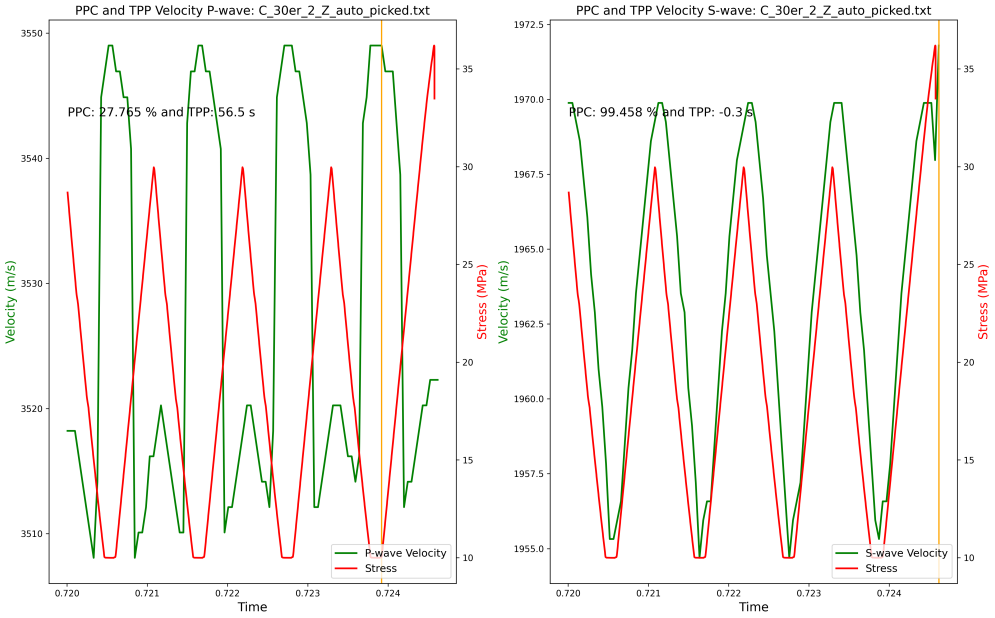

Figure 38: P- and S-wave velocity (green) and stress (red) plotted over last 400 seconds of the cyclic "C 30er 2 Z" test. With the PPC being P-wave: 27.61 % and S-wave: 99.46 % and the TPP being P-wave: 56.5 s and S-wave: -0.3s.

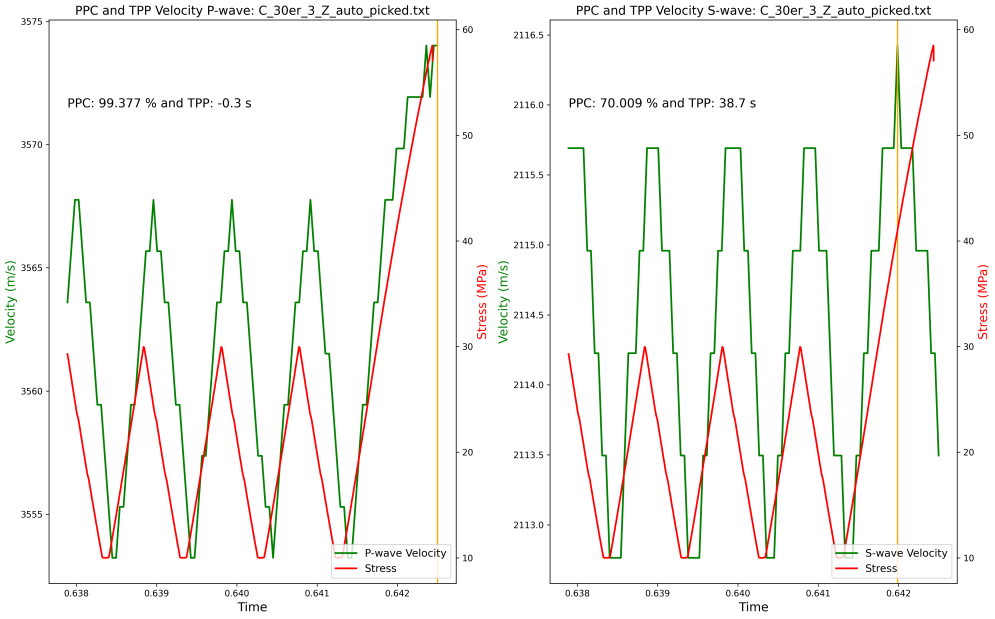

Figure 39: P- and S-wave velocity (green) and stress (red) plotted over last 400 seconds of the cyclic "C 30er 3 Z" test. With the PPC being P-wave: 99.38 % and S-wave: 70.01 % and the TPP being P-wave: -0.3 s and S-wave: 38.7 s.

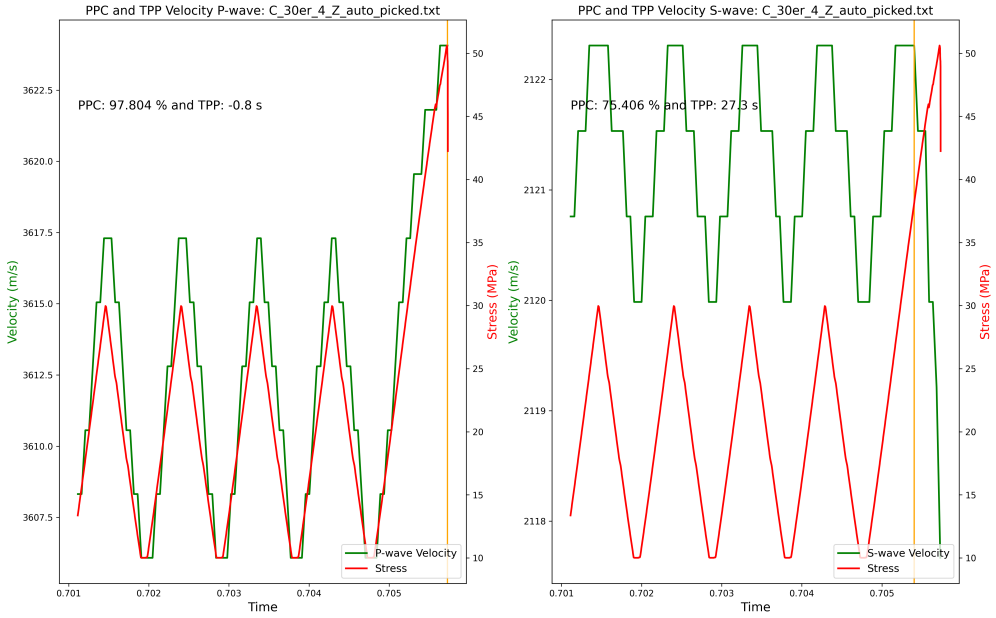

Figure 40: P- and S-wave velocity (green) and stress (red) plotted over last 400 seconds of the cyclic "C 30er 4 Z" test. With the PPC being P-wave: 97.80 % and S-wave: 75.41 % and the TPP being P-wave: -0.8 s and S-wave: 27.3 s.

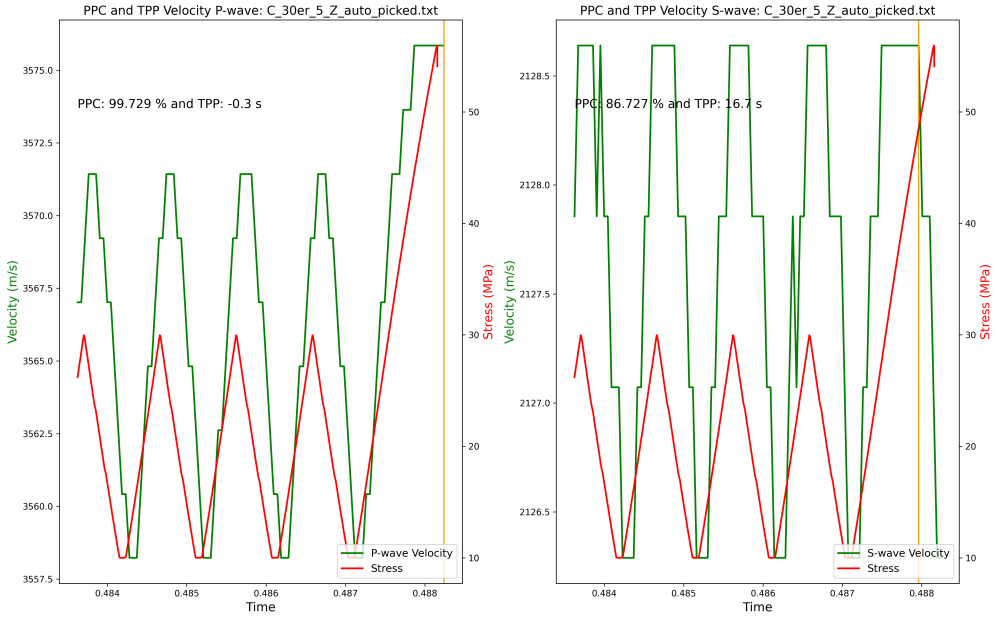

Figure 41: P- and S-wave velocity (green) and stress (red) plotted over last 400 seconds of the cyclic "C 30er 5 Z" test. With the PPC being P-wave: 99.73 % and S-wave: 86.73 % and the TPP being P-wave: -0.3 s and S-wave: 16.7 s.

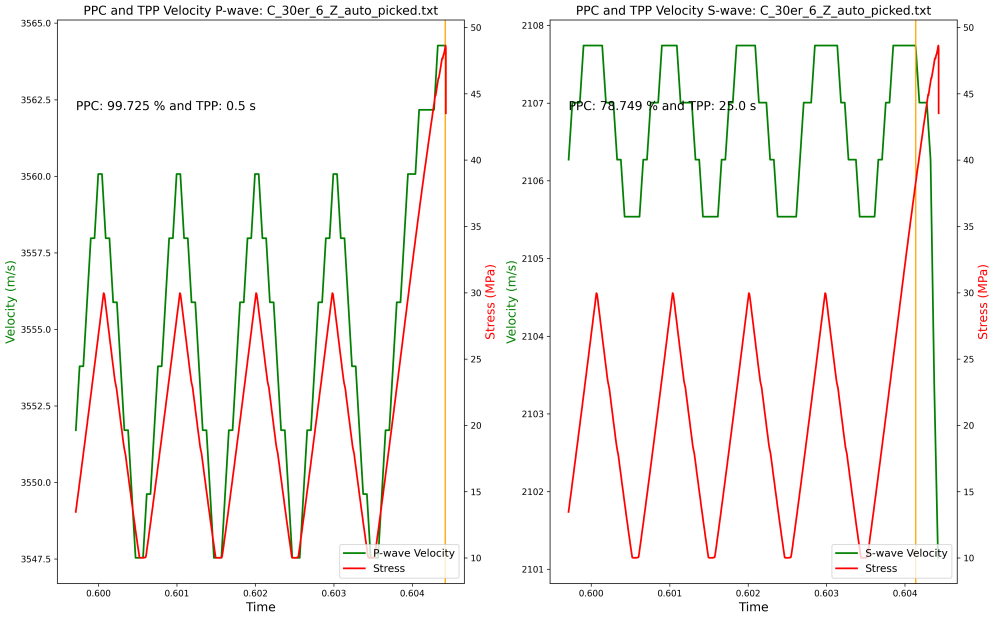

Figure 42: P- and S-wave velocity (green) and stress (red) plotted over last 400 seconds of the cyclic "C 30er 6 Z" test. With the PPC being P-wave: 99.73 % and S-wave: 78.75 % and the TPP being P-wave: 0.5 s and S-wave: 25.0 s.

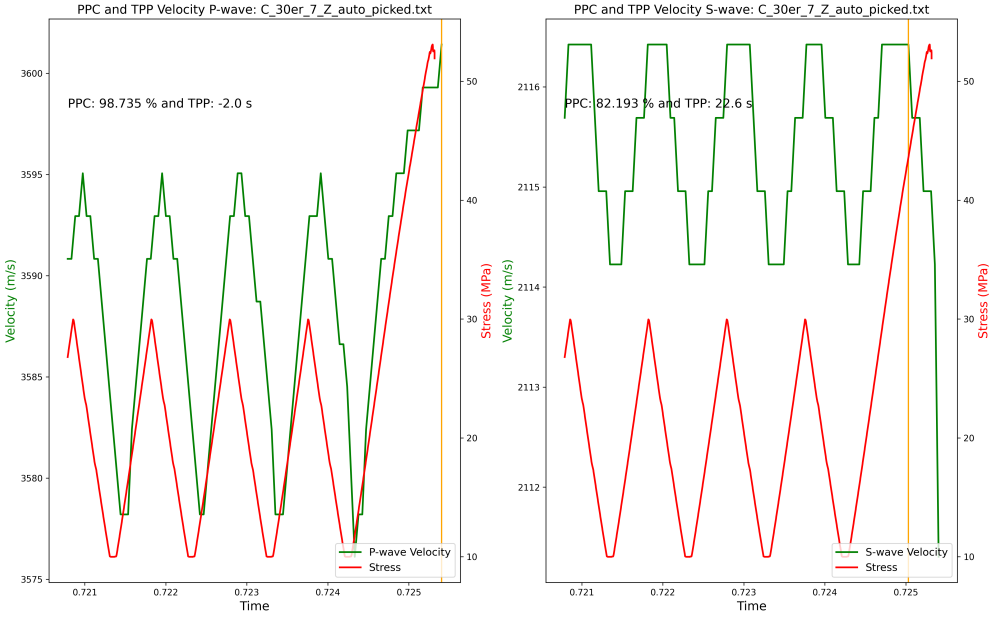

Figure 43: P- and S-wave velocity (green) and stress (red) plotted over last 400 seconds of the cyclic "C 30er 7 Z" test. With the PPC being P-wave:98.74 % and S-wave: 82.19 % and the TPP being P-wave: -2.0 s and S-wave: 22.6 s.

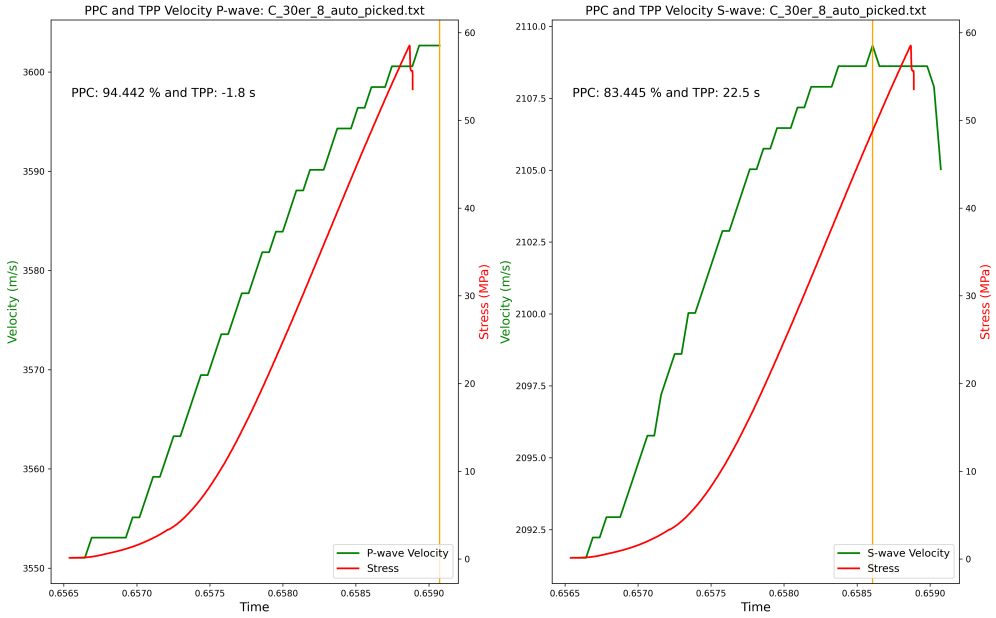

Figure 44: P- and S-wave velocity (green) and stress (red) plotted over the time of the "C 30er 8" test. With the PPC being P-wave: 94.44 % and S-wave: 83.45 % and the TPP being P-wave: -1.8 s and S-wave: 22.5 s.

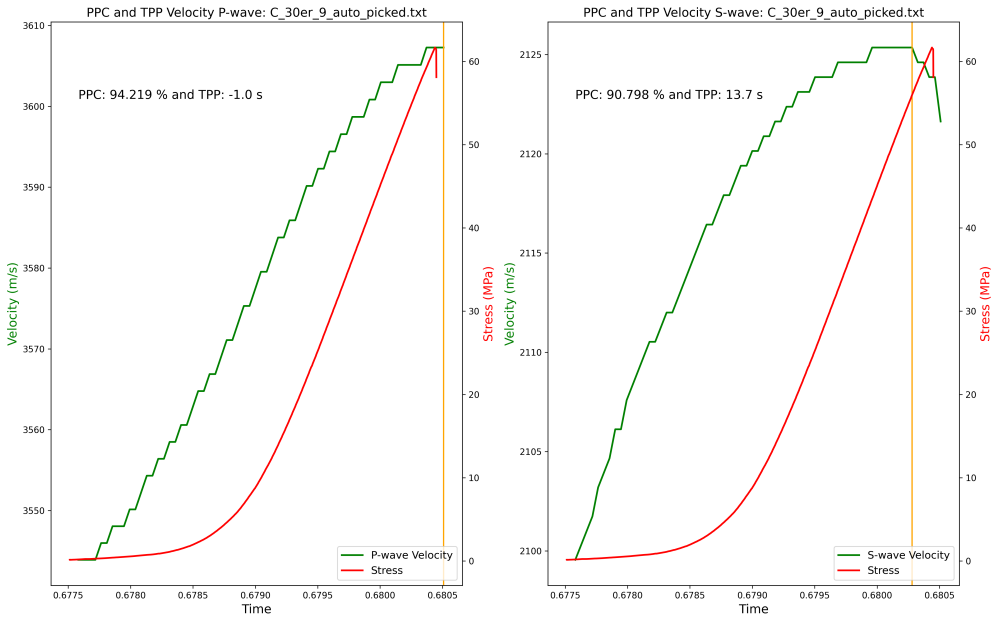

Figure 45: P- and S-wave velocity (green) and stress (red) plotted over the time of the "C 30er 9" test. With the PPC being P-wave: 94.22 % and S-wave: 90.8 % and the TPP being P-wave: -1.0 s and S-wave: 13.7 s.

IP and TIP

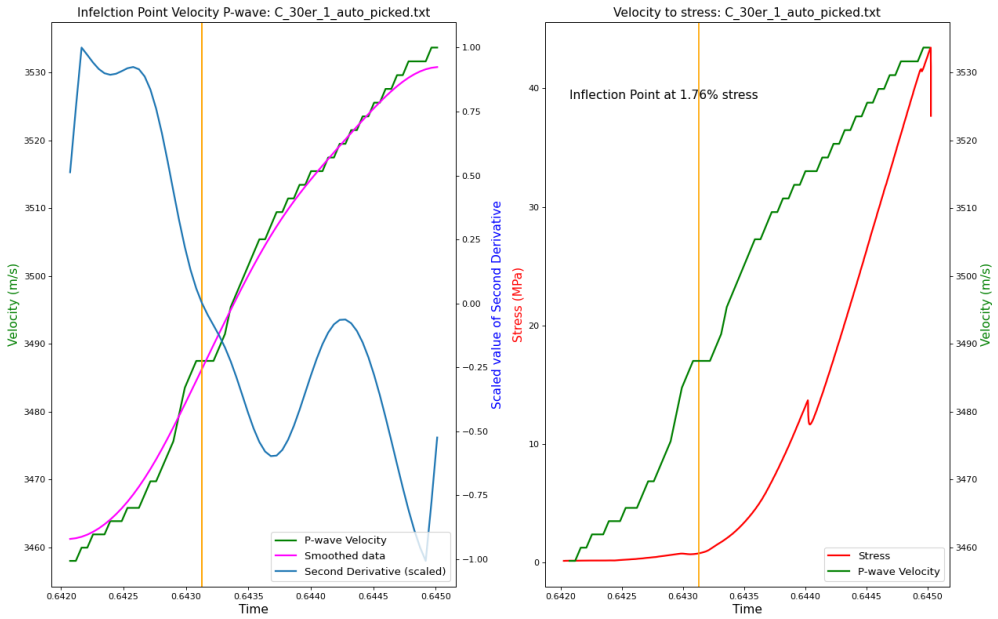

Figure 46: The **left** graph shows the P-wave velocity of the "C 30er 1" sample (green), the velocity data smoothed by a Gaussian filter (magenta), the second derivative of the smoothed data (blue), and the inflection point of the smoothed data (orange vertical line). The **right** graph shows stress (red) and velocity (green) over the time of the test. The last IP is at 1.76 % with a TIP of 163.9 s.

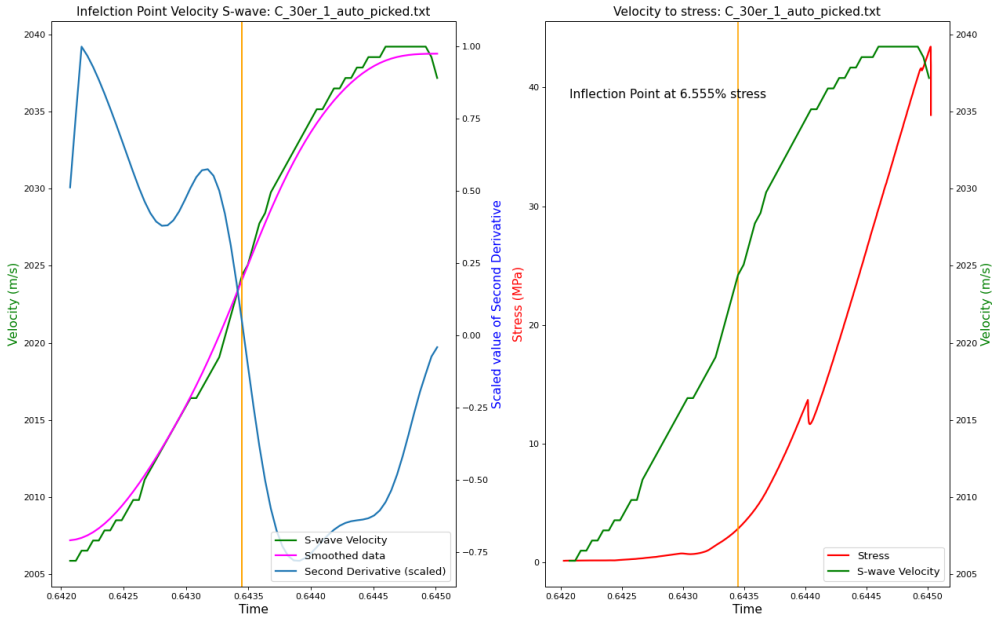

Figure 47: The **left** graph shows the S-wave velocity of the "C 30er 1" sample (green), the velocity data smoothed by a Gaussian filter (magenta), the second derivative of the smoothed data (blue), and the inflection point of the smoothed data (orange vertical line). The **right** graph shows stress (red) and velocity (green) over the time of the test. The last IP is at 6.56 % with a TIP of 136.1 s.

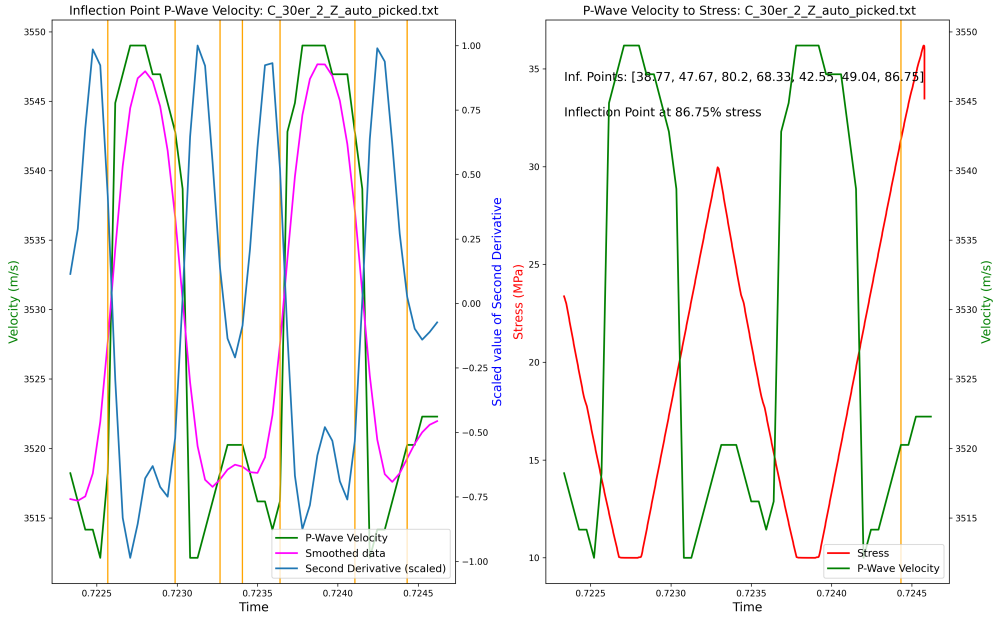

Figure 48: The **left** graph shows the P-wave velocity of the "C 30er 2 Z" sample (green), the velocity data smoothed by a Gaussian filter (magenta), the second derivative of the smoothed data (blue), and the inflection point of the smoothed data (orange vertical line). The **right** graph shows stress (red) and velocity (green) over the time of the test. The last IP is at 86.75 % with a TIP of 12.3 s.

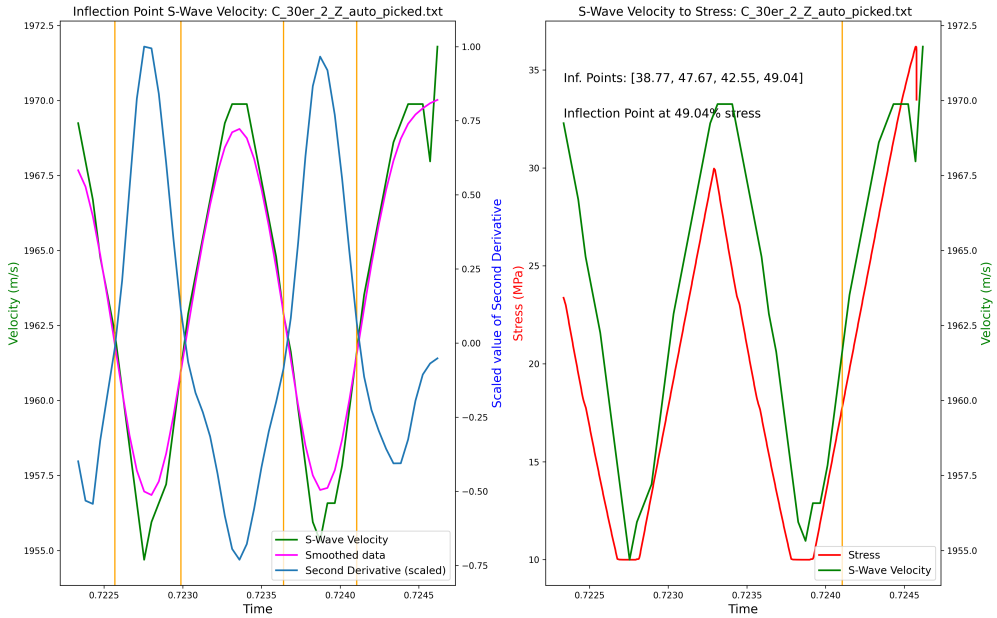

Figure 49: The **left** graph shows the S-wave velocity of the "C 30er 2 Z" sample (green), the velocity data smoothed by a Gaussian filter (magenta), the second derivative of the smoothed data (blue), and the inflection point of the smoothed data (orange vertical line). The **right** graph shows stress (red) and velocity (green) over the time of the test. The last IP is at 49.04 % with a TIP of 40.5 s.

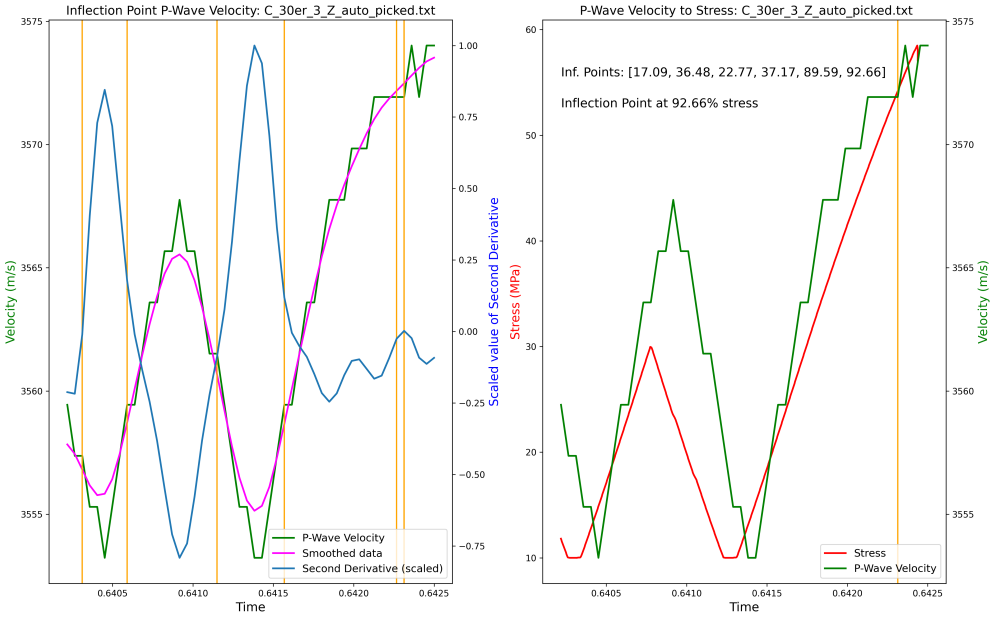

Figure 50: The **left** graph shows the P-wave velocity of the "C 30er 3 Z" sample (green), the velocity data smoothed by a Gaussian filter (magenta), the second derivative of the smoothed data (blue), and the inflection point of the smoothed data (orange vertical line). The **right** graph shows stress (red) and velocity (green) over the time of the test. The last IP is at 92.66 % with a TIP of 10.5 s.

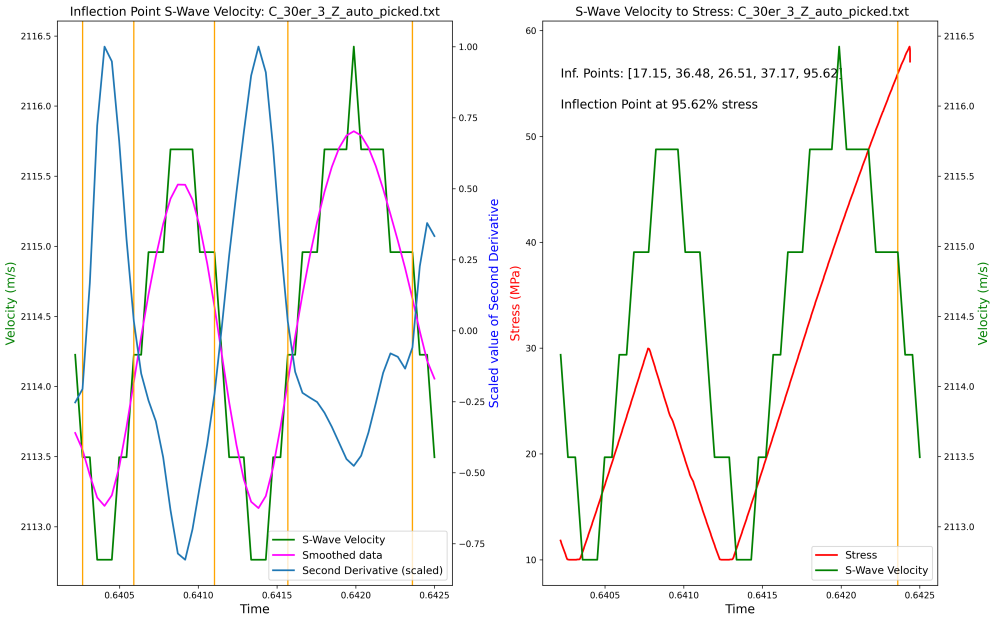

Figure 51: The **left** graph shows the S-wave velocity of the "C 30er 3 Z" sample (green), the velocity data smoothed by a Gaussian filter (magenta), the second derivative of the smoothed data (blue), and the inflection point of the smoothed data (orange vertical line). The **right** graph shows stress (red) and velocity (green) over the time of the test. The last IP is at 95.62 % with a TIP of 6.5 s.

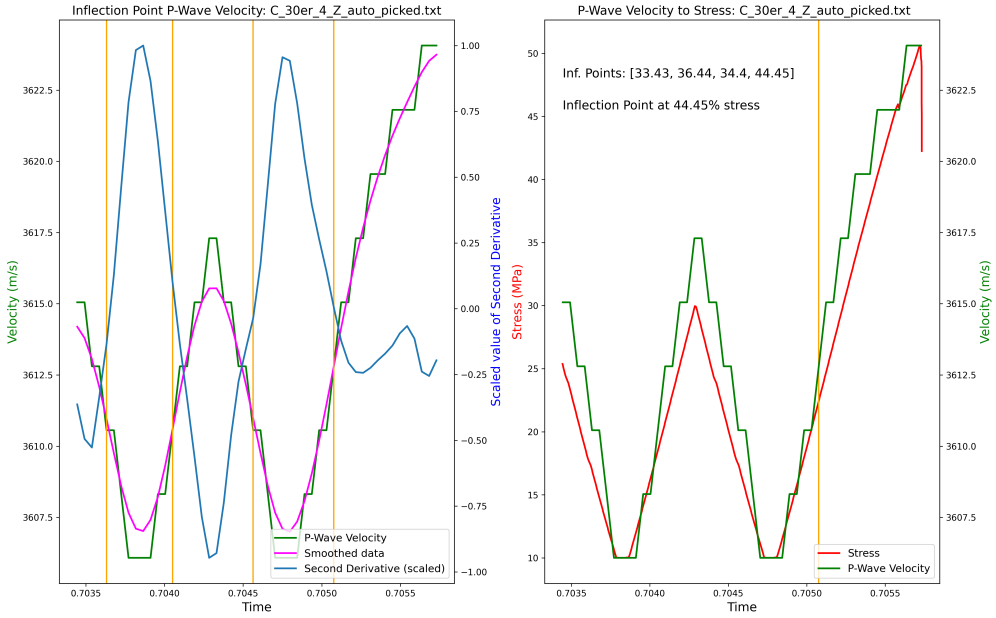

Figure 52: The **left** graph shows the P-wave velocity of the "C 30er 4 Z" sample (green), the velocity data smoothed by a Gaussian filter (magenta), the second derivative of the smoothed data (blue), and the inflection point of the smoothed data (orange vertical line). The **right** graph shows stress (red) and velocity (green) over the time of the test. The last IP is at 44.45 % with a TIP of 55.6 s.

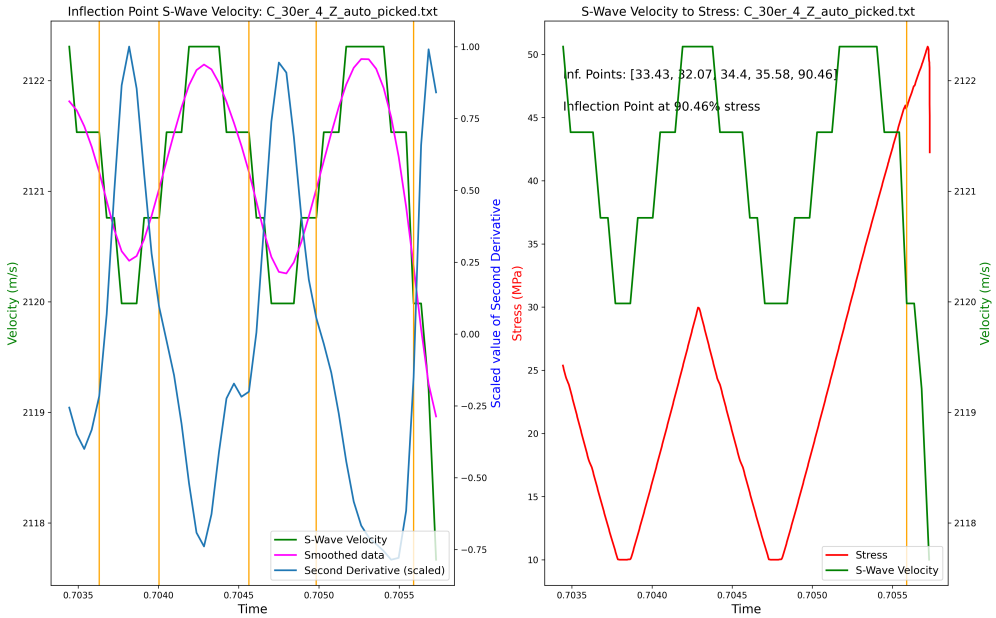

Figure 53: The **left** graph shows the S-wave velocity of the "C 30er 4 Z" sample (green), the velocity data smoothed by a Gaussian filter (magenta), the second derivative of the smoothed data (blue), and the inflection point of the smoothed data (orange vertical line). The **right** graph shows stress (red) and velocity (green) over the time of the test. The last IP is at 90.46 % with a TIP of 11.3 s.

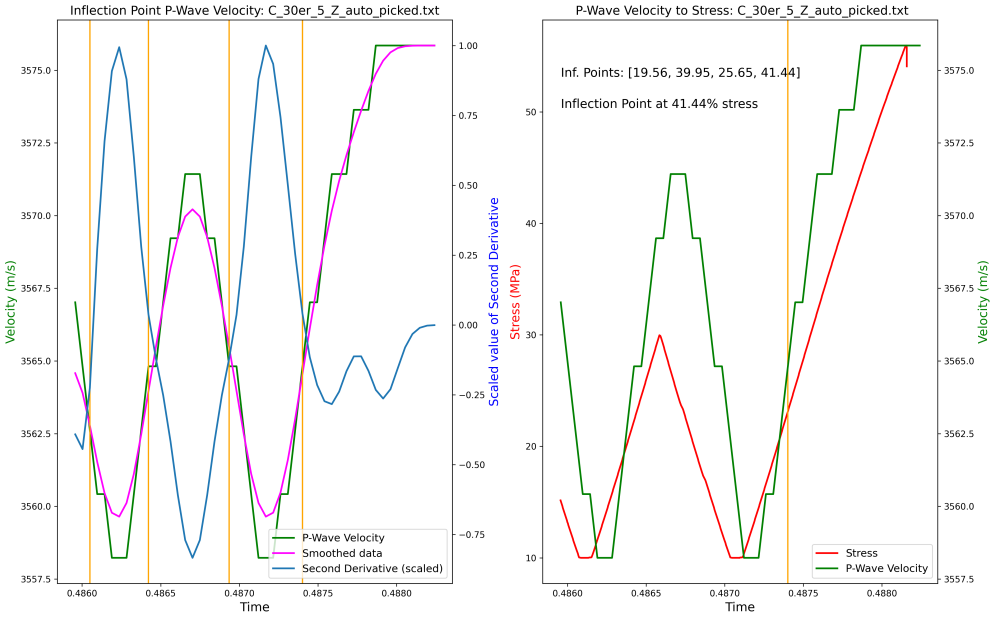

Figure 54: The **left** graph shows the P-wave velocity of the "C 30er 5 Z" sample (green), the velocity data smoothed by a Gaussian filter (magenta), the second derivative of the smoothed data (blue), and the inflection point of the smoothed data (orange vertical line). The **right** graph shows stress (red) and velocity (green) over the time of the test. The last IP is at 41.44 % with a TIP of 65.1 s.

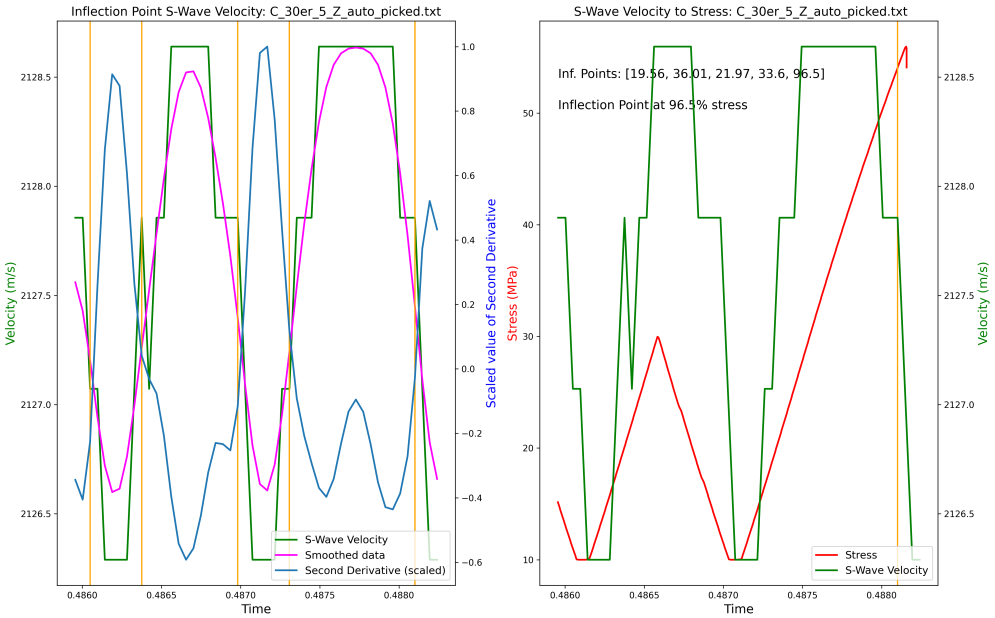

Figure 55: The **left** graph shows the S-wave velocity of the "C 30er 5 Z" sample (green), the velocity data smoothed by a Gaussian filter (magenta), the second derivative of the smoothed data (blue), and the inflection point of the smoothed data (orange vertical line). The **right** graph shows stress (red) and velocity (green) over the time of the test. The last IP is at 96.5 % with a TIP of 4.7 s.

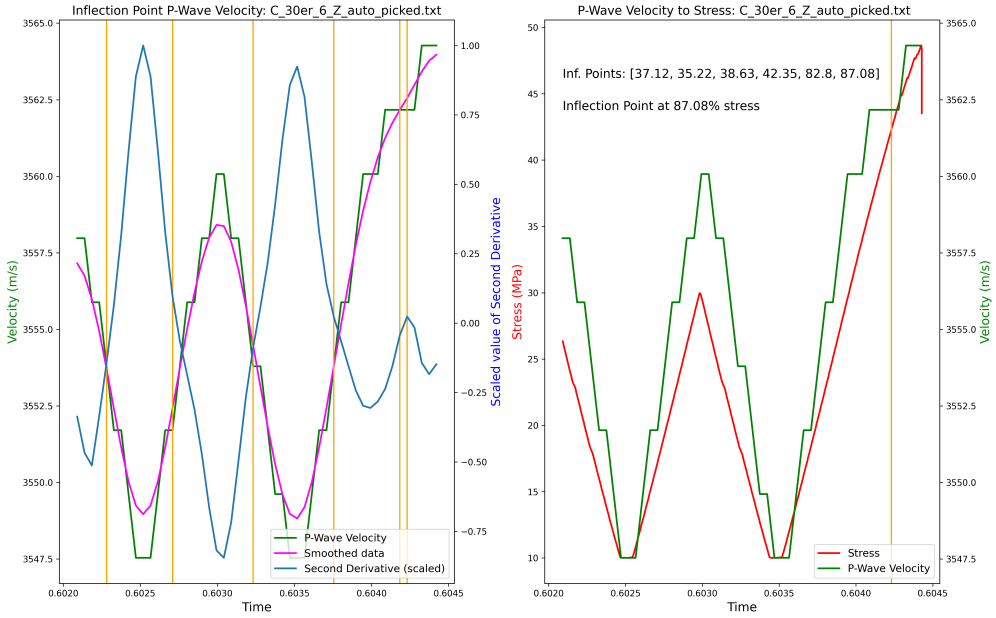

Figure 56: The **left** graph shows the P-wave velocity of the "C 30er 6 Z" sample (green), the velocity data smoothed by a Gaussian filter (magenta), the second derivative of the smoothed data (blue), and the inflection point of the smoothed data (orange vertical line). The **right** graph shows stress (red) and velocity (green) over the time of the test. The last IP is at 87.08 % with a TIP of 16.8 s.

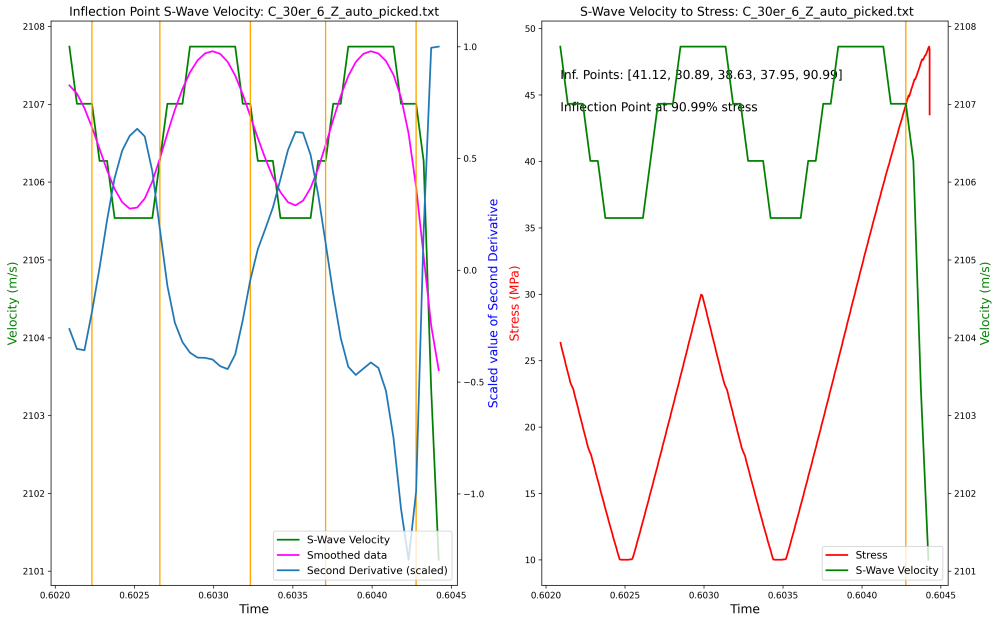

Figure 57: The **left** graph shows the S-wave velocity of the "C 30er 6 Z" sample (green), the velocity data smoothed by a Gaussian filter (magenta), the second derivative of the smoothed data (blue), and the inflection point of the smoothed data (orange vertical line). The **right** graph shows stress (red) and velocity (green) over the time of the test. The last IP is at 90.99 % with a TIP of 12.7 s.

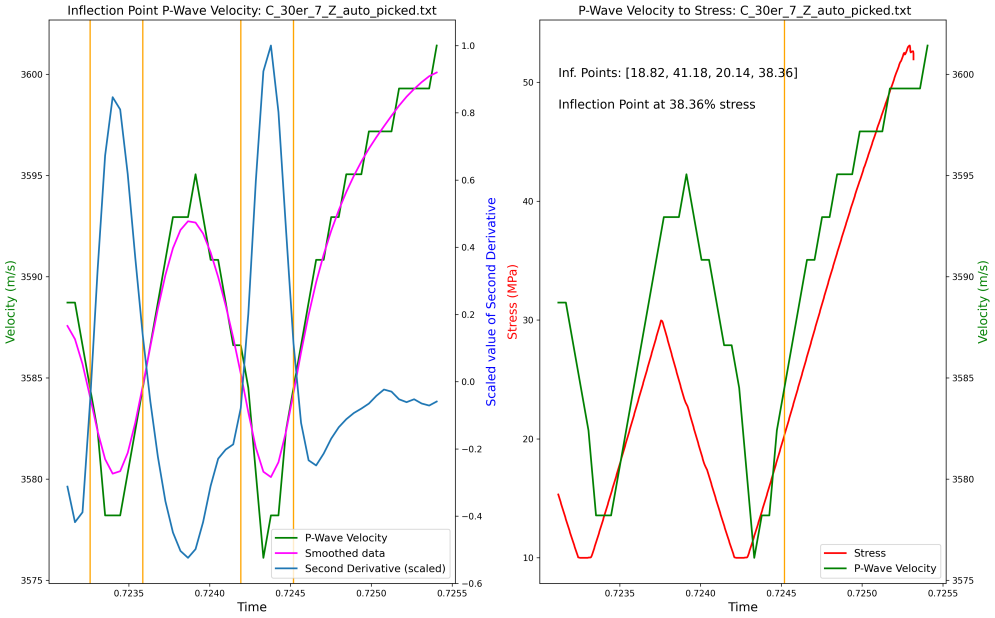

Figure 58: The **left** graph shows the P-wave velocity of the "C 30er 7 Z" sample (green), the velocity data smoothed by a Gaussian filter (magenta), the second derivative of the smoothed data (blue), and the inflection point of the smoothed data (orange vertical line). The **right** graph shows stress (red) and velocity (green) over the time of the test. The last IP is at 38.36 % with a TIP of 67.0 s.

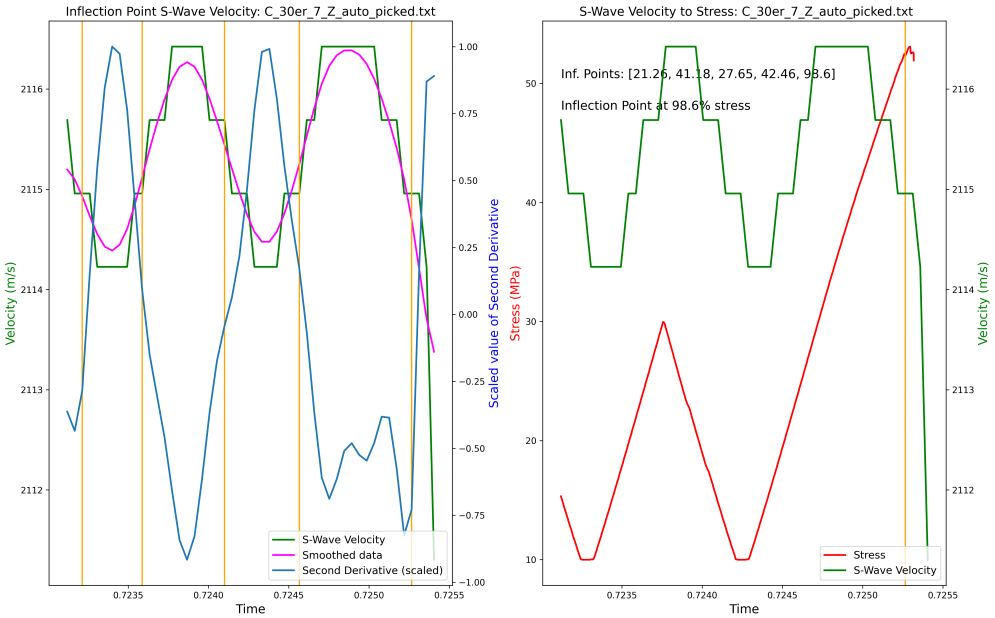

Figure 59: The **left** graph shows the S-wave velocity of the "C 30er 7 Z" sample (green), the velocity data smoothed by a Gaussian filter (magenta), the second derivative of the smoothed data (blue), and the inflection point of the smoothed data (orange vertical line). The **right** graph shows stress (red) and velocity (green) over the time of the test. The last IP is at 98.6 % with a TIP of 2.6 s.

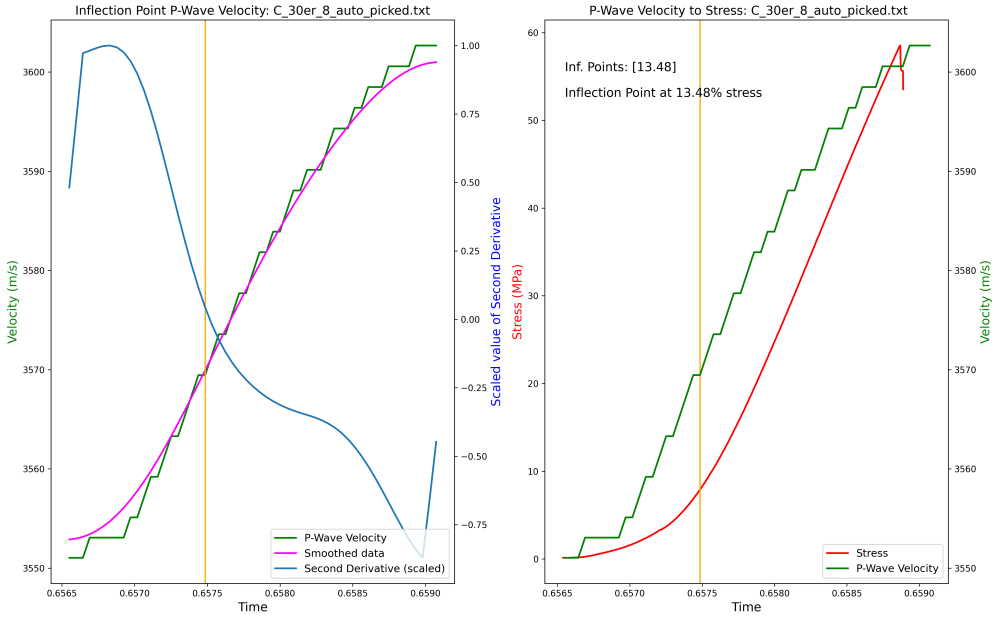

Figure 60: The **left** graph shows the P-wave velocity of the "C 30er 8" sample (green), the velocity data smoothed by a Gaussian filter (magenta), the second derivative of the smoothed data (blue), and the inflection point of the smoothed data (orange vertical line). The **right** graph shows stress (red) and velocity (green) over the time of the test. The last IP is at 13.48 % with a TIP of 119.5 s.

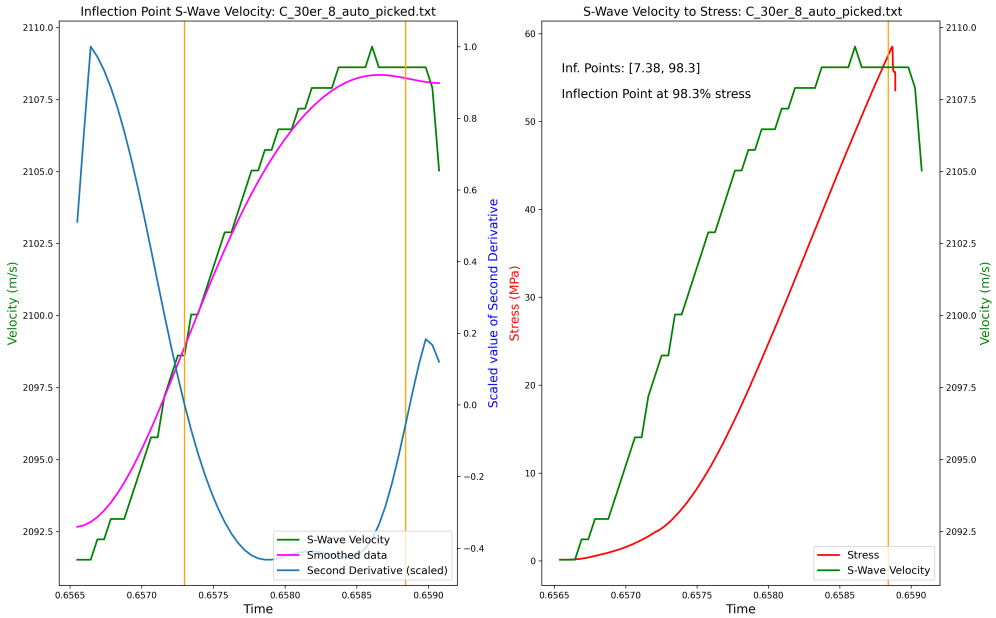

Figure 61: The **left** graph shows the S-wave velocity of the "C 30er 8" sample (green), the velocity data smoothed by a Gaussian filter (magenta), the second derivative of the smoothed data (blue), and the inflection point of the smoothed data (orange vertical line). The **right** graph shows stress (red) and velocity (green) over the time of the test. The last IP is at 98.3 % with a TIP of 2.4 s.

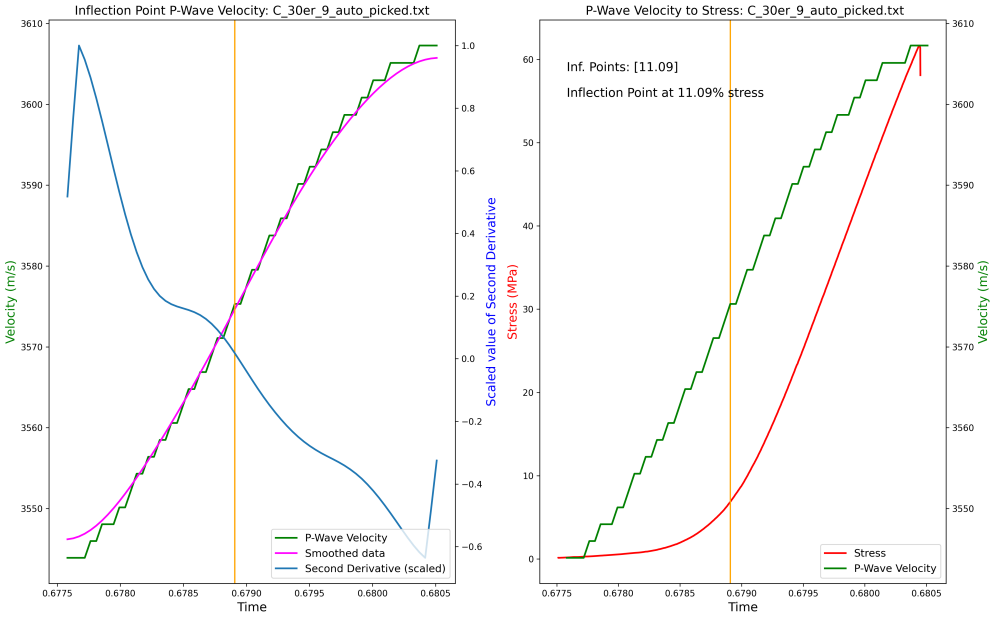

Figure 62: The **left** graph shows the P-wave velocity of the "C 30er 9" sample (green), the velocity data smoothed by a Gaussian filter (magenta), the second derivative of the smoothed data (blue), and the inflection point of the smoothed data (orange vertical line). The **right** graph shows stress (red) and velocity (green) over the time of the test. The last IP is at 11.09 % with a TIP of 132.4 s.

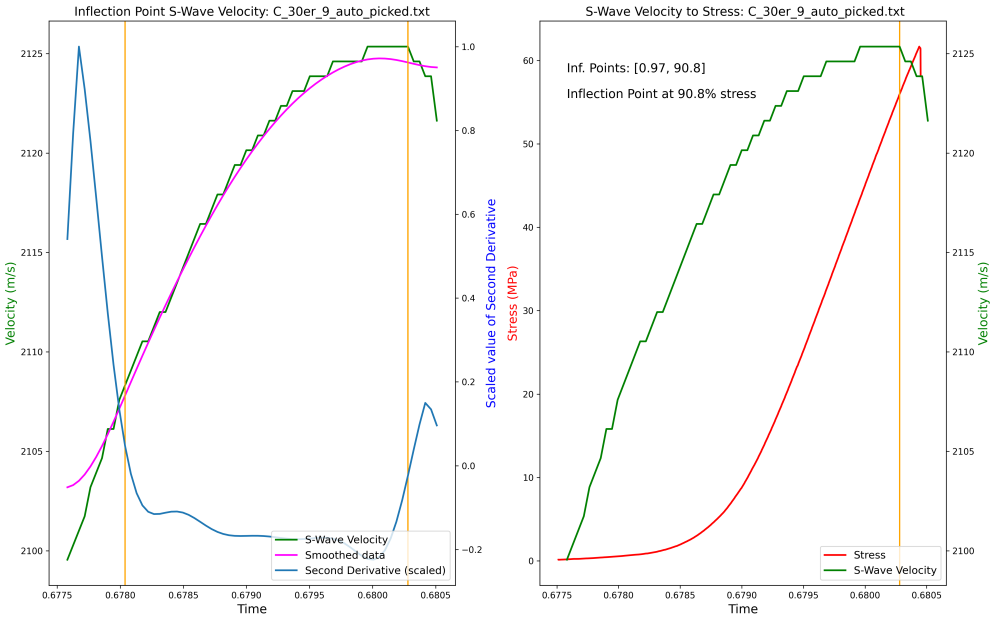

Figure 63: The **left** graph shows the S-wave velocity of the "C 30er 9" sample (green), the velocity data smoothed by a Gaussian filter (magenta), the second derivative of the smoothed data (blue), and the inflection point of the smoothed data (orange vertical line). The **right** graph shows stress (red) and velocity (green) over the time of the test. The last IP is at 90.80 % with a TIP of 13.8 s.

Gneiss 50 mm Diameter

PPC and TPP

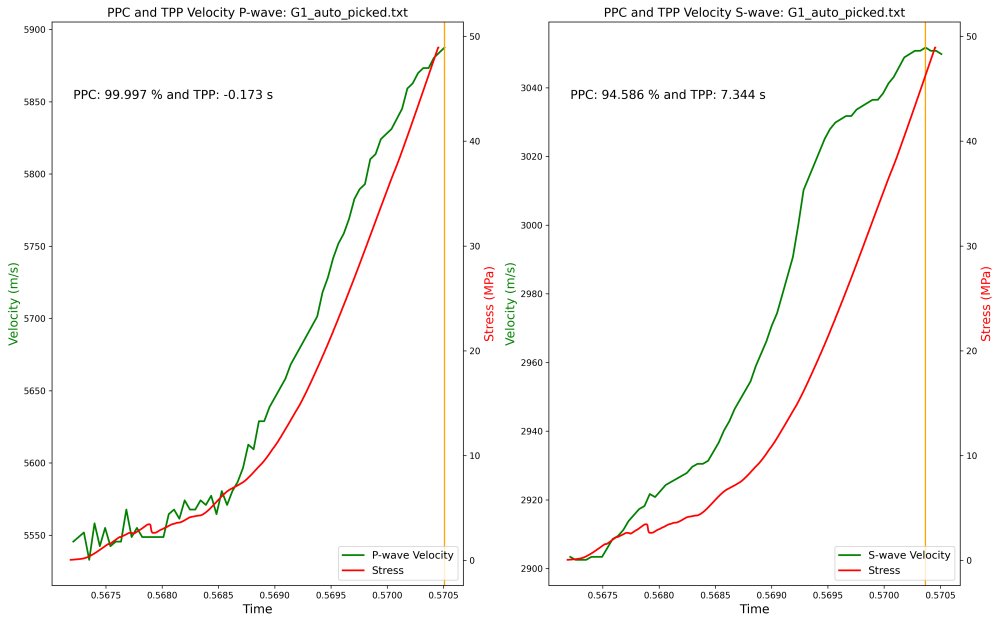

Figure 64: P- and S-wave velocity (green) and stress (red) plotted over the time of the "G1" test. With the PPC being P-wave: 100.0 % and S-wave: 94.6% and the TPP being P-wave: -0.2 s and S-wave: 7.3 s.

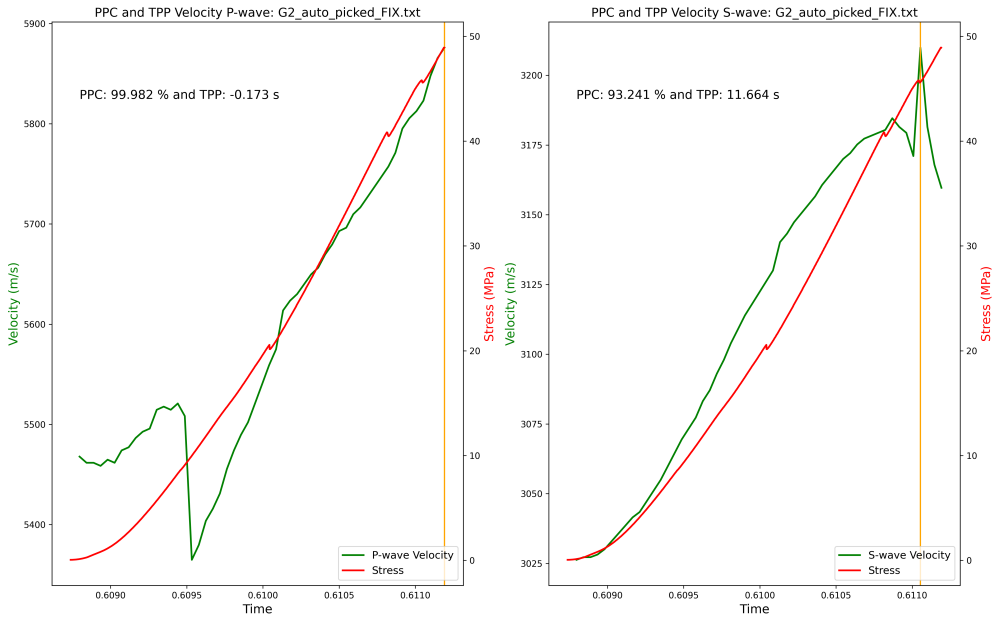

Figure 65: P- and S-wave velocity (green) and stress (red) plotted over the time of the "G2" test. With the PPC being P-wave: 100.0 % and S-wave: 93.2 % and the TPP being P-wave: -0.2 s and S-wave: 11.7 s.

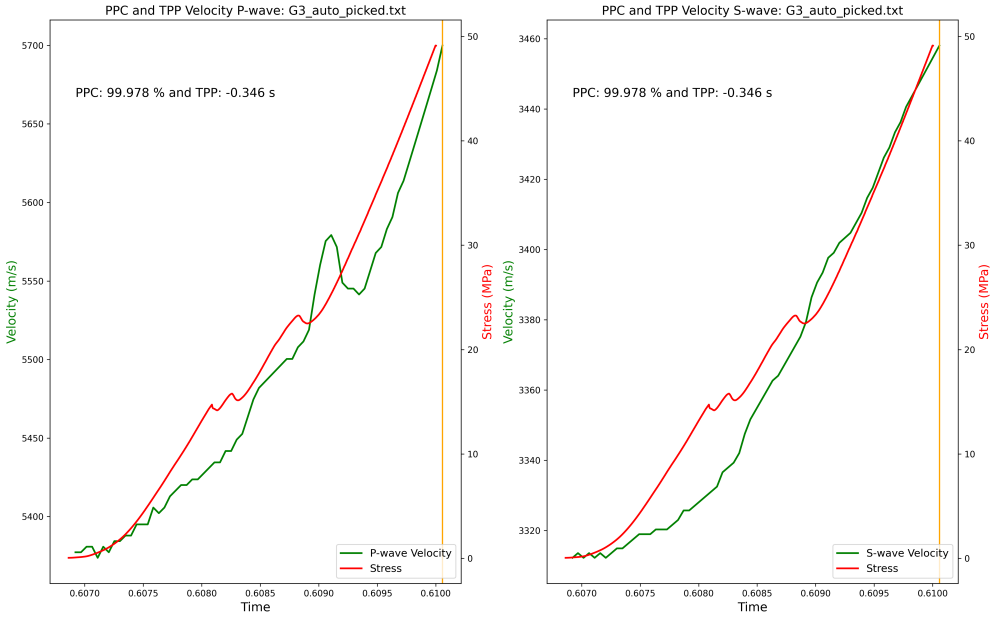

Figure 66: P- and S-wave velocity (green) and stress (red) plotted over the time of the "G3" test. With the PPC being P-wave: 100.0 % and S-wave: 100.0 % and the TPP being P-wave: -0.3 s and S-wave: -0.3 s.

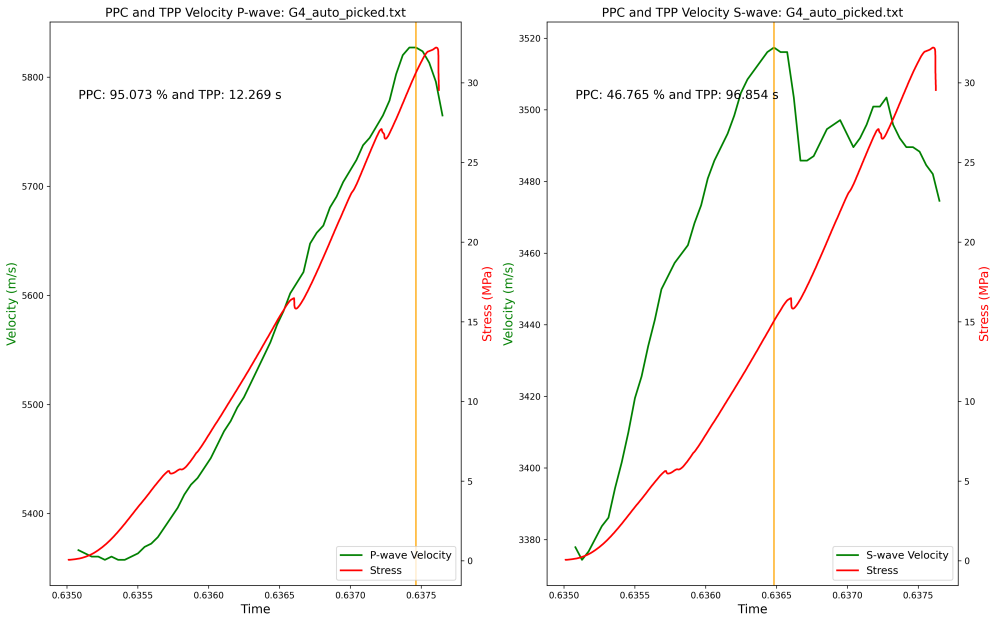

Figure 67: P- and S-wave velocity (green) and stress (red) plotted over the time of the "G4" test. With the PPC being P-wave: 95.1 % and S-wave: 46.8 % and the TPP being P-wave: 12.3 s and S-wave: 96.9 s.

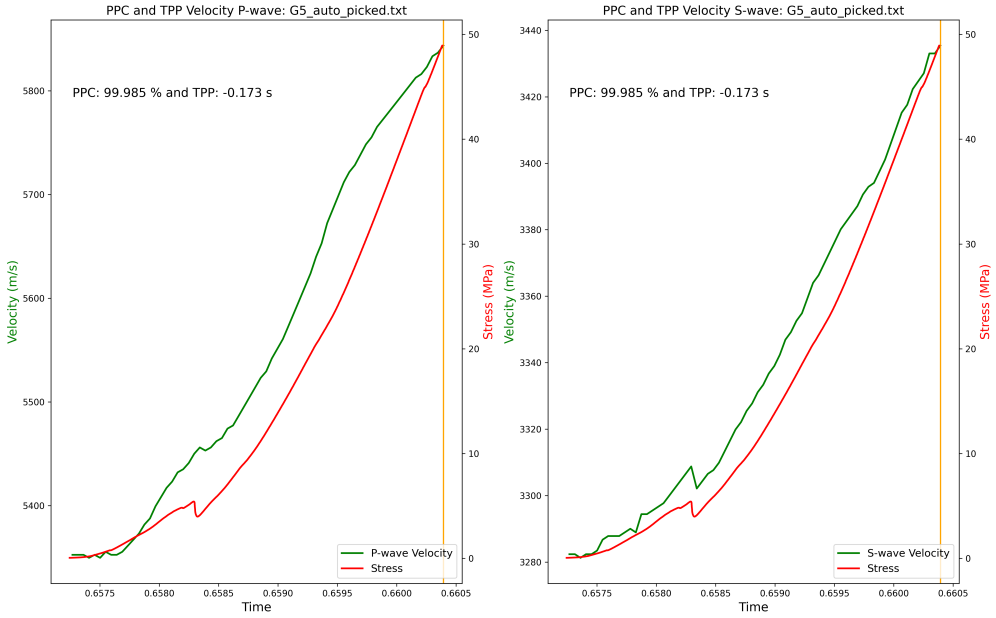

Figure 68: P- and S-wave velocity (green) and stress (red) plotted over the time of the "G5" test. With the PPC being P-wave: 100.0 % and S-wave: 100.0 % and the TPP being P-wave: -0.2 s and S-wave: -0.2 s.

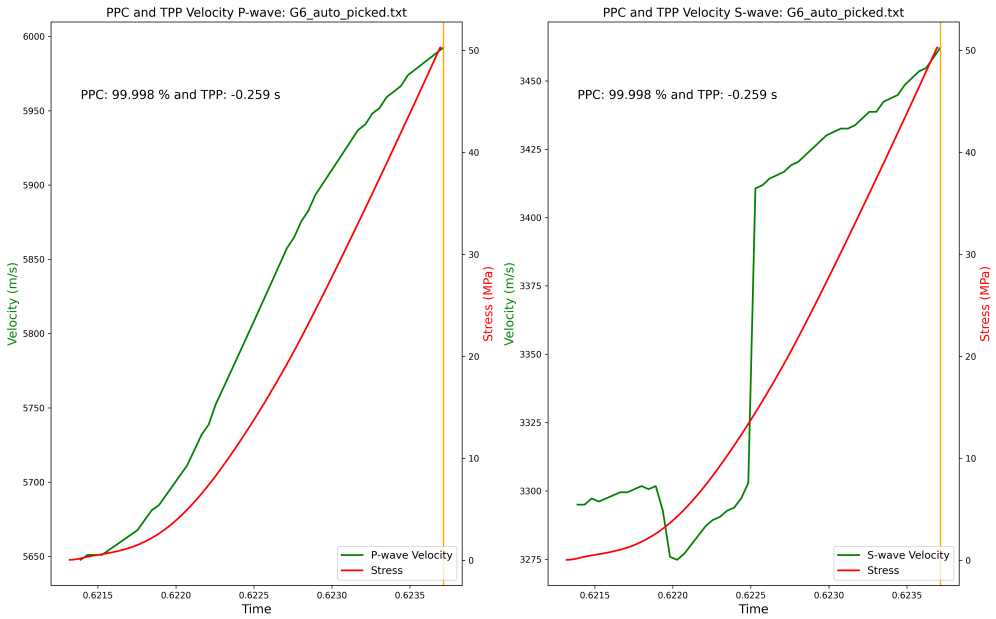

Figure 69: P- and S-wave velocity (green) and stress (red) plotted over the time of the "G6" test. With the PPC being P-wave: 100.0 % and S-wave: 100.0 % and the TPP being P-wave: -0.3 s and S-wave: -0.3 s.

IP and TIP

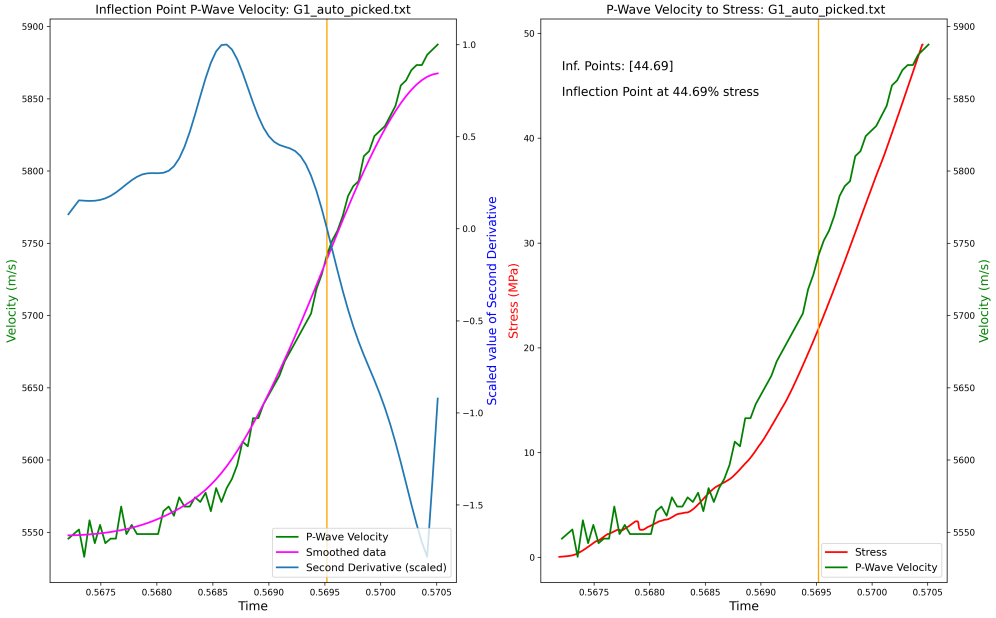

Figure 70: The **left** graph shows the P-wave velocity of the "G 1" sample (green), the velocity data smoothed by a Gaussian filter (magenta), the second derivative of the smoothed data (blue), and the inflection point of the smoothed data (orange vertical line). The **right** graph shows stress (red) and velocity (green) over the time of the test. The last IP is at 44.69 % with a TIP of 80.6 s.

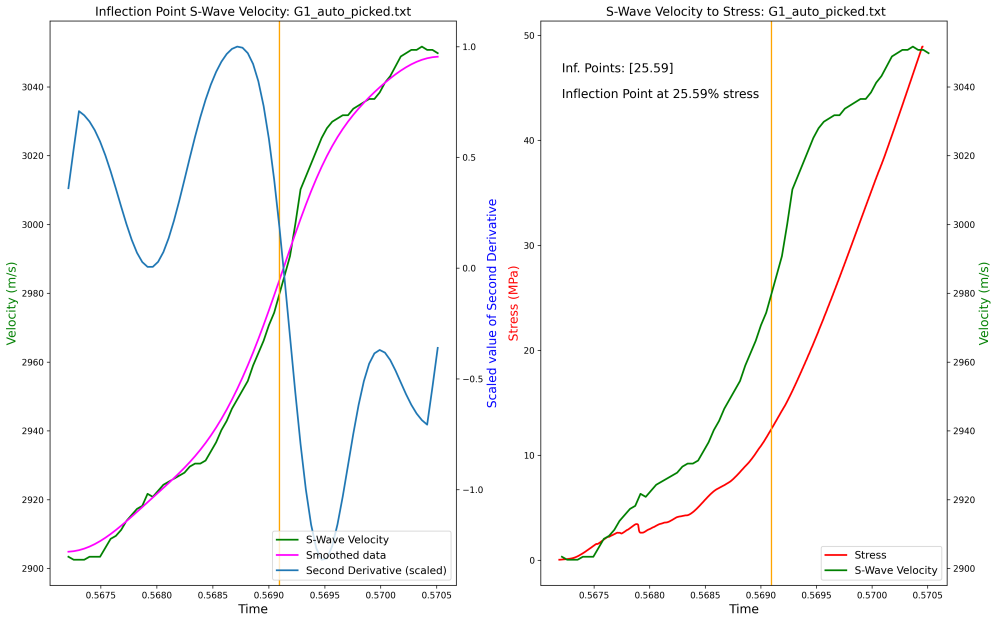

Figure 71: The **left** graph shows the S-wave velocity of the "G 1" sample (green), the velocity data smoothed by a Gaussian filter (magenta), the second derivative of the smoothed data (blue), and the inflection point of the smoothed data (orange vertical line). The **right** graph shows stress (red) and velocity (green) over the time of the test. The last IP is at 25.59 % with a TIP of 117.3 s.

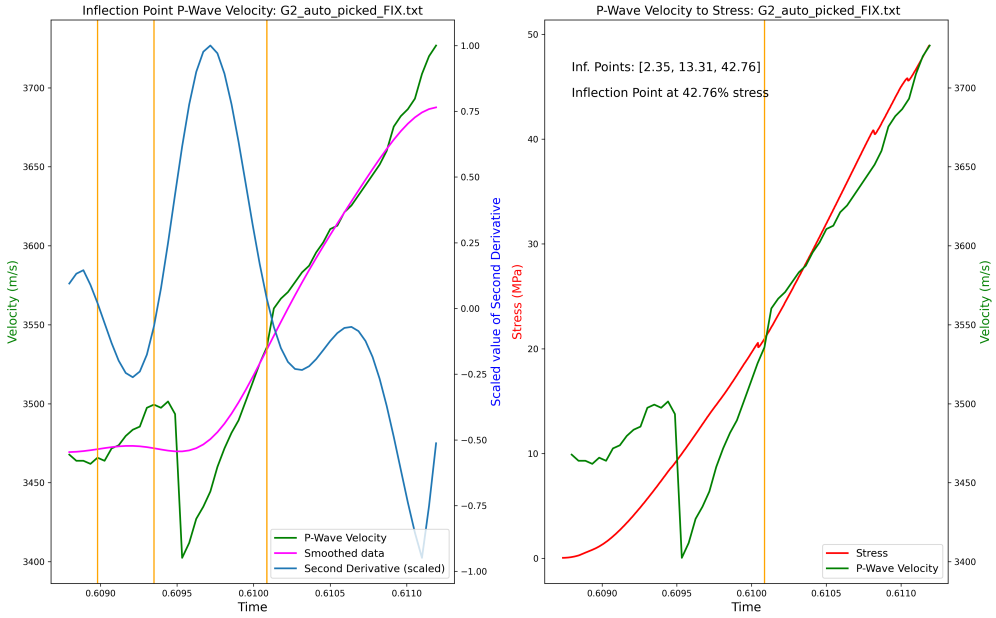

Figure 72: The **left** graph shows the P-wave velocity of the "G 2" sample (green), the velocity data smoothed by a Gaussian filter (magenta), the second derivative of the smoothed data (blue), and the inflection point of the smoothed data (orange vertical line). The **right** graph shows stress (red) and velocity (green) over the time of the test. The last IP is at 42.76 % with a TIP of 31.6 s.

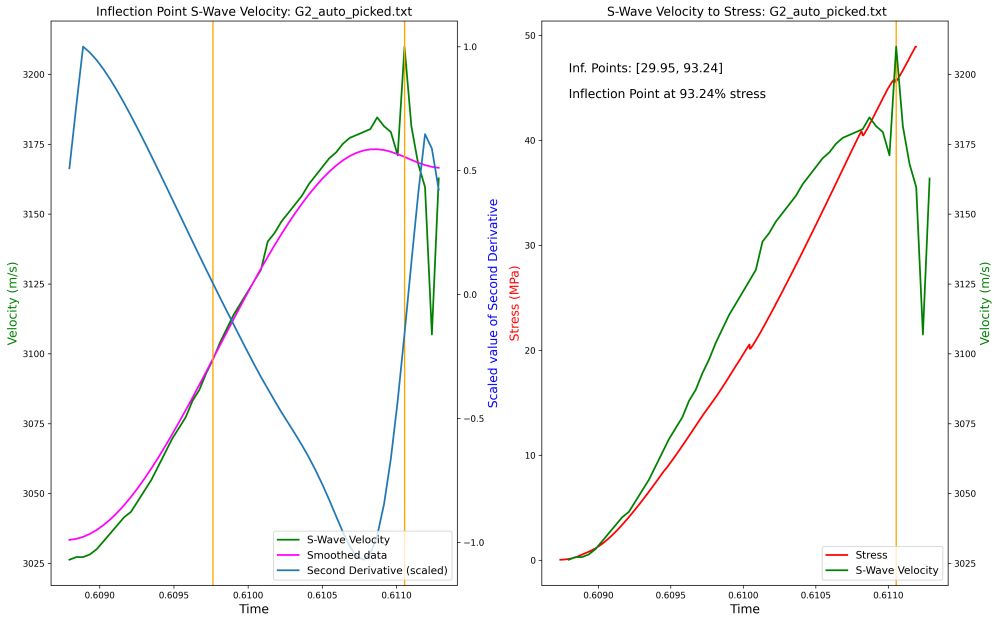

Figure 73: The **left** graph shows the S-wave velocity of the "G 2" sample (green), the velocity data smoothed by a Gaussian filter (magenta), the second derivative of the smoothed data (blue), and the inflection point of the smoothed data (orange vertical line). The **right** graph shows stress (red) and velocity (green) over the time of the test. The last IP is at 93.24 % with a TIP of 11.6 s.

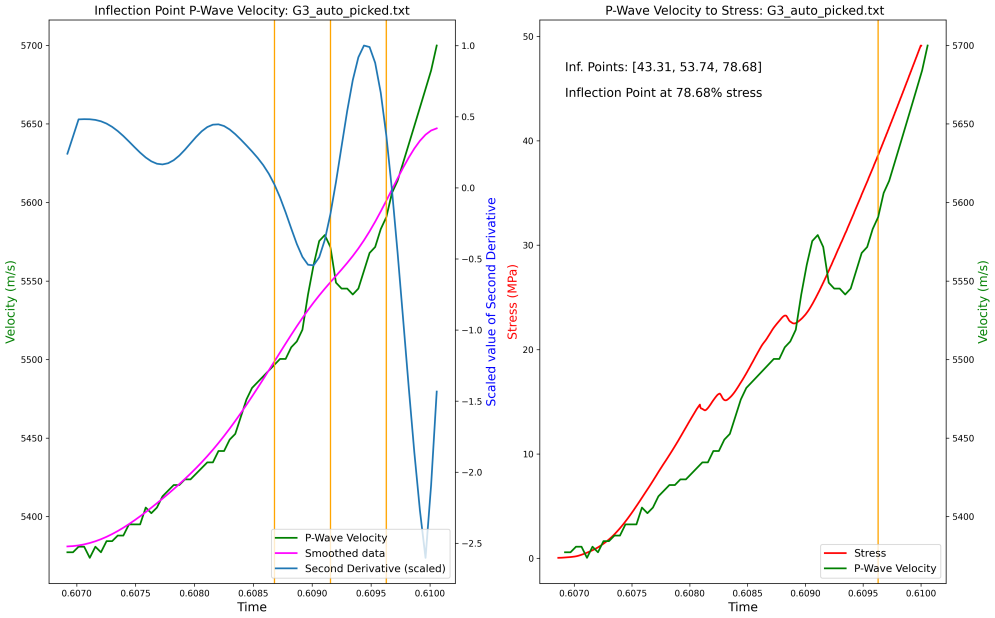

Figure 74: The **left** graph shows the P-wave velocity of the "G 3" sample (green), the velocity data smoothed by a Gaussian filter (magenta), the second derivative of the smoothed data (blue), and the inflection point of the smoothed data (orange vertical line). The **right** graph shows stress (red) and velocity (green) over the time of the test. The last IP is at 78.68 % with a TIP of 31.9 s.

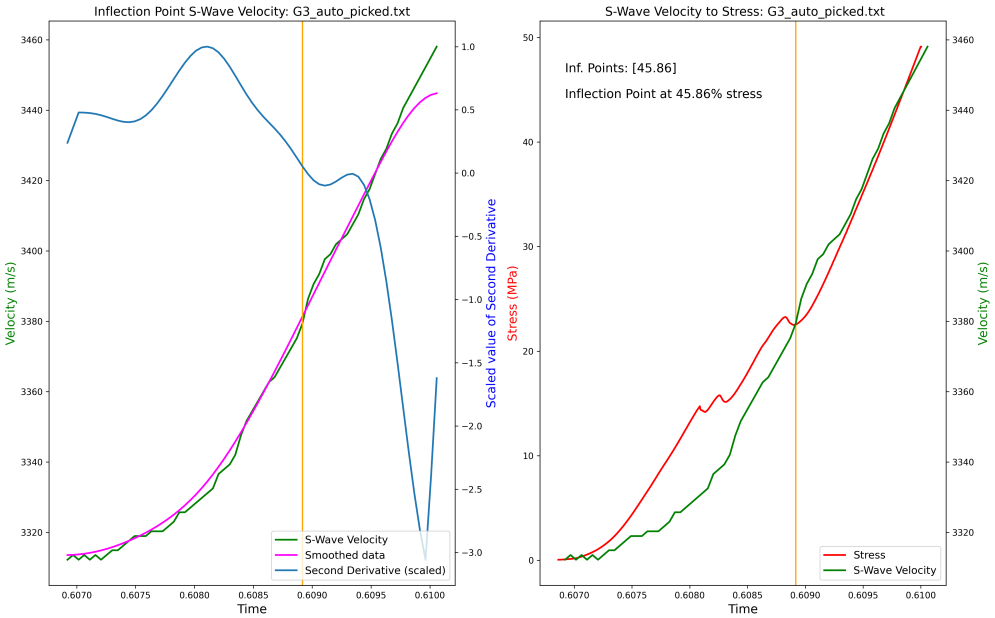

Figure 75: The **left** graph shows the S-wave velocity of the "G 3" sample (green), the velocity data smoothed by a Gaussian filter (magenta), the second derivative of the smoothed data (blue), and the inflection point of the smoothed data (orange vertical line). The **right** graph shows stress (red) and velocity (green) over the time of the test. The last IP is at 45.86 % with a TIP of 93.5 s.

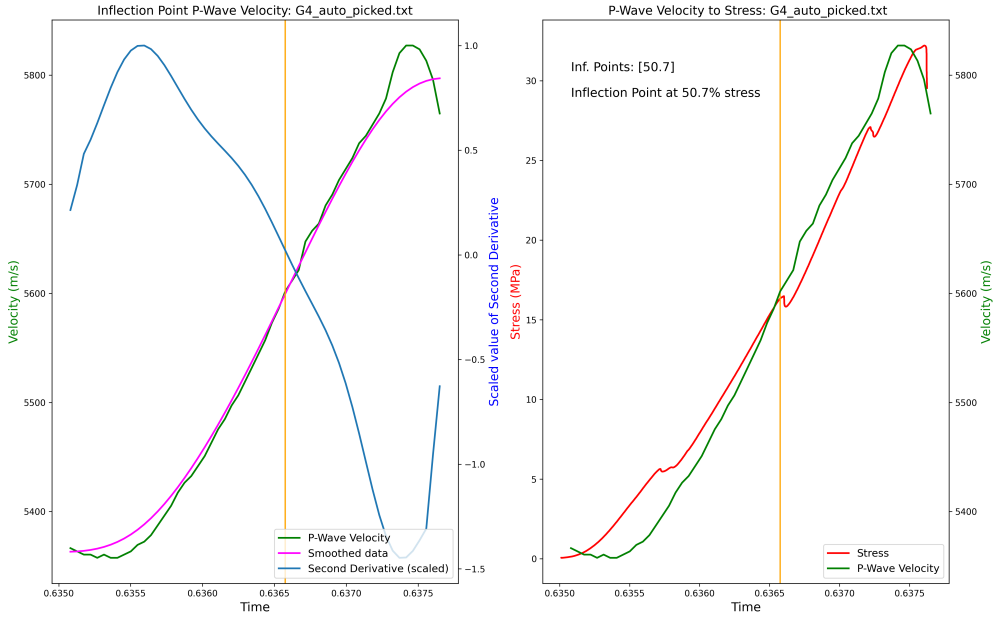

Figure 76: The **left** graph shows the P-wave velocity of the "G 4" sample (green), the velocity data smoothed by a Gaussian filter (magenta), the second derivative of the smoothed data (blue), and the inflection point of the smoothed data (orange vertical line). The **right** graph shows stress (red) and velocity (green) over the time of the test. The last IP is at 50.70 % with a TIP of 88.9 s.

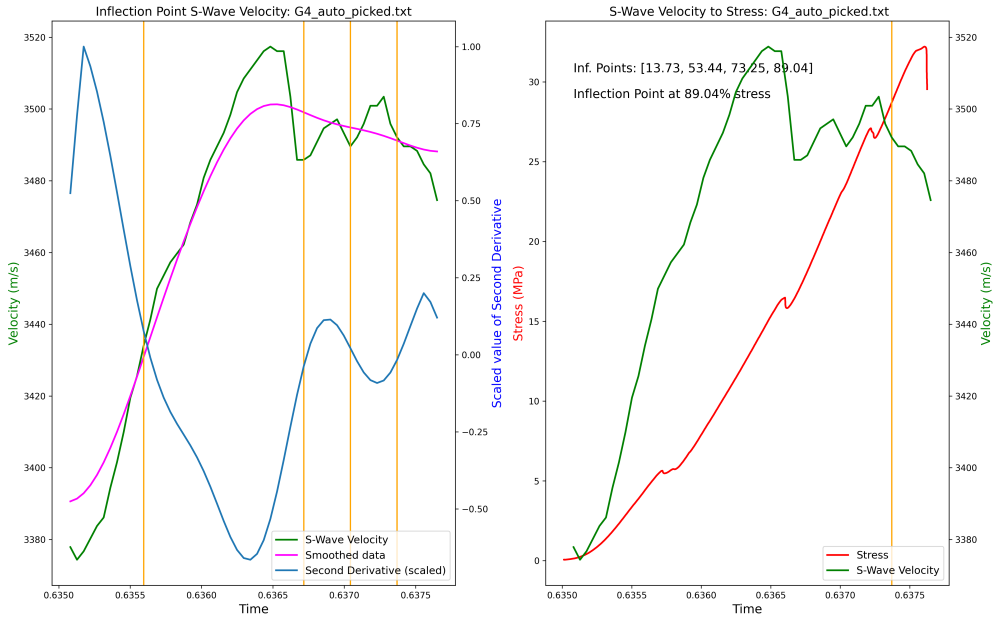

Figure 77: The **left** graph shows the S-wave velocity of the "G 4" sample (green), the velocity data smoothed by a Gaussian filter (magenta), the second derivative of the smoothed data (blue), and the inflection point of the smoothed data (orange vertical line). The **right** graph shows stress (red) and velocity (green) over the time of the test. The last IP is at 89.05 % with a TIP of 20.3 s.

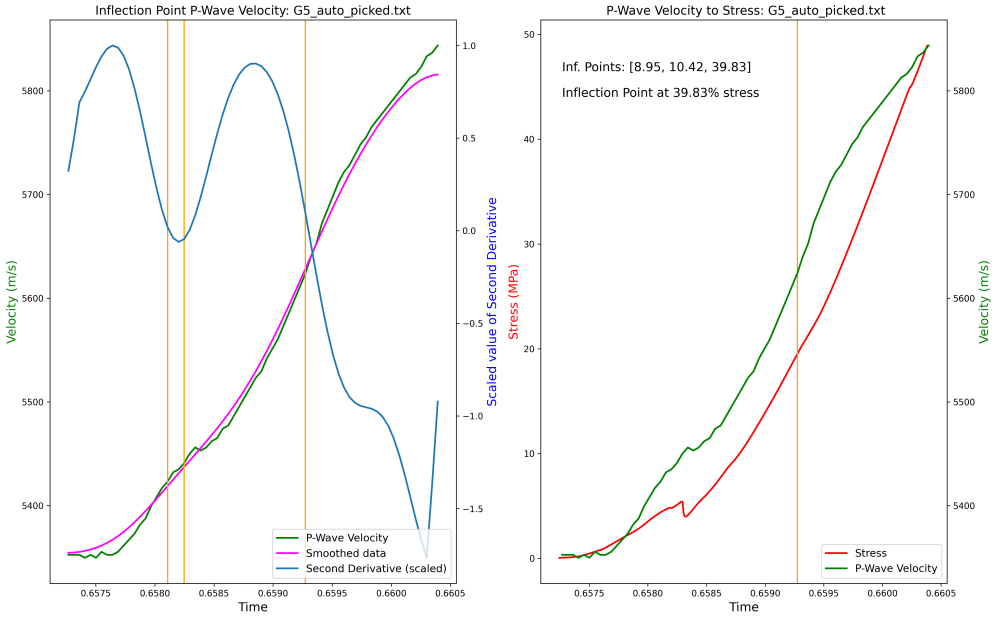

Figure 78: The **left** graph shows the P-wave velocity of the "G 5" sample (green), the velocity data smoothed by a Gaussian filter (magenta), the second derivative of the smoothed data (blue), and the inflection point of the smoothed data (orange vertical line). The **right** graph shows stress (red) and velocity (green) over the time of the test. The last IP is at 39.83 % with a TIP of 95.8 s.

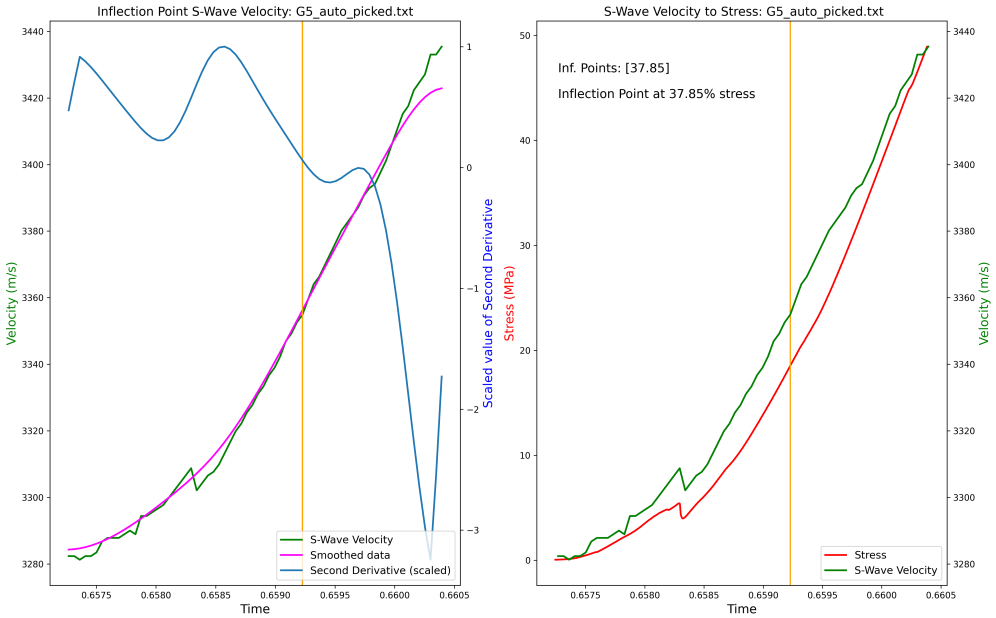

Figure 79: The **left** graph shows the S-wave velocity of the "G 5" sample (green), the velocity data smoothed by a Gaussian filter (magenta), the second derivative of the smoothed data (blue), and the inflection point of the smoothed data (orange vertical line). The **right** graph shows stress (red) and velocity (green) over the time of the test. The last IP is at 37.85 % with a TIP of 99.8 s.

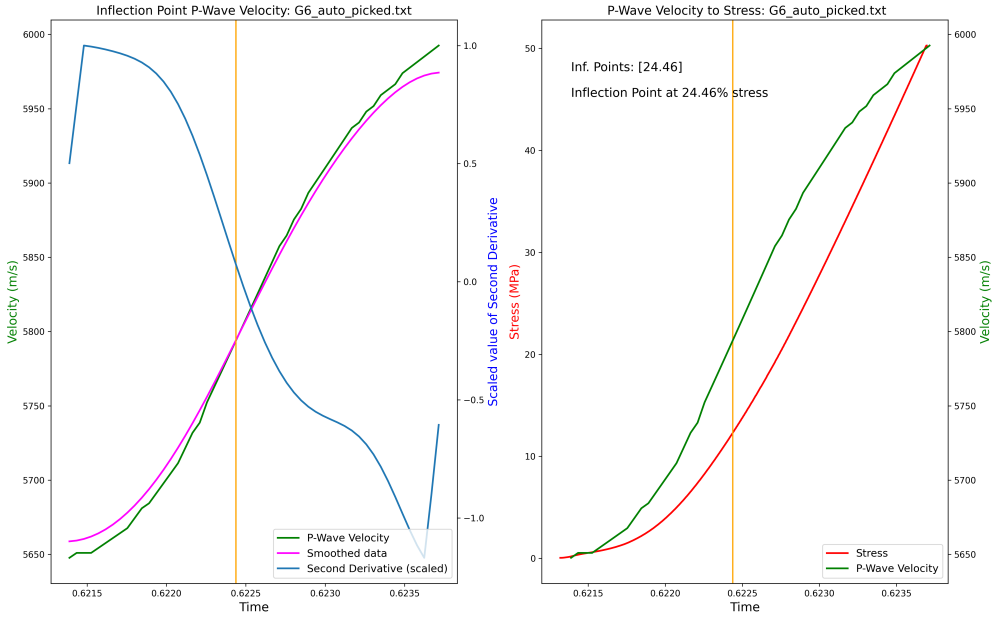

Figure 80: The **left** graph shows the P-wave velocity of the "G 6" sample (green), the velocity data smoothed by a Gaussian filter (magenta), the second derivative of the smoothed data (blue), and the inflection point of the smoothed data (orange vertical line). The **right** graph shows stress (red) and velocity (green) over the time of the test. The last IP is at 24.46 % with a TIP of 108.5 s.

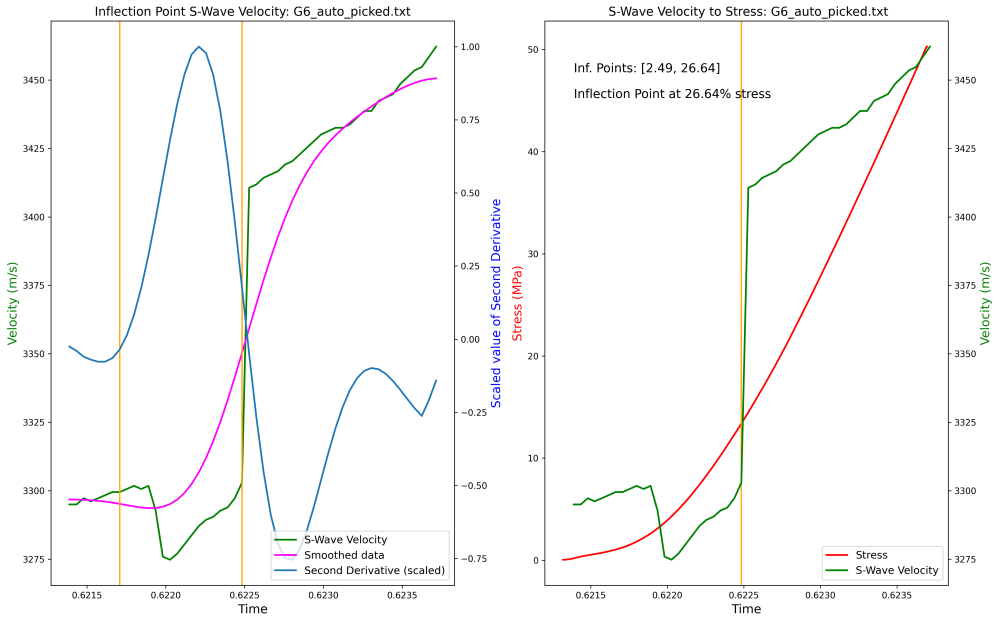

Figure 81: The **left** graph shows the S-wave velocity of the "G 6" sample (green), the velocity data smoothed by a Gaussian filter (magenta), the second derivative of the smoothed data (blue), and the inflection point of the smoothed data (orange vertical line). The **right** graph shows stress (red) and velocity (green) over the time of the test. The last IP is at 26.64 % with a TIP of 104.6 s.

Gneiss 30 mm Diameter

PPC and TPP

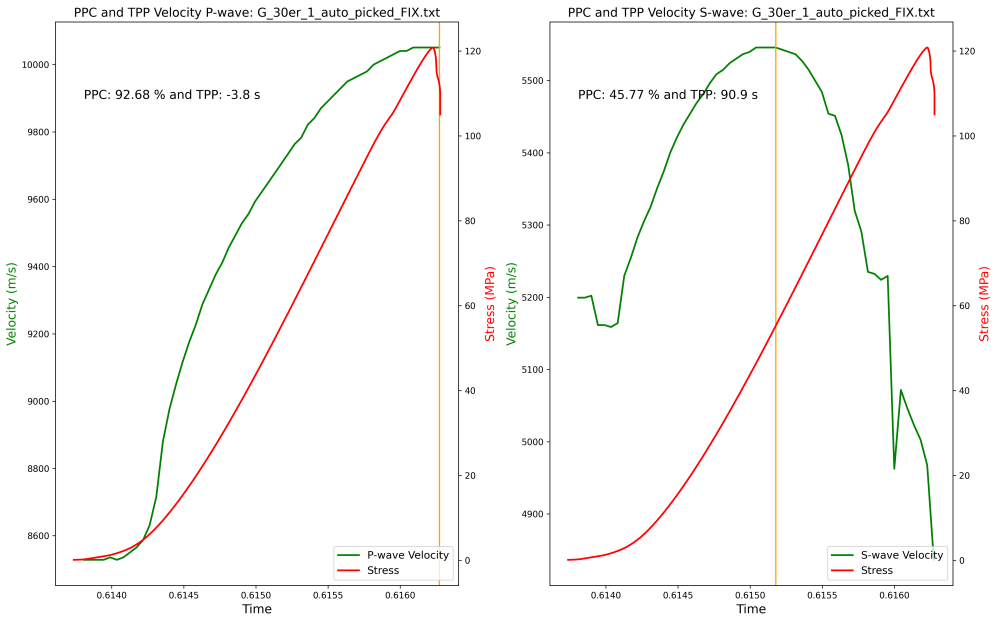

Figure 82: P- and S-wave velocity (green) and stress (red) plotted over the time of the "G 30er 1" test. With the PPC being P-wave: 92.68 % and S-wave: 45.77 % and the TPP being P-wave: -3.8 s and S-wave: 90.9 s.

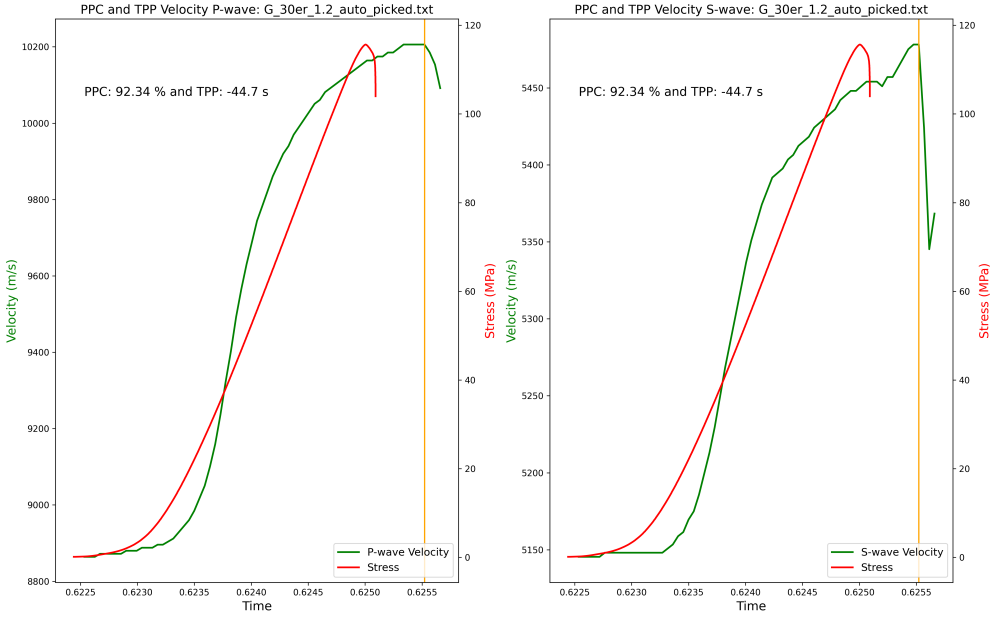

Figure 83: P- and S-wave velocity (green) and stress (red) plotted over the time of the "G 30er 1.2" test. With the PPC being P-wave: 92.34 % and S-wave: 92.34 % and the TPP being P-wave: -44.7 s and S-wave: -44.7 s.

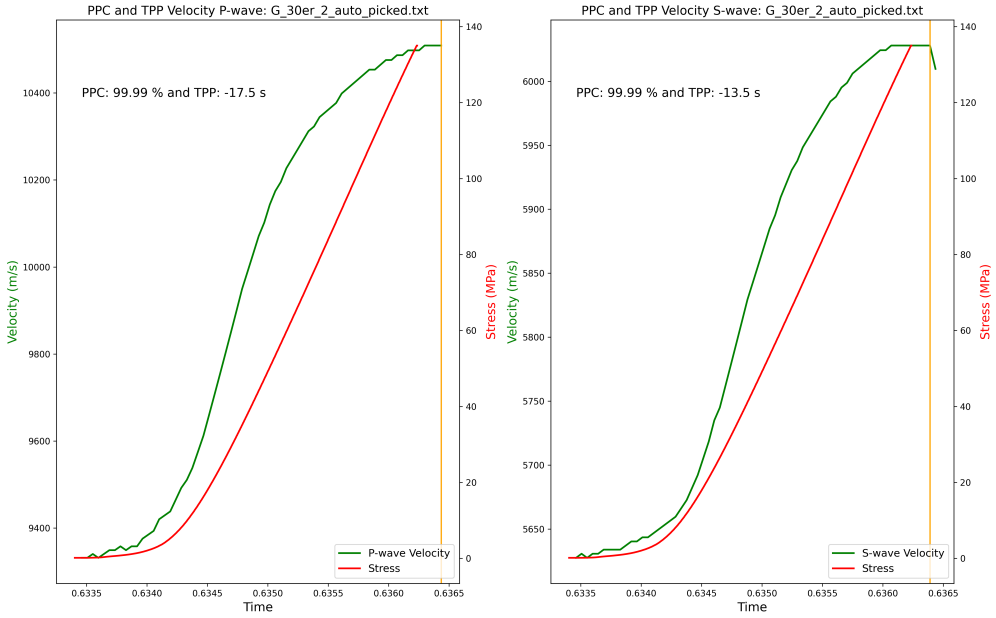

Figure 84: P- and S-wave velocity (green) and stress (red) plotted over the time of the "G 30er 2" test. With the PPC being P-wave: 99.99 % and S-wave: 99.99 % and the TPP being P-wave: -17.5 s and S-wave: -13.5 s.

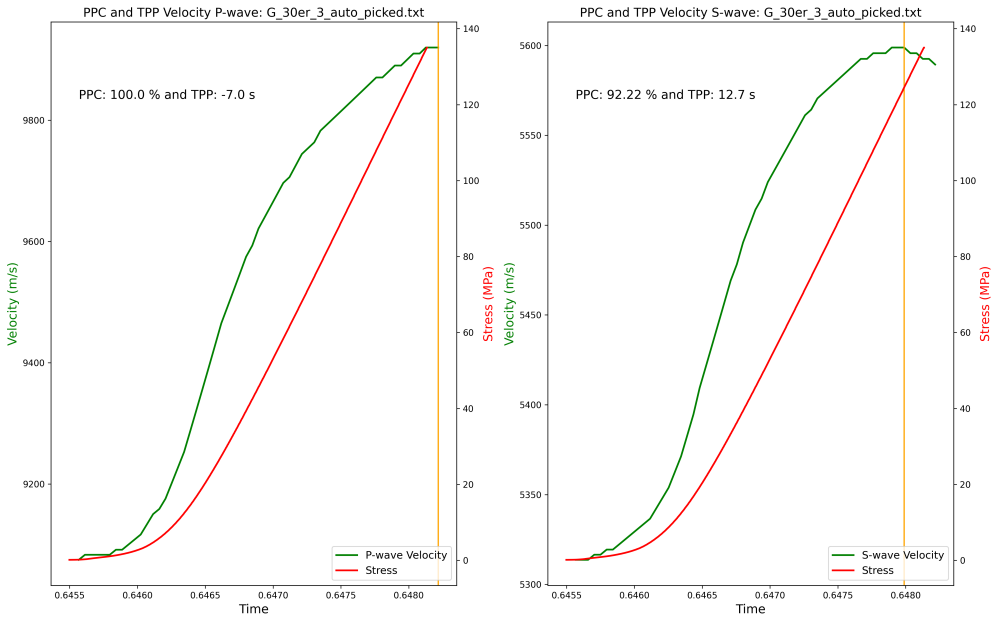

Figure 85: P- and S-wave velocity (green) and stress (red) plotted over the time of the "G 30er 3" test. With the PPC being P-wave: 100.0 % and S-wave: 92.22 % and the TPP being P-wave: -7.0 s and S-wave: 12.7 s.

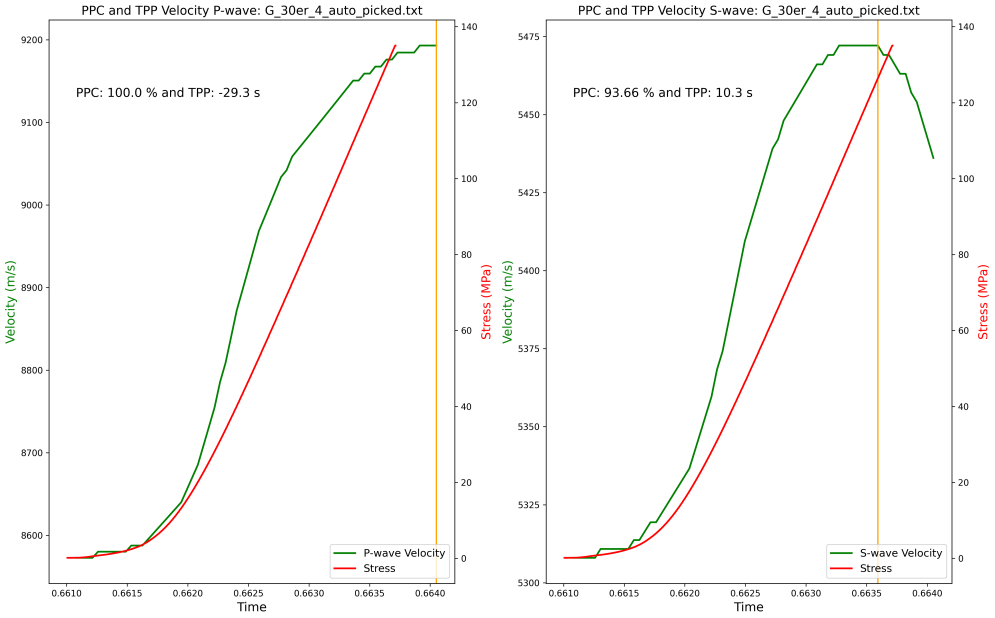

Figure 86: P- and S-wave velocity (green) and stress (red) plotted over the time of the "G 30er 4" test. With the PPC being P-wave: 100.0 % and S-wave: 93.66 % and the TPP being P-wave: -29.3 s and S-wave: 10.3 s.

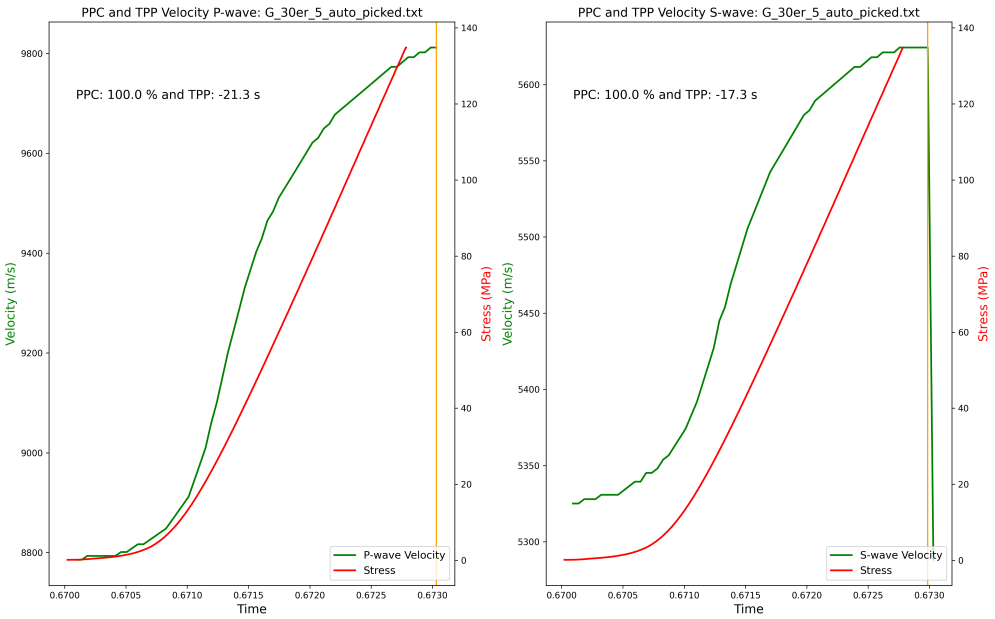

Figure 87: P- and S-wave velocity (green) and stress (red) plotted over the time of the "G 30er 5" test. With the PPC being P-wave: 100.0 % and S-wave: 100.0 % and the TPP being P-wave: -21.3 s and S-wave: -17.3 s.

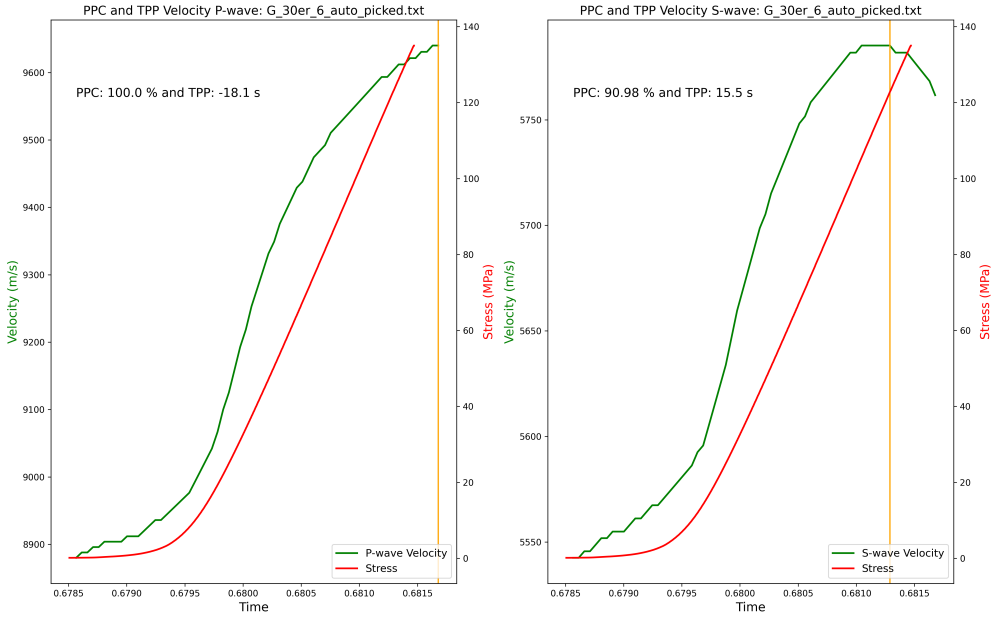

Figure 88: P- and S-wave velocity (green) and stress (red) plotted over the time of the "G 30er 6" test. With the PPC being P-wave: 100.0 % and S-wave: 90.98 % and the TPP being P-wave: -18.1 s and S-wave: 15.5 s.

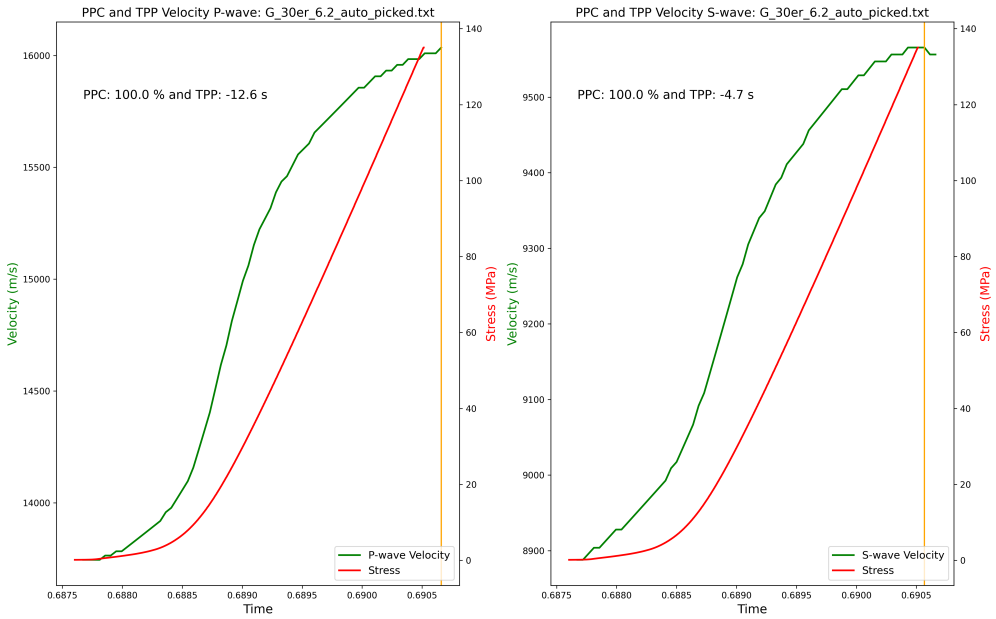

Figure 89: P- and S-wave velocity (green) and stress (red) plotted over the time of the "G 30er 6.2" test. With the PPC being P-wave: 100.0 % and S-wave: 100.0 % and the TPP being P-wave: -12.6 s and S-wave: 4.7 s.

IP and TIP

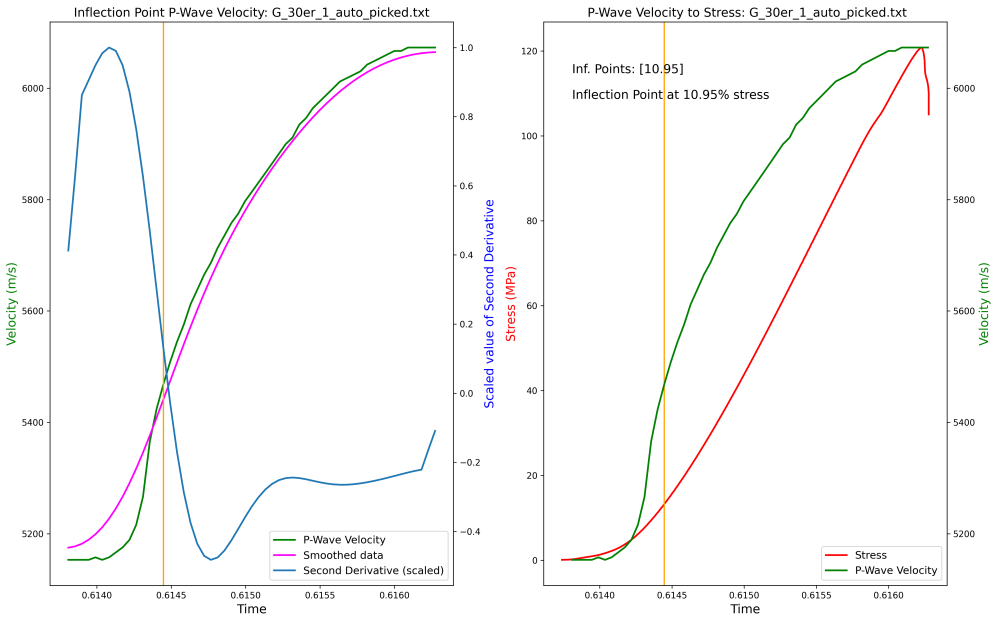

Figure 90: The **left** graph shows the P-wave velocity of the "G 30er 1" sample (green), the velocity data smoothed by a Gaussian filter (magenta), the second derivative of the smoothed data (blue), and the inflection point of the smoothed data (orange vertical line). The **right** graph shows stress (red) and velocity (green) over the time of the test. The last IP is at 10.95 % with a TIP of 154.0 s.

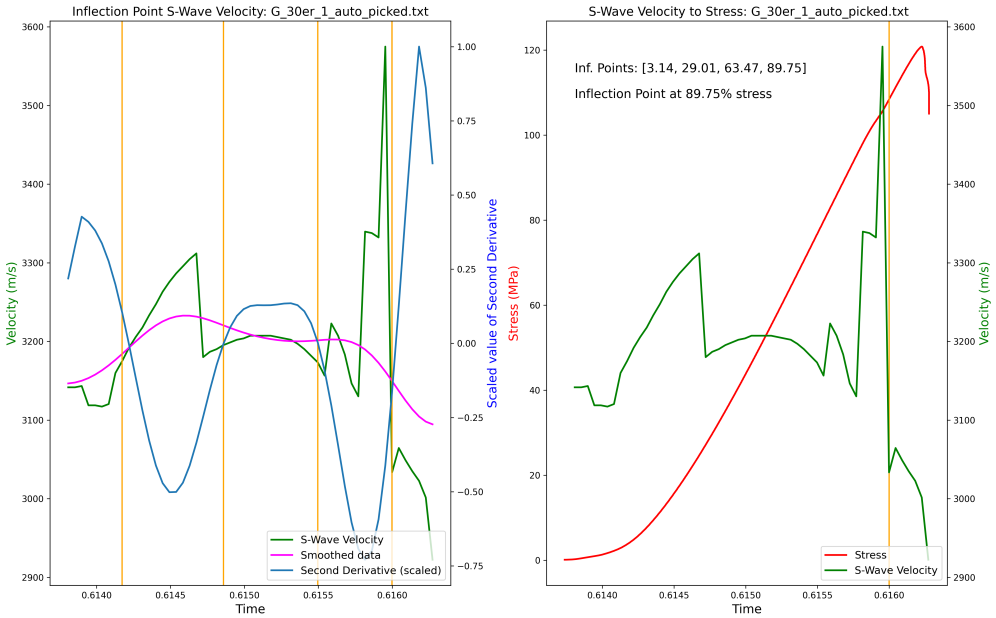

Figure 91: The **left** graph shows the S-wave velocity of the "G 30er 1" sample (green), the velocity data smoothed by a Gaussian filter (magenta), the second derivative of the smoothed data (blue), and the inflection point of the smoothed data (orange vertical line). The **right** graph shows stress (red) and velocity (green) over the time of the test. The last IP is at 81.14 % with a TIP of 35.6 s.

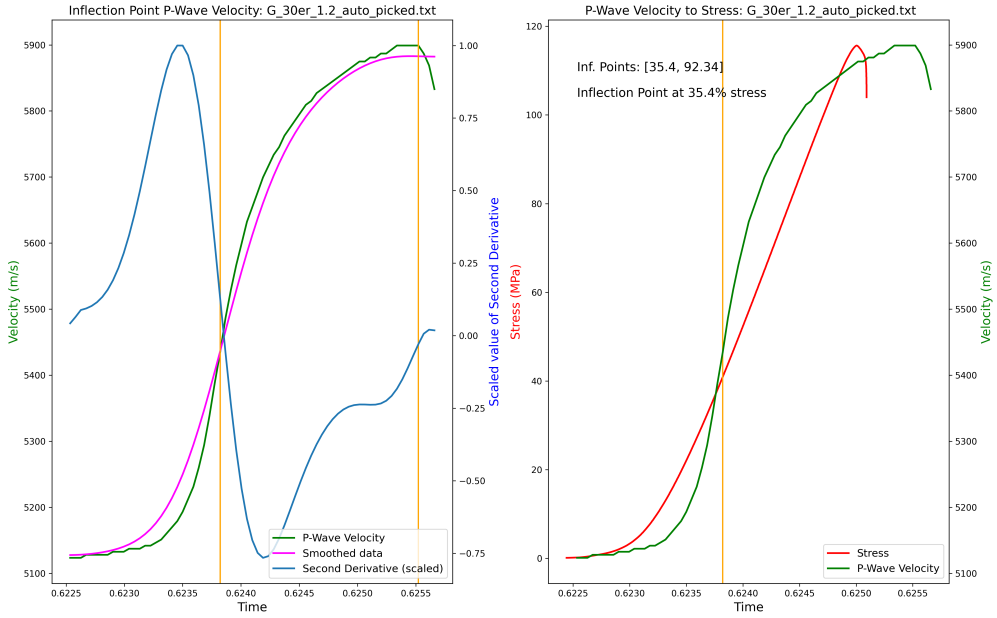

Figure 92: The **left** graph shows the P-wave velocity of the "G 30er 2" sample (green), the velocity data smoothed by a Gaussian filter (magenta), the second derivative of the smoothed data (blue), and the inflection point of the smoothed data (orange vertical line). The **right** graph shows stress (red) and velocity (green) over the time of the test. The last IP is at 35.40 % with a TIP of 102.3 s.

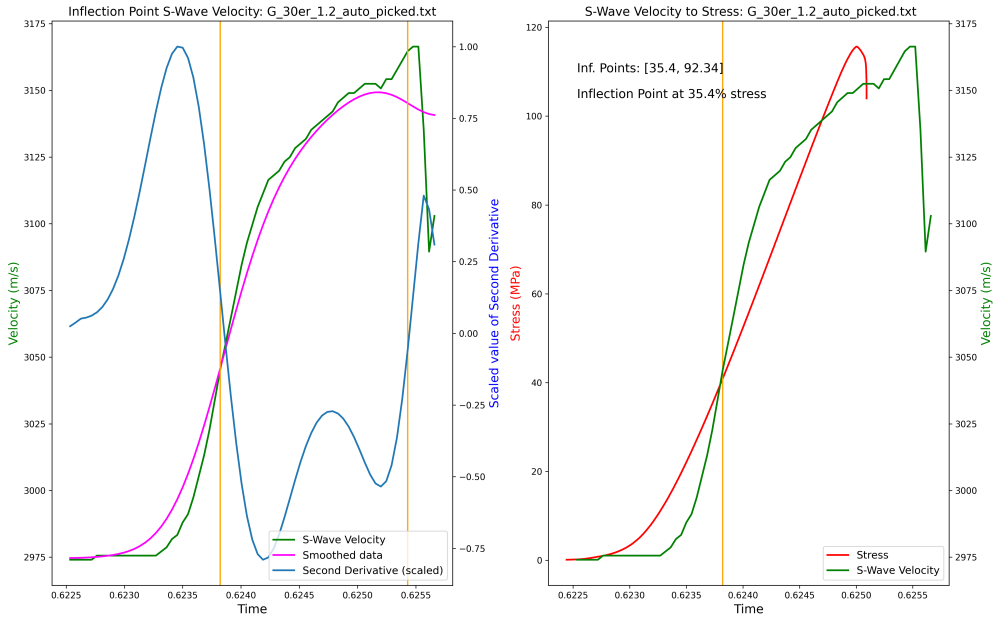

Figure 93: The **left** graph shows the S-wave velocity of the "G 30er 2" sample (green), the velocity data smoothed by a Gaussian filter (magenta), the second derivative of the smoothed data (blue), and the inflection point of the smoothed data (orange vertical line). The **right** graph shows stress (red) and velocity (green) over the time of the test. The last IP is at 35.40 % with a TIP of 102.3 s.

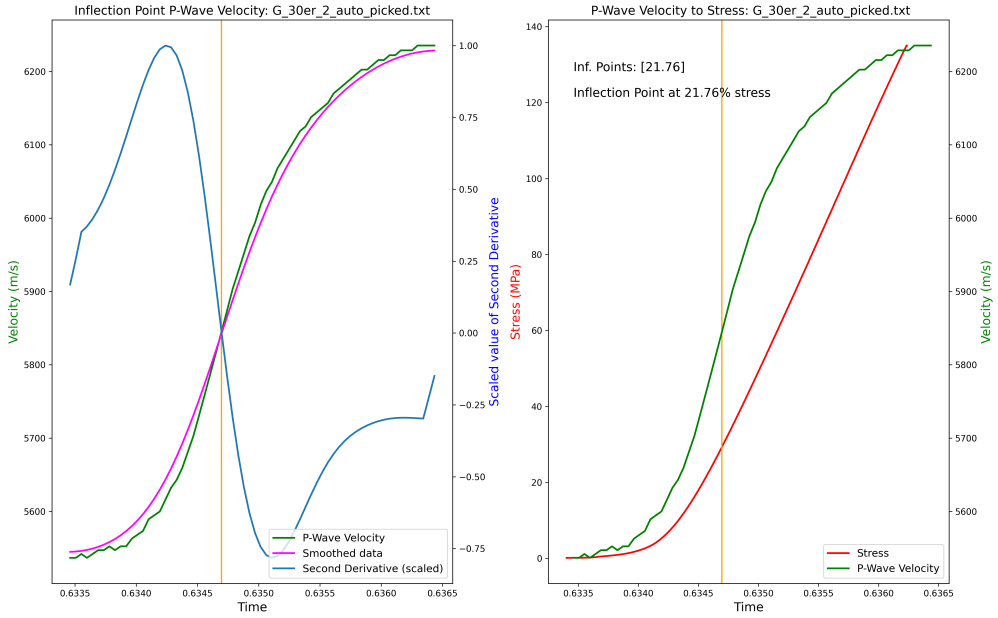

Figure 94: The **left** graph shows the P-wave velocity of the "G 30er 2" sample (green), the velocity data smoothed by a Gaussian filter (magenta), the second derivative of the smoothed data (blue), and the inflection point of the smoothed data (orange vertical line). The **right** graph shows stress (red) and velocity (green) over the time of the test. The last IP is at 21.76 % with a TIP of 132.8 s.

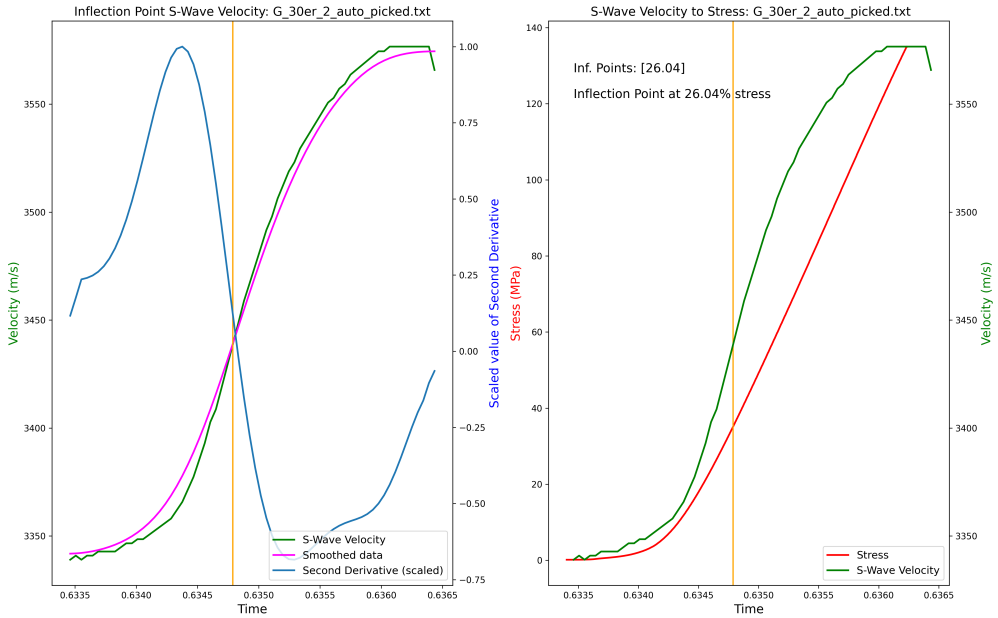

Figure 95: The **left** graph shows the S-wave velocity of the "G 30er 2" sample (green), the velocity data smoothed by a Gaussian filter (magenta), the second derivative of the smoothed data (blue), and the inflection point of the smoothed data (orange vertical line). The **right** graph shows stress (red) and velocity (green) over the time of the test. The last IP is at 26.04 % with a TIP of 124.9 s.

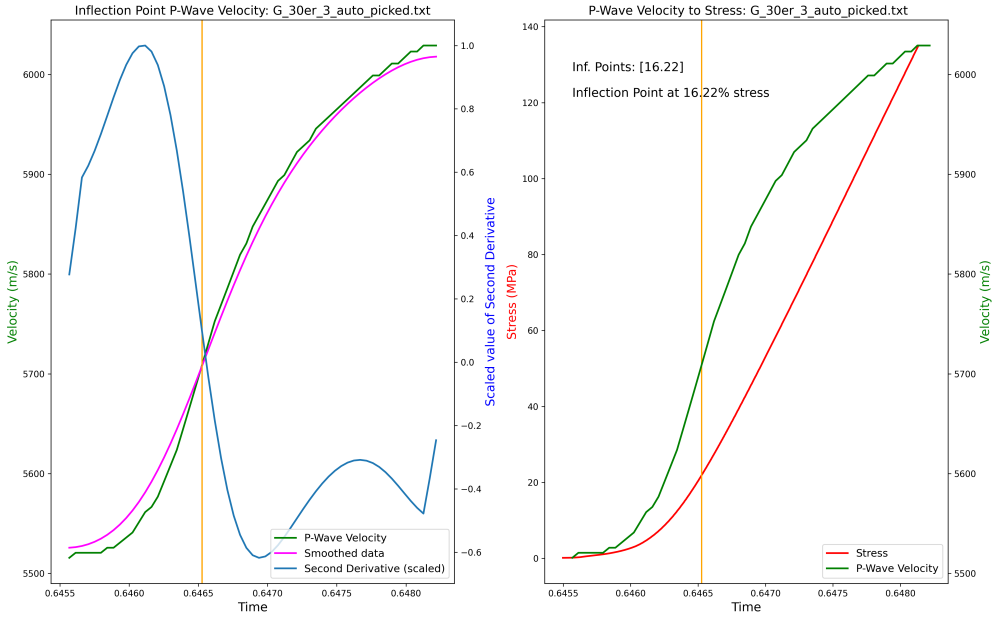

Figure 96: The **left** graph shows the P-wave velocity of the "G 30er 3" sample (green), the velocity data smoothed by a Gaussian filter (magenta), the second derivative of the smoothed data (blue), and the inflection point of the smoothed data (orange vertical line). The **right** graph shows stress (red) and velocity (green) over the time of the test. The last IP is at 16.22 % with a TIP of 139.0 s.

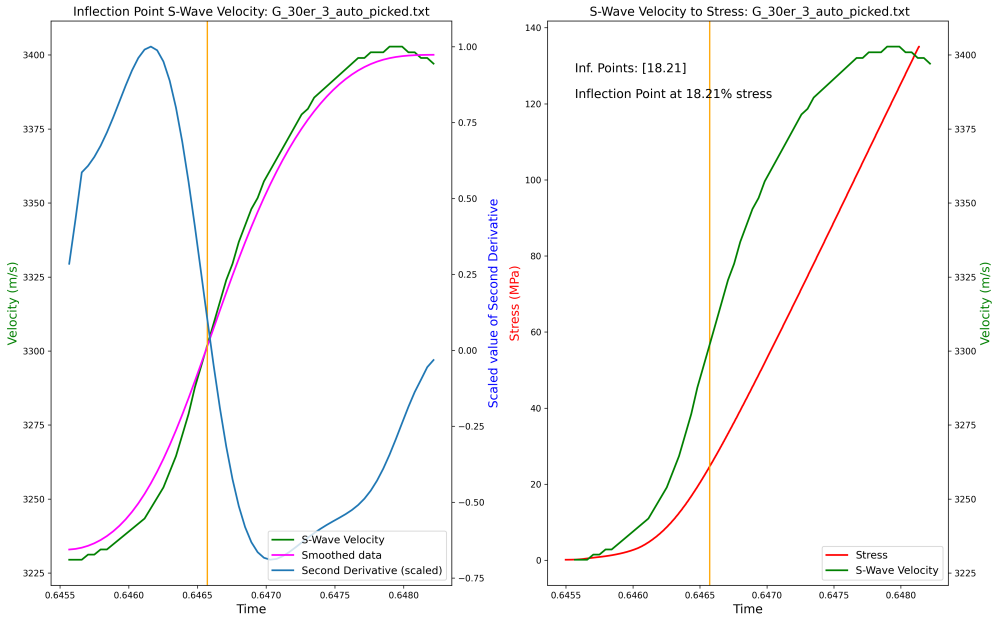

Figure 97: The **left** graph shows the S-wave velocity of the "G 30er 3" sample (green), the velocity data smoothed by a Gaussian filter (magenta), the second derivative of the smoothed data (blue), and the inflection point of the smoothed data (orange vertical line). The **right** graph shows stress (red) and velocity (green) over the time of the test. The last IP is at 18.21 % with a TIP of 135.1 s.

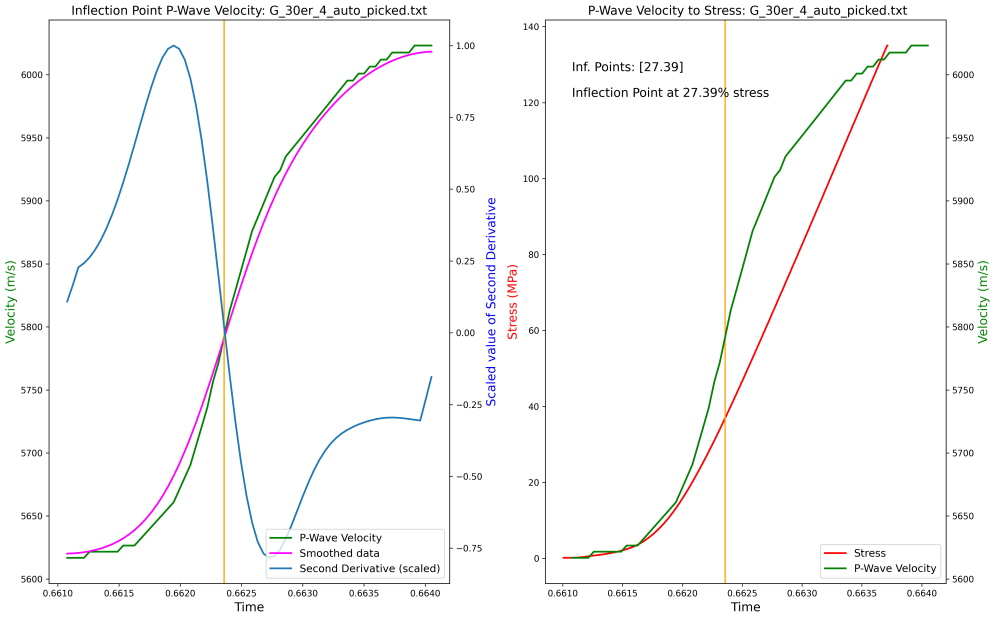

Figure 98: The **left** graph shows the P-wave velocity of the "G 30er 4" sample (green), the velocity data smoothed by a Gaussian filter (magenta), the second derivative of the smoothed data (blue), and the inflection point of the smoothed data (orange vertical line). The **right** graph shows stress (red) and velocity (green) over the time of the test. The last IP is at 27.39 % with a TIP of 117.0 s.

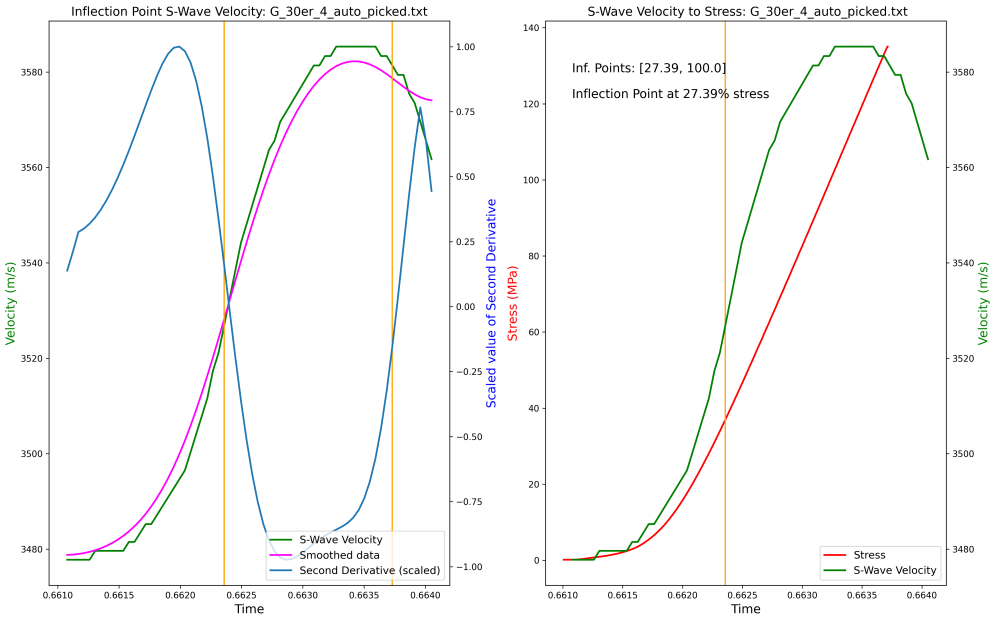

Figure 99: The **left** graph shows the S-wave velocity of the "G 30er 4" sample (green), the velocity data smoothed by a Gaussian filter (magenta), the second derivative of the smoothed data (blue), and the inflection point of the smoothed data (orange vertical line). The **right** graph shows stress (red) and velocity (green) over the time of the test. The last IP is at 27.39 % with a TIP of 117.0 s.

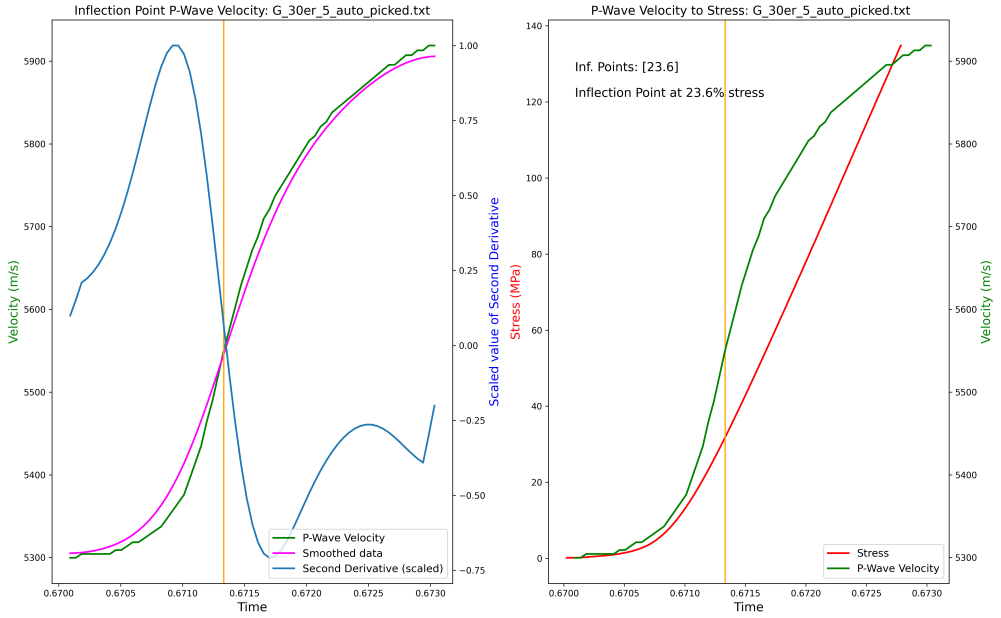

Figure 100: The **left** graph shows the P-wave velocity of the "G 30er 5" sample (green), the velocity data smoothed by a Gaussian filter (magenta), the second derivative of the smoothed data (blue), and the inflection point of the smoothed data (orange vertical line). The **right** graph shows stress (red) and velocity (green) over the time of the test. The last IP is at 23.60 % with a TIP of 125.6 s.

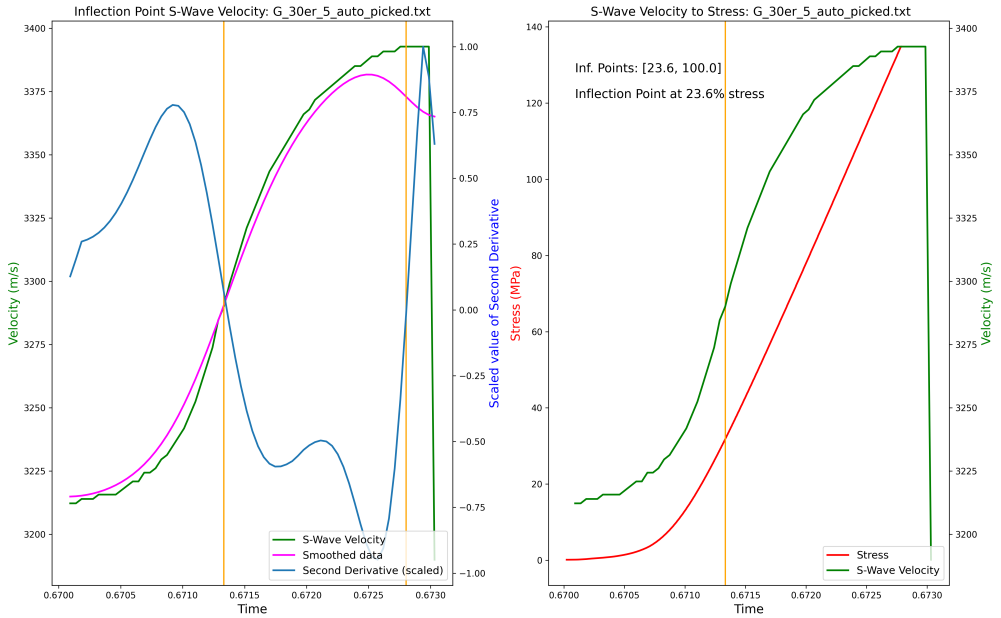

Figure 101: The **left** graph shows the S-wave velocity of the "G 30er 5" sample (green), the velocity data smoothed by a Gaussian filter (magenta), the second derivative of the smoothed data (blue), and the inflection point of the smoothed data (orange vertical line). The **right** graph shows stress (red) and velocity (green) over the time of the test. The last IP is at 23.60 % with a TIP of 125.6 s.

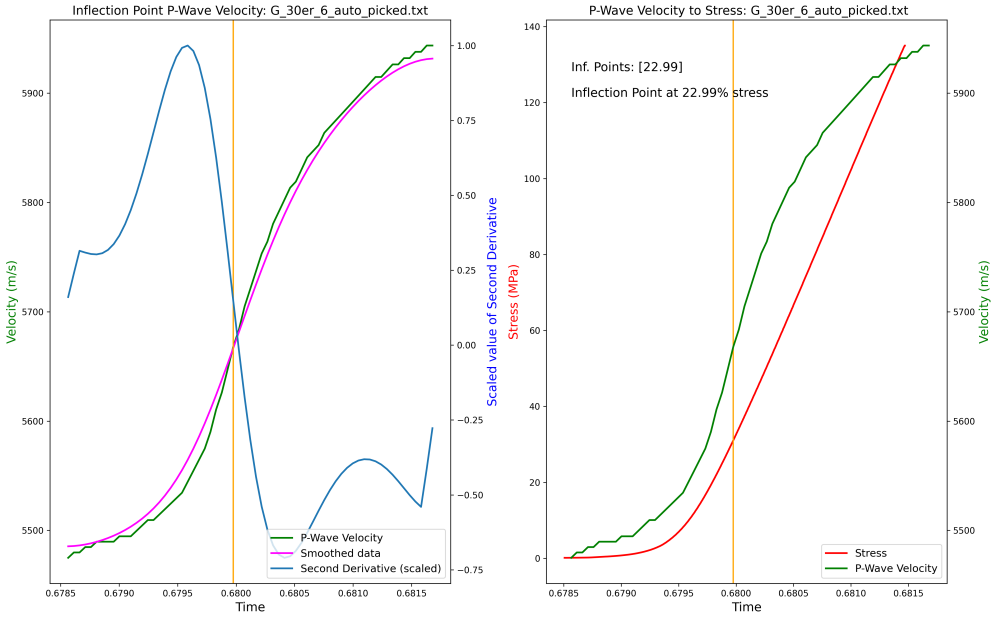

Figure 102: The **left** graph shows the P-wave velocity of the "G 30er 6" sample (green), the velocity data smoothed by a Gaussian filter (magenta), the second derivative of the smoothed data (blue), and the inflection point of the smoothed data (orange vertical line). The **right** graph shows stress (red) and velocity (green) over the time of the test. The last IP is at 22.99 % with a TIP of 129.0 s.

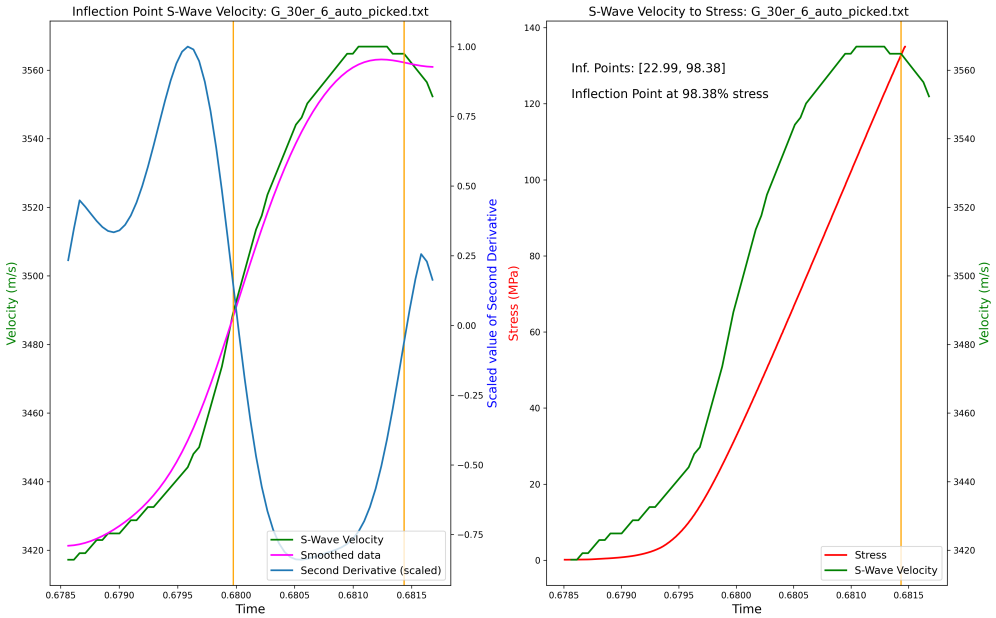

Figure 103: The **left** graph shows the S-wave velocity of the "G 30er 6" sample (green), the velocity data smoothed by a Gaussian filter (magenta), the second derivative of the smoothed data (blue), and the inflection point of the smoothed data (orange vertical line). The **right** graph shows stress (red) and velocity (green) over the time of the test. The last IP is at 98.38 % with a TIP of 2.9 s.

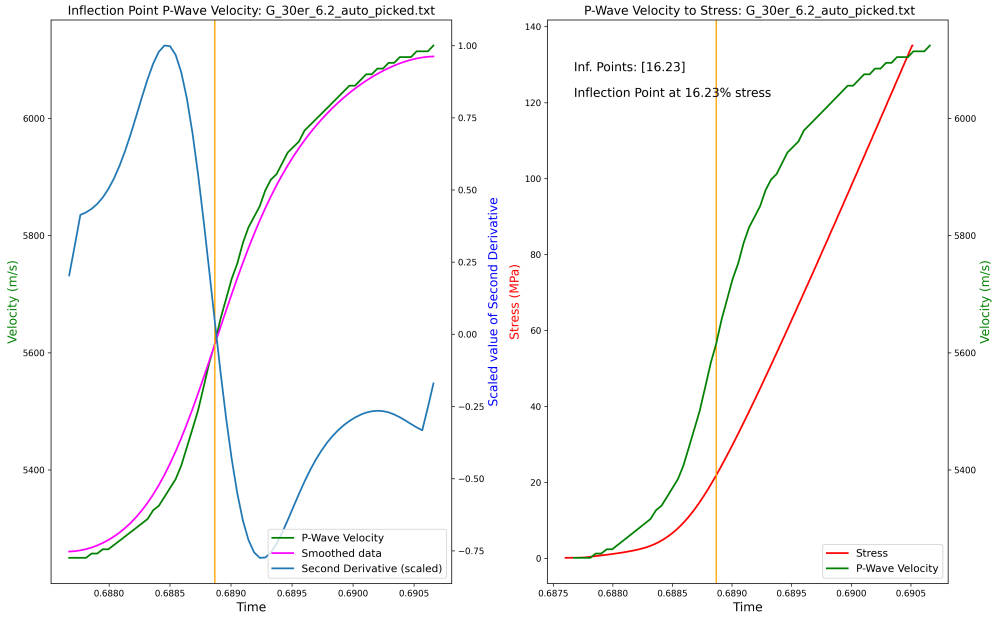

Figure 104: The **left** graph shows the P-wave velocity of the "G 30er 6.2" sample (green), the velocity data smoothed by a Gaussian filter (magenta), the second derivative of the smoothed data (blue), and the inflection point of the smoothed data (orange vertical line). The **right** graph shows stress (red) and velocity (green) over the time of the test. The last IP is at 16.23 % with a TIP of 142.2 s.

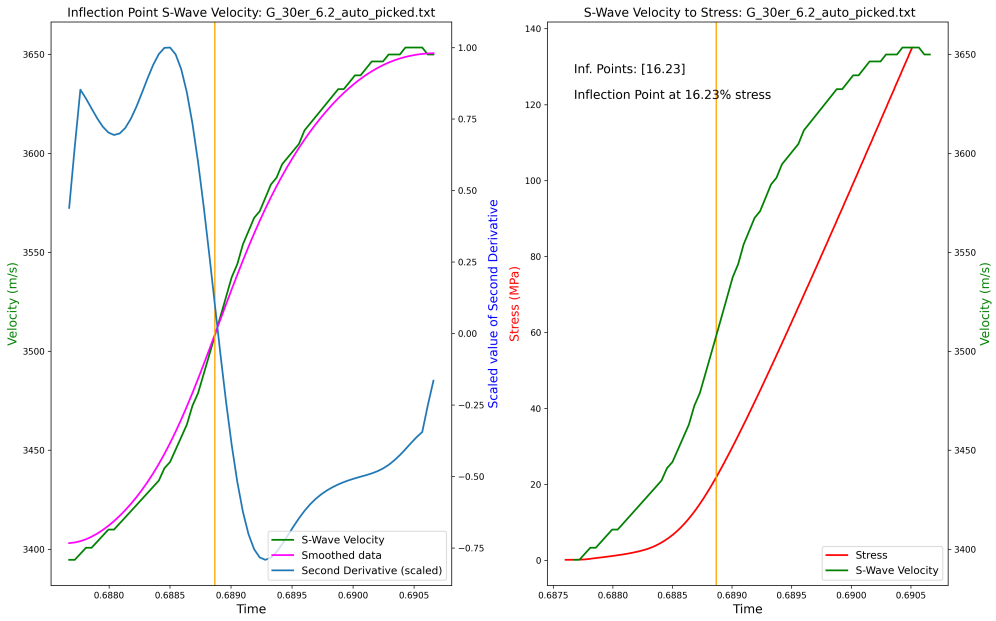

Figure 105: The **left** graph shows the S-wave velocity of the "G 30er 6.2" sample (green), the velocity data smoothed by a Gaussian filter (magenta), the second derivative of the smoothed data (blue), and the inflection point of the smoothed data (orange vertical line). The **right** graph shows stress (red) and velocity (green) over the time of the test. The last IP is at 16.23 % with a TIP of 142.2 s.